EFFECTS OF A TRANSVERSE MAGNETIC FIELD ON THE SMALL SIGNAL ADMITTANCE OF GaAs DIODES

by

Colmon Wood-Chuen Wong

A dissertation submitted to the Graduate Faculty in Engineering in partial fulfillment of the requirements for the degree of Doctor of Philosophy, The City University of New York.

1976

This manuscript has been read and accepted for the Graduate Faculty in Engineering in satisfaction of the dissertation requirement for the degree of Doctor of Philosophy.

March 24, 1976 — Joseph S. Nadan
date — Chairman of Examining Committee

March 24, 1976 — Jacques E. Benveniste
date — Executive Officer

Prof. Samir A. Ahmed

Prof. Morris Ettenberg

Prof. Joseph S. Nadan (Chairman)

Prof. Carl Shulman
Supervisory Committee

The City University of New York

ACKNOWLEDGEMENTS

I wish to express my gratitude to all members of my doctoral committee. In particular, I wish to thank my mentor Professor Joseph S. Nadan for his guidance, encouragement and confidence in my work. The assistance of Mr. Abraham Glasser in the fabrication of the devices is much appreciated. I am indebted to the City University of New York for the Summer Research Assistantship in 1973. Lastly, I am most gratful to my wife, Tammy, whose high spirit makes difficult tasks seem a lot easier. Her enthusiasm in the preparation of the manuscript is the most recent example.

TO

TAMMY

Abstract

EFFECTS OF A TRANSVERSE MAGNETIC FIELD ON
THE SMALL SIGNAL ADMITTANCE OF GaAs DIODES

by

Colmon Wood-Chuen Wong

Advisor: Professor Joseph S. Nadan

The dc and microwave properties of GaAs (Gunn) diodes under the influence of a transverse magnetic field are studied through calculation and measurement of the device admittance with the magnetic field as parameter.

The zero magnetic field static V-I characteristics of the devices tested are measured and expressed analytically. The results are then used to calculate device properties for non-zero magnetic field cases. The non-linearity in the static characteristic is modeled in terms of a carrier temperature dependent drift mobility. The uniform electric field model in which the electric field is assumed to be uniform across the entire device is used, resulting in analytical expressions for the device admittance. Microstrip circuits are built for testing purposes. External circuit effects are taken into consideration using equivalent lumped circuit elements and appropriate sections of transmission lines. Microwave measurements are made employing the microwave network analyzer.

The major effect of the magnetic field is in altering the carrier transit time at which small signal measurements are made. It is shown that reduction of the transit time by the magnetic field results in a reduction in the frequency at which small signal gain occurs. The measured and calculated results are presented graphically.

The magnetic field is demonstrated to be useful as a diagnostic tool. In the static case, the magnetic field provides an independent means of obtaining the device mobility. In the small signal case, it allows the device model, in which the small signal admittance is calculated as a function of the transit time , to be evaluated. Furthermore, the magnetic field may be used as a tuning element since it alters the device amplification characteristics as a function of frequency.

TABLE OF CONTENTS

TABLE OF CONTENTS

LIST OF FIGURES

LIST OF FIGURES

LIST OF FIGURES

LIST OF FIGURES

LIST OF TABLES

CHAPTER 1 INTRODUCTION AND BACKGROUND

1.1 Discovery of Negative Differential Conductance (NDC) in Gallium Arsenide (GaAs)

In 1961, Ridley and Watkins [1] first proposed the electron transfer mechanism, in which electrons are transferred from a high mobility band to a low mobility band by raising the static electric field, as a possible source of negative differential conductance (NDC) in certain semiconductors. The term NDC is used here to describe the negative slope in the average carrier drift velocity versus electric field (v_d-E) characteristic. The energy band structure of GaAs [2], Fig. 1.1:1, with its high mobility lower conduction band valley and low mobility upper conduction band valley, satisfies the basic requirements for such a mechanism to occur.

In 1963, while investigating the effects of high electric fields in solids, Gunn [3,4] observed that when the applied voltage across the terminals of devices fabricated from GaAs and InP exceeded a definite threshold voltage, current oscillations resulted. Using a specially designed capacitive probe [5], he determined the time dependent potential distribution within the devices. The results indicated that current oscillations occured in conjunction with the cyclic formation of a high electric field domain (region) and a low electric field domain within the sample.

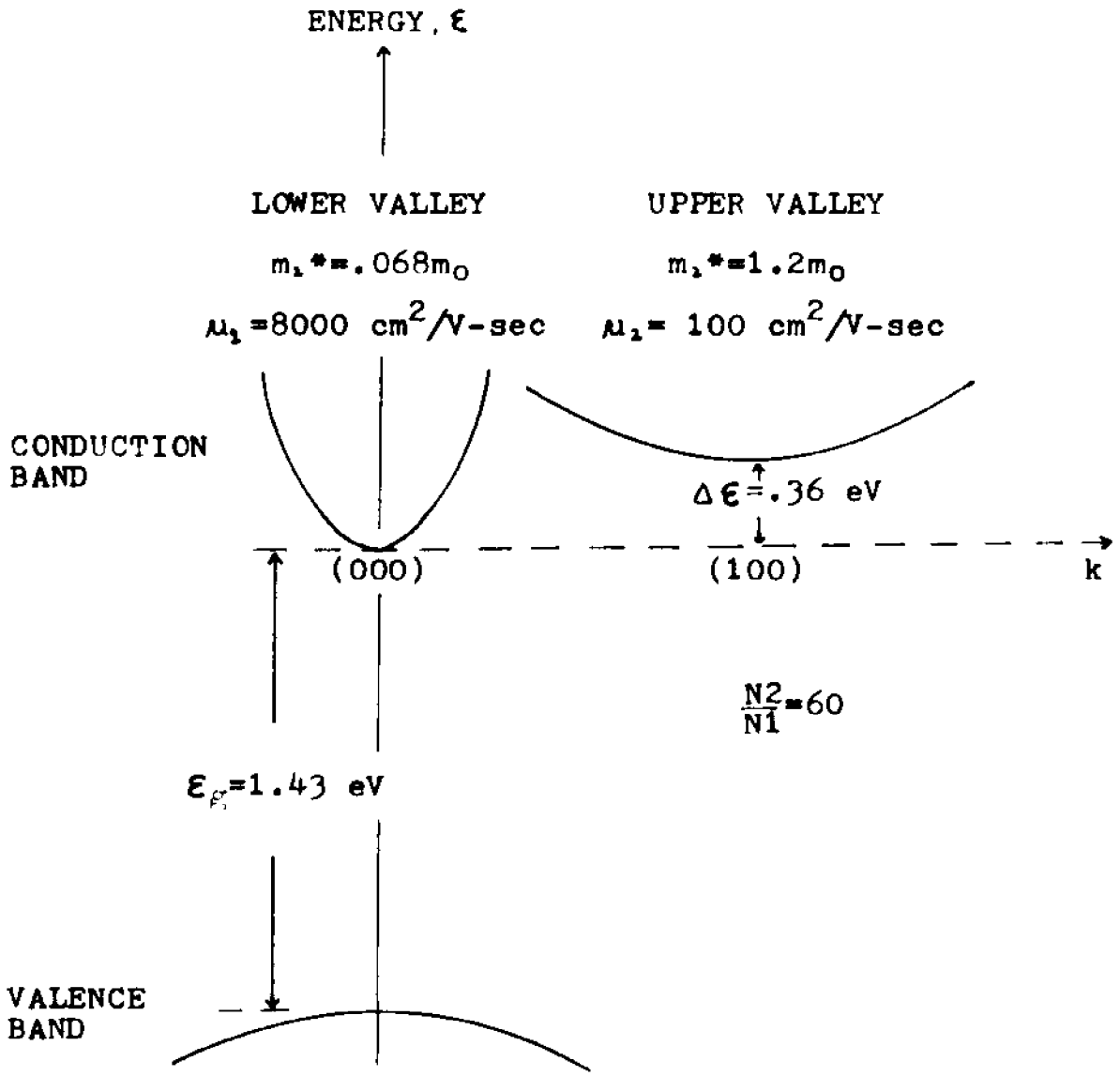

FIGURE 1.1.1 ENERGY BAND STRUCTURE OF GaAs [2]

Sequentially, as shown in Fig. 1.1:2, the high field domain nucleates at the cathode, grows in magnitude while remaining stationery, detaches from the cathode, drifts towards the anode and finally drains at the anode. While the high field domain is in transit, much of the externally applied voltage is developed across this high field region which is narrow compared to the physical lengths of the devices in Gunn's experiments. As a result, the electric field across the rest of the sample is much lower than the value if the high field domain did not exist. Externally, this is observed as a reduction in current as determined by the electric field external to the high field domain. When the domain makes its exit at the anode, the excess voltage is redistributed to the rest of the sample resulting in a current rise. One cycle of current oscillation is completed when the high field domain completely drains at the anode and a new one is nucleated at the cathode. This phenomenon subsequently came to be known as the Gunn effect.

Together with the description of the experimental results, Gunn [3,4] proposed several possible mechanisms to explain the experimental observations. One of the models that he considered was the existence of NDC in the medium resulting from the transfer of electrons to the upper valley with increasing electric field. However, in view of the considerable size of the band gap ($\Delta\mathcal{E}\sim.36$eV), Gunn estimated that for intervalley transfer to be significant, an electron temperature of 4,000°K would be required. Since the high

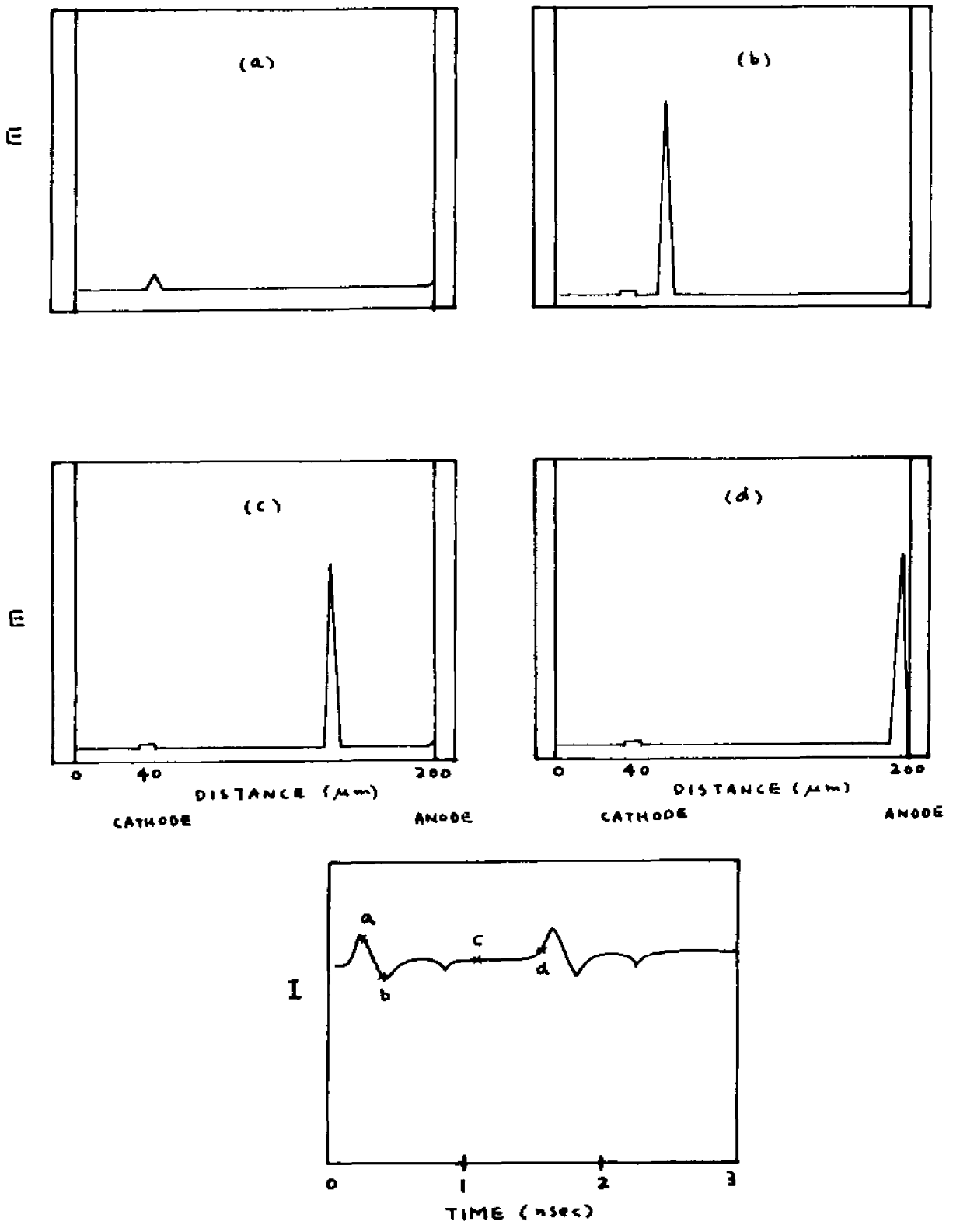

FIGURE 1.1:2 DOMAIN DYNAMICS IN GUNN OSCILLATIONS [14]

temperature was not substantiated in other measurements, the transferred electron mechanism was rejected as being unlikely to cause the Gunn effect. Independently, and prior to Gunn's experiments, significant theorectical results existed in this area. In 1962, Hilsum [6] calculated and obtained the NDC region in GaAs using the transferred electron model. The formation of high and low electric field domains in such a medium was further predicted by Ridley [7] in 1963 using general thermodynamic arguments. Subsequently, in 1964, Kroemer [8] pointed out that the theorectical results are consistent with Gunn's experimental observations due to the ratio of the density of states in the upper valley, N2, to that in the lower valley, N1, with typically (N2/N1)=60. This high ratio predicts a much higher probability of electron transfer from the lower to the upper valley at a much lower electron temperature than the one Gunn considered necessary.

A number of experiments have been performed that conclusively demonstrated that the electron transfer mechanism is responsible for the NDC observed in GaAs. In one experiment [9], the band gap, $\Delta\mathcal{E}$, was varied by hydrostatic pressure. It was found that decreasing $\Delta\mathcal{E}$ by increasing the pressure decreased the threshold voltage. In the second experiment [10], $\Delta\mathcal{E}$ was varied by forming a series of solid solutions between GaAs and GaP. The same correlation between $\Delta\mathcal{E}$ and the threshold voltage was found. The transferred electron mechanism is hence well established as

the cause of NDC and the resulting Gunn effect in GaAs.

Measurement of the average carrier drift velocity versus electric field (v_d-E) characteristic was done by Ruch and Kino [11] in 1967 on semi-insulating GaAs. The result, together with that calculated earlier by Butcher and Fawcett [12], are shown in Fig. 1.1:3. In 1970, Braslau and Hauge [13] adopted a microwave technique to measure the characteristic in doped samples. The results indicated that the v_d-E characteristics are somewhat dependent on the fabrication processes. No conclusive explanations were given for the variations.

Since the original experiments by Gunn, numerous publications on theorectical and experimental treatments of Gunn effect have been presented [14-23]. In addition to the Gunn oscillations described above, consideration of the external circuit and device parameters lead to the discovery of other modes of operations which are summarized below:

1. Quenched, delayed and multiple domain modes [24,25] which are Gunn oscillations with the frequencies modified by a high-Q external circuit.
2. The limited space-charge accumulation (LSA) mode discovered by Copeland [26,27] in which the external circuit is tuned to such a high frequency that a domain does not have time to form; in its place, an electron accumulation layer propagates across the sample.

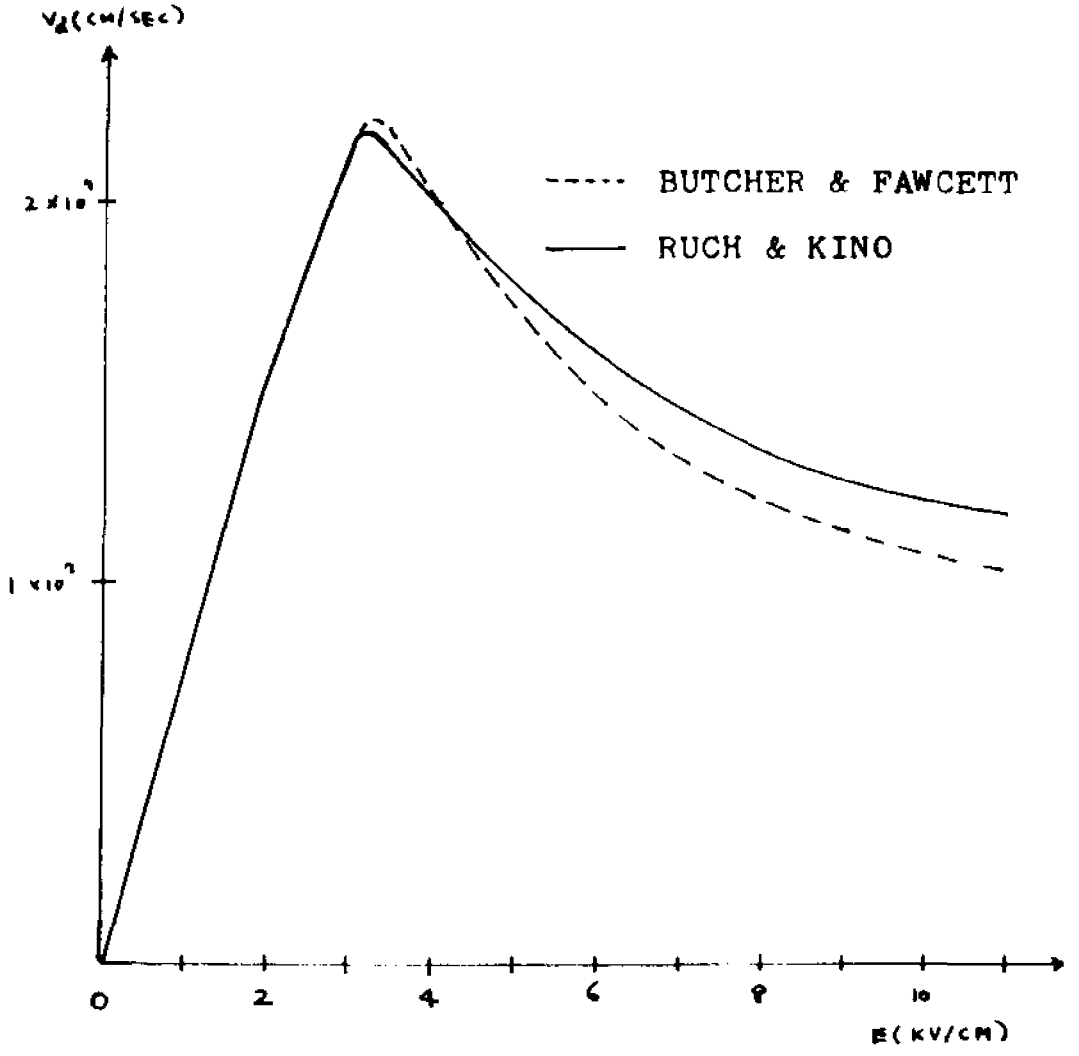

FIGURE 1.1.3 v_d-E CHARACTERISTIC OF GaAs [11,12]

3. Bias circuit oscillations [28] which resemble relaxation oscillations in a low-Q circuit.
4. Stable, linear amplification [19,29] in which no microwave output is detected with zero input. This is to be distinguished from injection-locked amplification [30] in which the device is oscillating at all times.

A good summary discussion of the various modes of operations is found in a paper by Copeland [31]. In this paper, a figure is presented in which the dependence of these possible modes on doping concentration and frequency is shown. This is reproduced in Fig. 1.1:4.

The stable amplification region is the topic of interest in this work and will be discussed in more detail here and in the next section. As Fig. 1.1:4 shows, the transition from Gunn oscillations to stable amplification occurs at a value of $n_oL \approx 10^{12}/cm^2$. Furthermore, there is only a narrow frequency region, $fL \approx 10^7$ cm/sec, where this mode of operation is possible. Therefore, to operate the device in the stable amplification mode, it is necessary to

1. keep the doping concentration, n_o, low enough such that $n_oL \lesssim 10^{12}/cm^2$, and
2. pick the proper sample length L such that gain occurs at $fL \simeq 10^7$ cm/sec.

There are other complications such as non-uniform electric field distribution within the device, bias circuit oscillations, temperature effects, etc., to be discussed

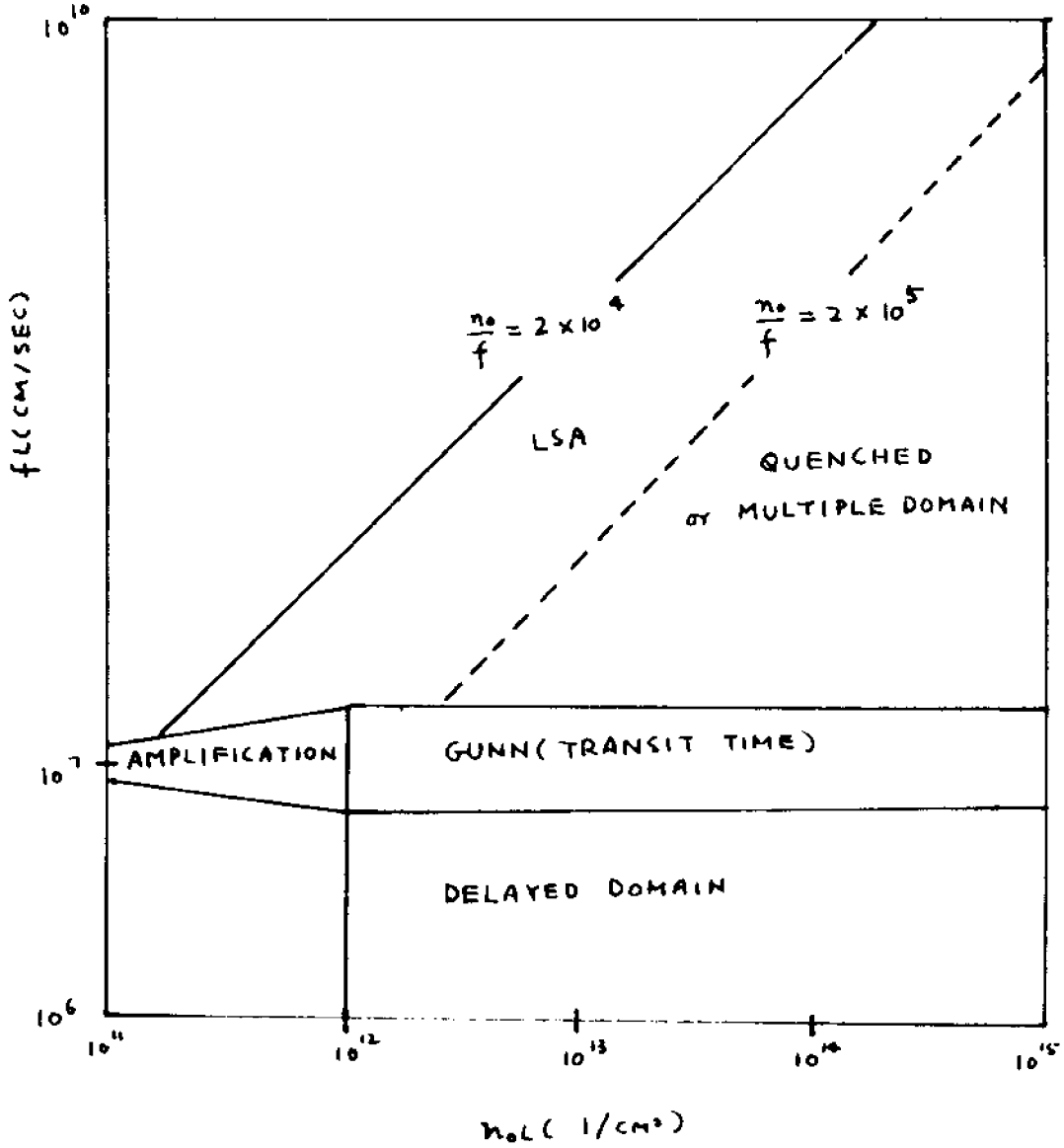

FIGURE 1.1:4 MODE CHART [31]

as needed throughout the text.

1.2 Outline of This Study

In 1965, Thim, Barber, Hakki, Knight and Uenohara [32] proposed the use of a NDC device for small signal microwave amplification. Detailed experimental results were published by Thim and Barber [19] in 1966. Theoretical works in this area were further carried out by other authors; among them were McCumber and Chynoweth [14], Engelmann and Quate [16], Kroemer [22], Hakki [29], and Ohmi and Hasuo [33]. Other publications concentrated on the necessary external networks required to obtain stable operations [34-37]. In a few publications [38-40] which included some most recent papers in this area, the possibility of a non-uniform electric field distribution within the device is considered. All these results are further discussed in Chp. 3 where the small signal admittance is calculated.

Amplification in a GaAs device is made possible by the existence of a NDC region in the average carrier drift velocity versus electric field (v_d-E) characteristic. Whereas a negative slope in the v_d-E characteristic is necessary for amplification to occur, the static value, v_d, is of particular importance in determining the frequency region at which it occurs. Publications on the magnetoresistance effects in GaAs [41-44] showed that the application of a static transverse magnetic field alters the v_d-E characteristic. Considering two characteristics, v_d-E(B=0)

and v_d-E(B≠0), the same value of negative slope will occur for two different values of v_d's. As the discussions above indicate, the frequency at which maximum gain occurs would be different. If the values for the two v_d's are measured or calculated accurately, measured and calculated changes in the frequency at which maximum gain occurs allows one to evaluate the accuracy of the model used in the calculations. One difficulty is that the v_d-E characteristics for the devices used in the amplification experiments are not directly measurable. Rather, they are derived from measured voltage-current (V-I) characteristics. In Sec. 2.3, it is shown that the V-I characteristic is not simply related to the ideal v_d-E characteristic through a scalar constant. Interpretation of the measured current in terms of the average carrier drift velocity is then carried out. The results are used in evaluating the microwave measurements in Chp. 4. The topics studied are summarized below:

1. In Chp. 1, historical backgrounds are introduced and an outline for the thesis is presented.
2. In Chp. 2, static magnetoresistance effects are studied. A simple method is then derived to model these results. Finally, measurements are correlated to calculated values.
3. In Chp. 3, using the results of Chp. 2, amplification properties are studied with the magnetic field as a parameter. Towards this end, the

dispersion equation is derived, and solved; the small signal admittance is then calculated.

4. In Chp. 4, the large number of a-c experiments used to verify the model are discussed. The microstrip circuit model used in these measurements is first developed and evaluated. The small signal gain is then measured for various circuit configurations with the magnetic field and bias voltage as parameters.

5. In Chp. 5, concluding remarks about the successes and limitations of the theorectical and experimental works are presented. Possible future studies towards better results are suggested.

CHAPTER 2 THE STATIC v_d-E CHARACTERISTICS OF TRANSFERRED ELECTRON DEVICES

2.1 Introduction

The negative slope in the static drift velocity versus electric field (v_d-E) characteristic makes possible small signal amplification in transferred electron devices (TED's). However, the two terminal voltage-current (V-I) characteristic (the only directly measurable quantities) may be related to the v_d-E characteristic only when the electric field distribution is known (or assumed uniform) across the sample. The latter requirement may not be satisfied for non-ideal ohmic contacts to the cathode or with inhomogeneous doping [38-40]; this effect will be discussed in greater detail in Sec. 2.2. Previously reported d-c measurements of the static V-I characteristics on doped GaAs devices do not extend into the negative slope region. This is due to the occurrence of absolute instabilities as the negative slope region is reached. The various types of oscillations that may occur were discussed in Sec. 1.1. As a result of the instabilities, no correlations were obtained between the static V-I characteristic and the small signal negative conductance. In the present measurements, it is found that it is possible in some devices to measure the V-I characteristic well into the negative slope region. Most interestingly, it is found that even over

some regions of the negatively sloped static V-I characteristic, the measured small signal conductance is positive. The microwave results, and their relationships to the static measurements are discussed in Chp. 4. The interpretation of the measured negative differential conductance, in view of Shockley's positive conductance theorem [45], is discussed in App. 1. The theorem states that slope of the two terminal V-I characteristic of a device with negative differential mobility is always positive if the cathode is well behaved where a well behaved cathode implies positive differential mobility at the cathode.

The application of a transverse magnetic field alters the shape of the static v_d-E curve [41-44]. Therefore, the magnetic field influences a-c measurements. To understand the a-c behavior of the device under the influence of the magnetic field, it is necessary to first study the effects the magnetic field has on the static v_d-E characteristic. This is the topic of the following section.

2.2 Influence of a Static Transverse Magnetic Field on the Static v_d-E Characteristic

(A) Geometrical and Non-Geometrical Magnetoresistance

In the discussions to follow, the term magnetoresistance is used to denote the effect whereby the resistance of a device is altered due to the presence of an externally applied static magnetic field. The magnetic field in this case is transverse to the direction of current flow.

Distinction between the non-geometrical and geometrical type of magnetoresistance is made as follows:

1. The non-geometrical type of magnetoresistance denotes the effects on the device resistance when the Hall field on the average cancels out the $q\vec{v}_d \times \vec{B}$ force. The magnetic field acts on the drift velocity of the carriers indirectly through the reduction of high energy carriers (cooling). Since the abundunce of high energy carriers results from the existence of a high electric field, this cooling effect is only significant at electric fields above the threshold field for NDC in GaAs. Figure 2.?:1a shows the situation where only the non-geometrical type of magnetoresistance is present. Note that v_d is parallel to E.
2. Depending on device geometry, the Hall field may not be strong enough to cancel out the effect of the magnetic field on the average. In the limit, the Hall field may be considered non-existent [46]. In this case, the transverse magnetic field causes
    a. the carriers to drift at an angle to the electric field,
    b. the drift component parallel to the electric field to be reduced, and
    c. as a result of (b), the carrier energy

absorption to be reduced (geometrical type of cooling).

These effects, which again contribute to an alteration in the device resistance, are referred to as the geometrical type of magnetoresistance. Figure 2.2:1b indicates the situation where the geometrical as well as the non-geometrical type of magnetoresistance effects are present. In this case, v_d is not parallel to E.

To sum up the above discussions, the total magnetoresistance will always include the non-geometrical type while the geometrical type will be present only for appropriate device geometries. For appropriate geometries, the latter is significant in determining device behavior. The necessary conditions for this to occur is discussed in the following paragraphs.

For most commercially available X-band transferred electron devices (TED's), the linear transverse dimensions are large when compared to the length of the sample, with

$$\frac{L}{w} << 1 \qquad (2.2:1)$$

where L ≡ length of the sample,

and w ≡ linear transverse dimensions of the sample.

Under the condition specified by Eq. 2.2:1, Lippmann and Kuhrt [47] have shown that the Hall field is essentially shorted out by the contacts and therefore non-existent.

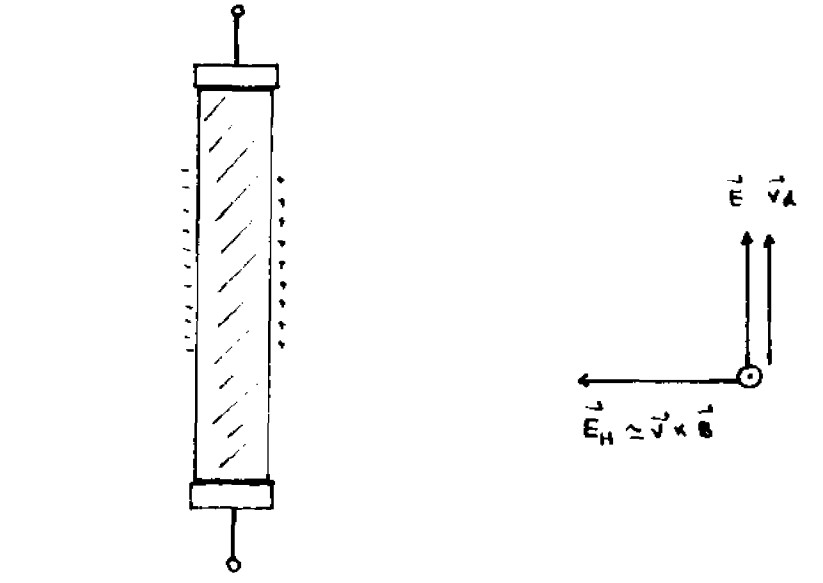

(a)

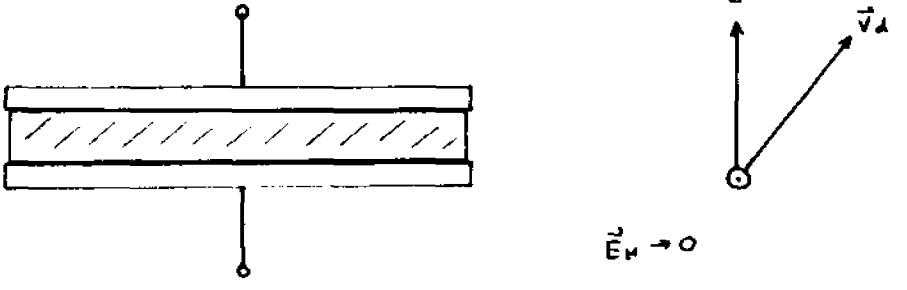

(b)

FIGURE 2.2:1 GEOMETRICAL EFFECTS IN MAGNETORESISTANCE CALCULATIONS

The effect of a finite L/w ratio, using a relationship formulated by these authors, is

$$\frac{\Delta R}{R_o} = \frac{\Delta R}{R_o}\bigg|_o \left(1.-.543 \frac{L}{w} \right) \qquad (2.2:2)$$

where $\frac{\Delta R}{R_o}\Big|_o$ is the magnetoresistance including the non-geometrical type. For finite L/w ratio, the latter is partially cancelled by the Hall field.

For the devices tested, $L \simeq 10\,\mu m$, $w \simeq 8$ mils, $L/w \simeq .05$ and $\frac{\Delta R}{R_o} \simeq \frac{\Delta R}{R_o}\Big|_o (.97) \simeq \frac{\Delta R}{R_o}\Big|_o$. Therefore, Hall field build-up is considered to be negligible and the geometrical type of magnetoresistance may be included in its entirety. In Sec. 2.2B, it is shown that the latter effect becomes dominant under certain situations. Since the geometrical type of magnetoresistance is of major interest, a general discussion on this subject is now presented.

As mentioned earlier in this section, when the Hall field is negligible, the transverse magnetic field causes the drifting carriers to have a component perpendicular to the electric field as shown in Fig. 2.2:2 with

$$\vec{E} = E_o \hat{a}z \qquad (2.2:3)$$

$$\vec{B} = -B_o \hat{a}y \qquad (2.2:4)$$

and $$\vec{v} = v_z \hat{a}z + v_x \hat{a}x \qquad (2.2:5)$$

where v represents the average carrier drift

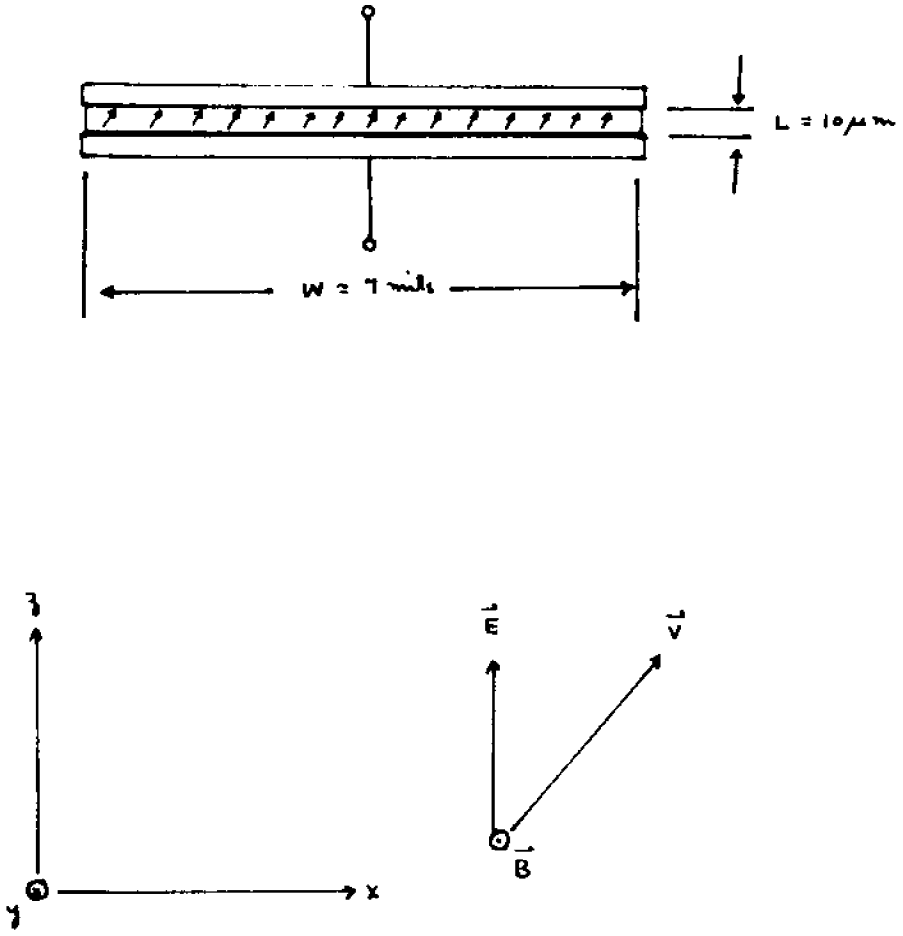

FIGURE 2.2.2 GEOMETRICAL CONFIGURATION FOR MAGNETORESISTANCE MEASUREMENTS

velocity defined earlier as v_d. The subscript'd' is dropped for convenience.

The momentum transfer equation [48] under static and spatially uniform conditions, where time and space derivatives are taken to be zero, reduces to

$$q\left(\vec{E}+\vec{v}\times\vec{B}\right)=\frac{m^*}{\tau_m}\vec{v} \qquad (2.2;6)$$

where τ_m = momentum relaxation time,

q = electron charge,

and m^* = effective mass of charge carrier.

Equations 2.2;3 - 2.2;6 may be put in matrix form as follows:

$$\begin{bmatrix}0\\0\\E_o\end{bmatrix}+\begin{bmatrix}\hat{a}_x & \hat{a}_y & \hat{a}_z\\ v_x & v_y & v_z\\ 0 & -B_o & 0\end{bmatrix}=\frac{1}{\mu}\begin{bmatrix}v_x\\v_y\\v_z\end{bmatrix} \qquad (2.2;7)$$

where $\mu = q\tau_m/m^*$ is the drift mobility of the carriers.

Solving for v from Eq. 2.2;7 gives

$$v_x=\frac{1}{1+(\mu B)^2}E_o \qquad (2.2;8)$$

$$v_z=\frac{\mu}{1+(\mu B)^2}E_o \qquad (2.2;9a)$$

or

$$v_z=\frac{v_z\big|_{B=0}}{1+(\mu B)^2} \qquad (2.2;9b)$$

where $v_z\big|_{B=0}=\mu E_o$ is the drift velocity of the carriers if the magnetic field were removed.

In Eq. 2.2:9, it is observed that the drift velocity parallel to the electric field, v_z, is reduced by a factor $1+(\mu B)^2$. In addition, v_x, a drift component perpendicular to the electric field, is also present. Since the device is open circuited at the sides, the return path for the carriers is through the ohmic contact region. If the mobility, μ, is assumed to be constant, v is completely determined with no further calculations necessary. Practically, however, it is well known [49,50] that μ is a function of carrier temperature. The carrier temperature, in turn, depends on the electric and magnetic fields. One method of simplifying the problem is to hold the electric field constant while the carrier temperature variation as a function of the magnetic field is calculated. This calculation is done in Sec. 2.2C. For the above discussions to apply to TED's, the mobility, μ, is interpreted as an effective mobility averaged over two carrier species. The details of this formulation are found in Secs. 2.2B and 2.2C.

(B) Magnetoresistance in GaAs

A clear demonstration of magnetoresistance in GaAs is through the changes in the v_d-E characteristic with zero and finite values of magnetic fields. The v_d-E characteristic may be calculated either by using a numerical method or with an assumed distribution function. Detailed Monte Carlo calculations for GaAs were made by Boardman, Fawcett

and Ruch [41]; similar results were obtained by Sasaki and Tanaka [42]. Calculations using displaced Maxwellian distribution functions were made by Heinle [43]; similar results were obtained by Levinshtein et. al. [44]. The results obtained by Heinle [43] and Levinshtein et. al. [44] indicated a smaller magnitude in the effect of the magnetic field at high bias electric fields where the non-geometrical type of cooling effect is significant. Results obtained by Heinle [43] and Boardman et. al. [41] are reproduced in Figs. 2.2:3 and 2.2:4 respectively. Both these figures show the total magnetoresistance effects. The difference in the results is, as mentioned earlier, due to the non-geometrical type of cooling effect at high bias electric fields. This is further demonstrated in Fig. 2.2:5 where the non-geometrical type of magnetoresistance effect obtained by Boardman et. al. [41] is shown. Heinle's results indicate much smaller changes in the carrier drift velocity at high bias electric field due to the magnetic field. The actual magnitudes of the changes still remain to be correlated to measurements.

Other than the alterations of the average carrier drift velocity at high bias electric fields, Fig. 2.2:5 indicates that the magnetic field does not significantly affect the v_d-E characteristic for electric field values up to the threshold electric field for NDC. A magnetic field of 20 kG, in this case, only shifts the NDC threshold slightly and has no effect on the low electric field

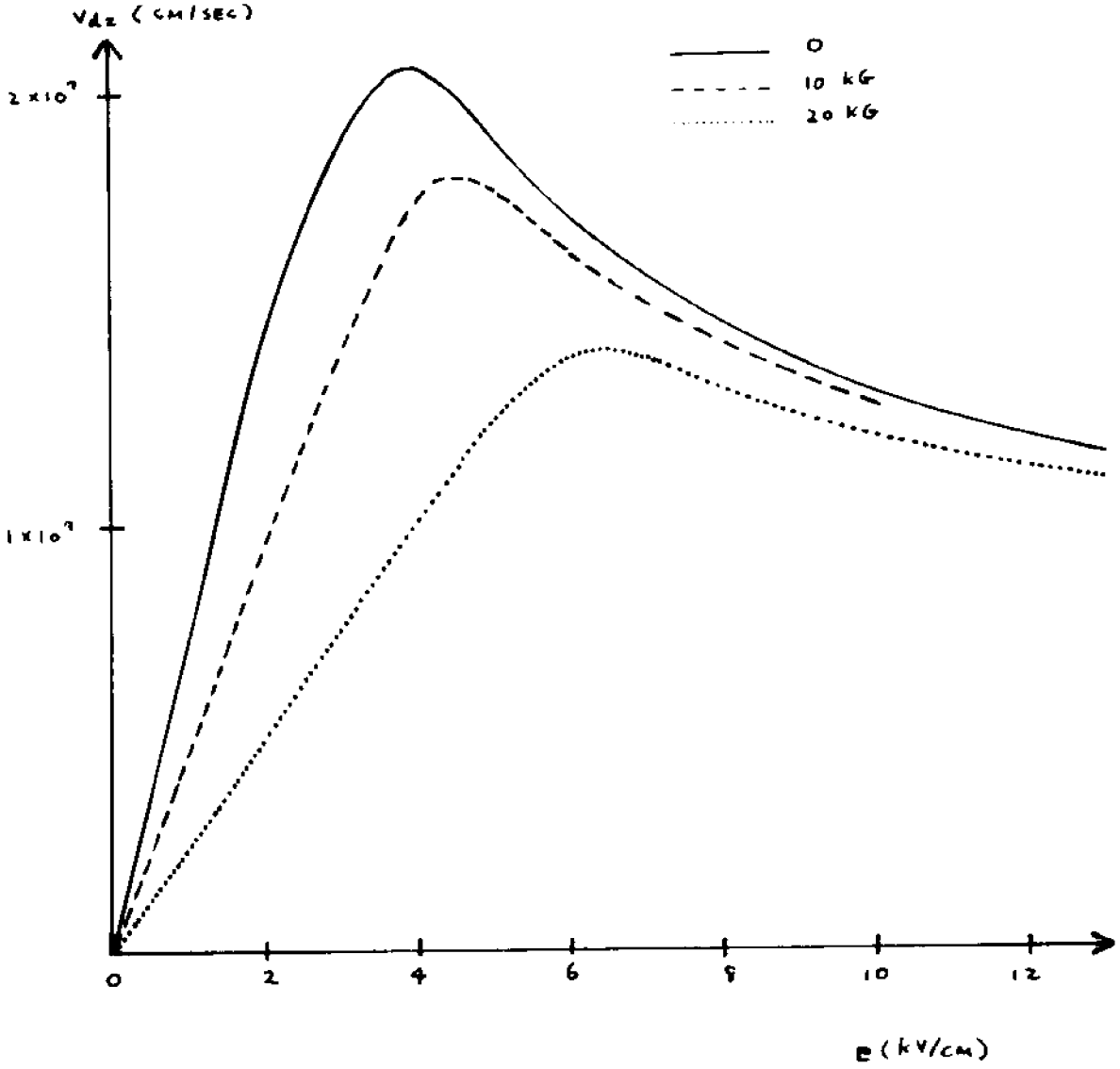

FIGURE 2.2:3 MAGNETORESISTANCE EFFECTS BY HEINLE [43]

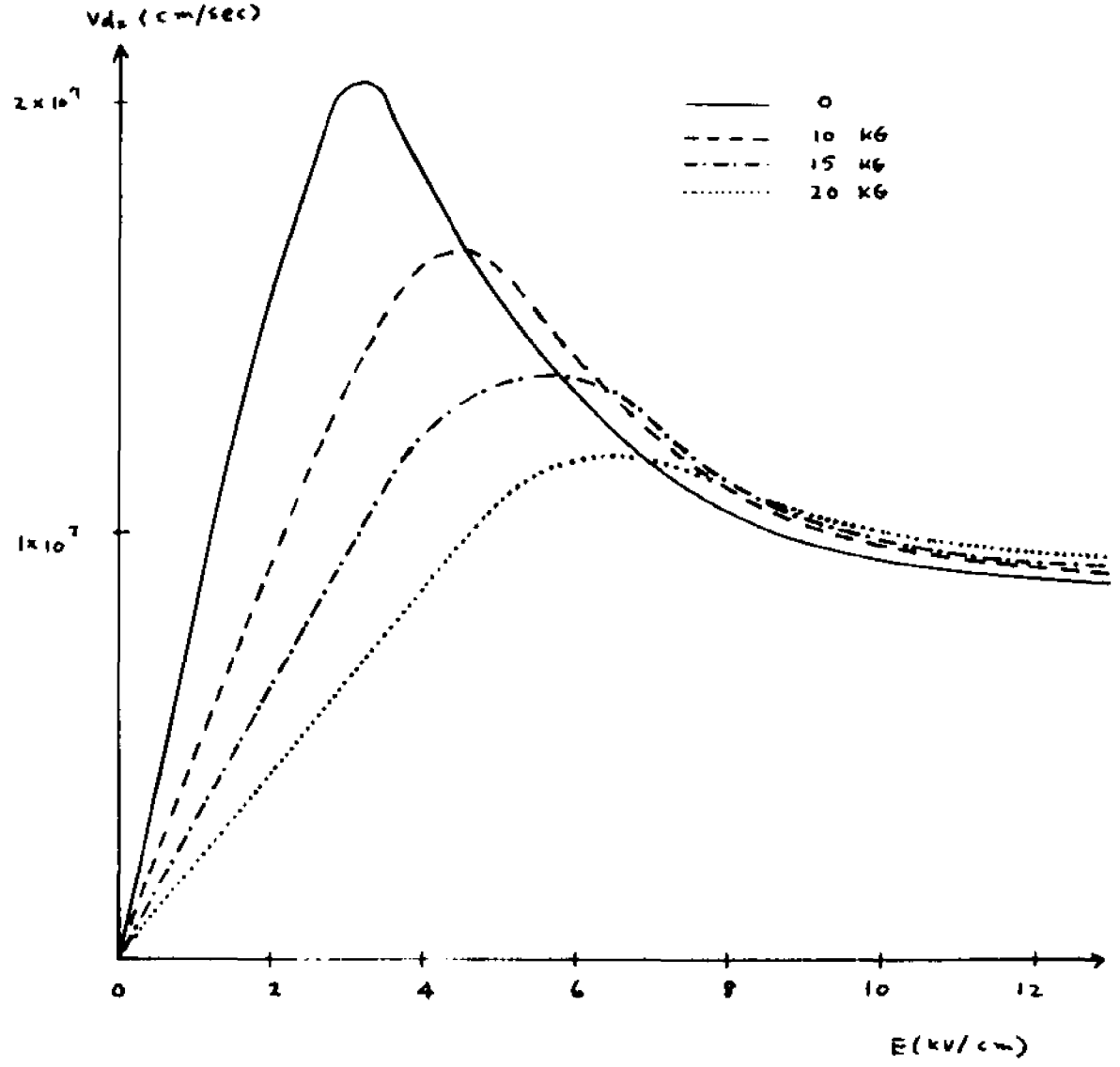

FIGURE 2.2.4 MAGNETORESISTANCE EFFECTS BY BOARDMAN ET. AL. [41]

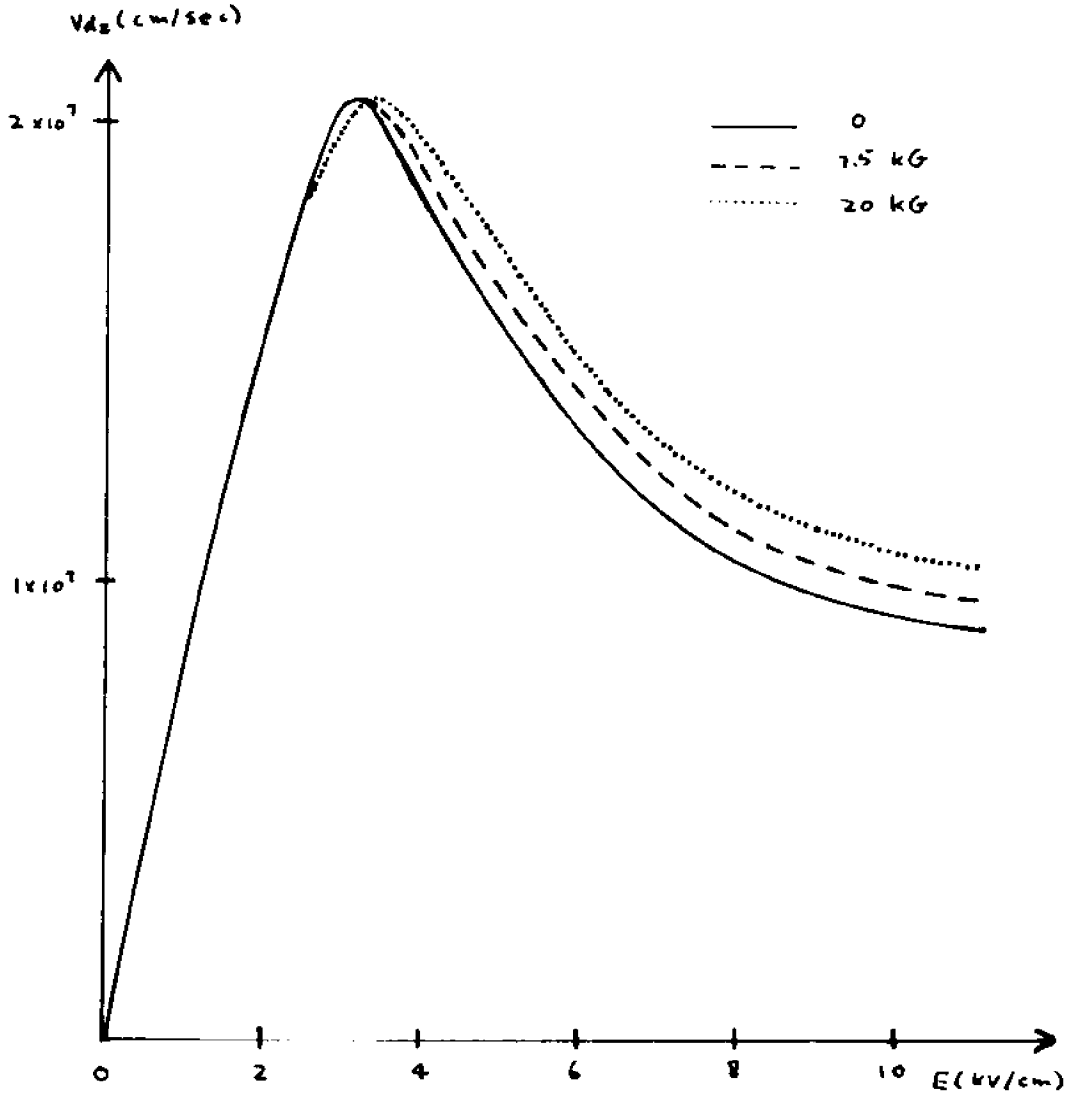

FIGURE 2.2:5 NON-GEOMETRICAL TYPE OF MAGNETORESISTANCE BY BOARDMAN ET. AL. [41]

resistance. Since Fig. 2.2:5 accounts for the non-geometrical type of magnetoresistance alone, all other effects, including significant changes in the low electric field resistance as well as significant shifts in the NDC threshold, are due entirely to geometrical effects.

In conclusion, existing theories indicate that for X-band TED's, the geometrical type of magnetoresistance dominates device behavior up to the threshold electric field for NDC. For small signal amplification experiments to be performed near the threshold, it is therefore necessary to consider only geometrical type of effects. On the other hand, if the drift velocity at high electric field is of interest, then it is necessary to consider the non-geometrical type of effects as well. In this case, the magnitude of the effect is not clear and experimental correlations are called for.

(C) Magnetoresistance in GaAs (A Simplified Method of Calculation)

As indicated in Sec. 2.2B, the geometrical type of magnetoresistance dominates device behavior for electric fields up to the threshold field for NDC. Since device behavior near the NDC threshold is of major interest for experiments to be described in Chp. 4, it is desirable to have a simple method of calculating the geometrical type of magnetoresistance effects. As shown in Eq. 2.2:9, the effective drift mobility, μ_B, in the presence of the

magnetic field is,

$$\mu_B = \frac{\mu}{1+(\mu B)^2} \quad . \qquad (2.2;10)$$

The mobility, μ, is a function of the magnetic field as the following explanations will show. For constant electric field, the carrier temperature is a function of the magnetic field only. Since μ is a function of the carrier temperature, μ is also a function of the magnetic field. In a GaAs device, μ can only represent an effective mobility averaged over two carrier species. The notation $\overline{\mu}$ is therefore used, with

$$\overline{\mu} = \frac{n_\ell}{n_o}\mu_\ell + \frac{n_u}{n_o}\mu_u \qquad (2.2;11)$$

where n_ℓ, n_u, μ_ℓ and μ_u are the lower and upper valley carrier number densities and drift mobilities respectively,

and $n_o \equiv (n_\ell + n_u)$ is the doping number density.

The dependence of $\overline{\mu}$ on carrier temperature arises from the dependences of (1) μ_ℓ and μ_u, and (2) n_ℓ and n_u on carrier temperature. The final objective in this formulation is to obtain the relationship between the magnetic field and the average mobility, $\overline{\mu}$, with the electric field as parameter. Towards this end, the relationship between the electric field and the average mobility, $\overline{\mu}$, is first formulated. It is then shown how the magnetic field modifies this relationship.

The average carrier drift velocity, v_d, for the two valley model is written in the form,

$$v_d = \frac{1}{n_o} (n_\ell v_\ell + n_u v_u)$$

$$= \frac{1}{n_o} (n_\ell \mu_\ell E + n_u \mu_u E)$$

$$= \left\{ \mu_\ell \frac{n_\ell}{n_o} + \mu_u (1 - \frac{n_\ell}{n_o}) \right\} E \qquad (2.2{:}12)$$

where v_ℓ and v_u are the lower and upper valley drift velocities respectively,

and the relationships $n_o = (n_\ell + n_u)$, $v_\ell = \mu_\ell E$ and $v_u = \mu_u E$ have been used.

Since is is desired to compare magnetoresistance effects calculated in this section and that obtained earlier by Boardman et. al. [41] discussed in Sec. 2.2B, it is necessary to formulate dependences of (n_ℓ/n_o), μ_ℓ and μ_u on the electric field such that the resulting v_d-E characteristic approximates that obtained by Boardman et. al. for the zero magnetic field case. The forms of the expressions used and the choices of the parameters involved for these quantities are discussed in App. 2. In Fig. 2.2:6, the resulting plot of v_d-E using expressions

$$\frac{n_\ell}{n_o} = \frac{1 + .27(E/4.8)^3}{1 + (E/4.8)^3} \qquad (2.2{:}13a)$$

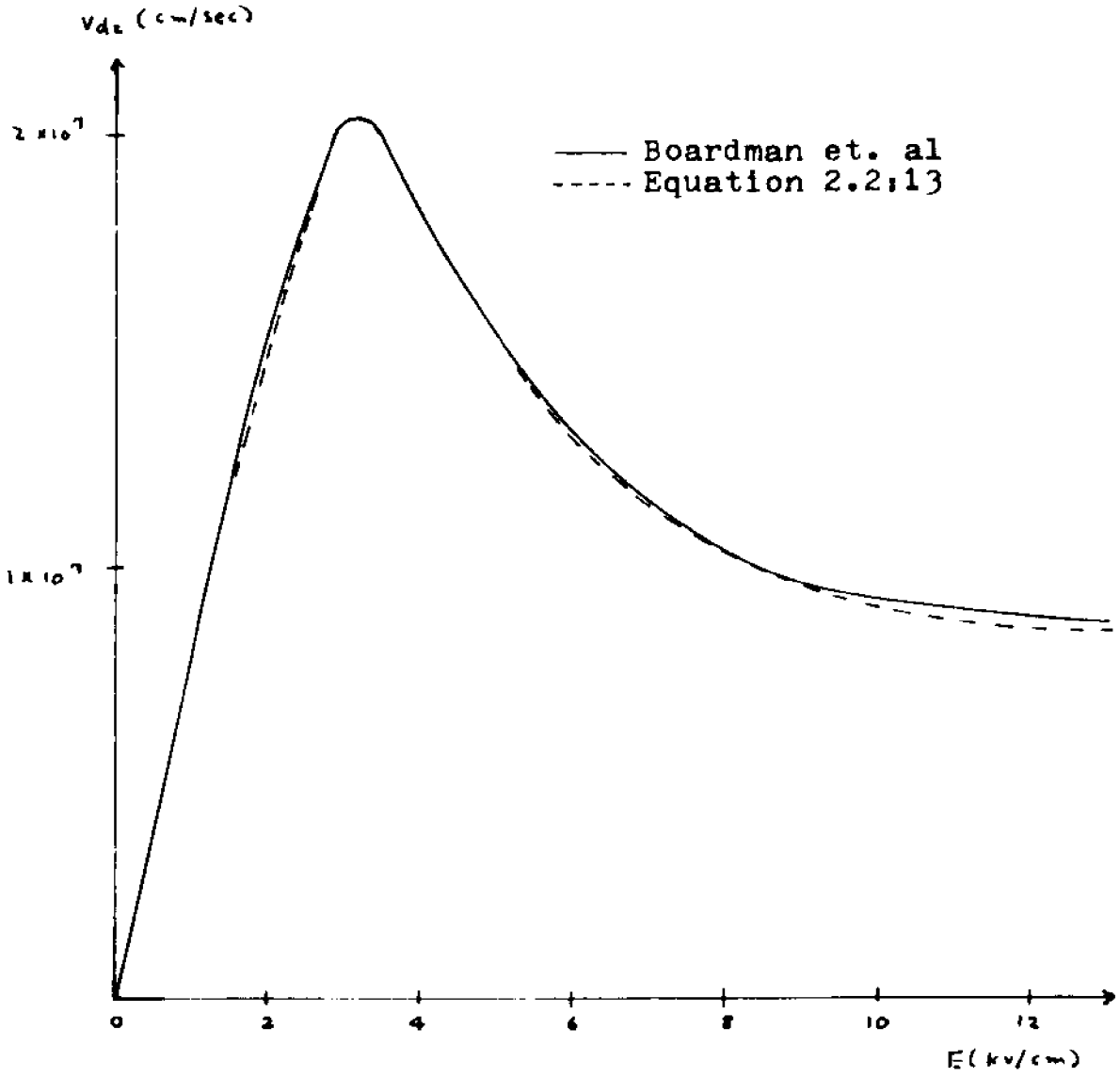

FIGURE 2.2:6 ZERO MAGNETIC FIELD v_d-E CHARACTERISTIC

$$\mu_L = \begin{cases} 8000 \text{ cm}^2/\text{V-sec} & \text{for } E \leq (2.5/.8) \text{ kV/cm} \\ 2.5/E \text{ cm}^2/\text{V-sec} & \text{for } E > (2.5/.8) \text{ kV/cm} \end{cases} \quad (2.2;13b)$$

$$\mu_u = 120 \text{ cm}^2/\text{V-sec} \quad (2.2;13c)$$

are shown. The v_d-E characteristic obtained by Boardman et. al. is superimposed for comparism. As Fig. 2.2;6 indicates, good graphical agreement is obtained.

Equations 2.2;12 and 2.2;13 gives the desired relationship between the electric field and the average mobility, $\overline{\mu}$. The relationship between the electric field and the carrier temperature is then obtained from the steady state energy transport equation [48] where spatial uniformity is also assumed,

$$\frac{3}{2} \frac{k_B (T-T_o)}{\tau_e} = \frac{1}{2} E v_z \quad (2.2;14)$$

where k_B ≡ Boltzmann's constant ,

T ≡ carrier temperature ,

T_o ≡ lattice temperature ,

and τ_e ≡ carrier energy relaxation time.

Using Eq. 2.2;9,

$$v_z = \frac{\mu}{1+(\mu B)^2} E \quad , \quad (2.2;9)$$

the energy transport equation, Eq. 2.2;14, for finite magnetic field becomes

$$\frac{3}{2} \frac{k_B (T-T_o)}{\tau_e} = \frac{1}{2} \frac{\mu}{1+(\mu B)^2} E^2$$

$$= \frac{1}{2}\mu \left\{ \frac{E}{\sqrt{1+(\mu B)^2}} \right\}^2$$

$$= \frac{1}{2}\mu E_{eff}^2 \qquad (2.2{:}15)$$

where $E_{eff} \equiv \dfrac{E}{\sqrt{1+(\mu B)^2}}$.

This may be interpreted as a reduction in the effective electric field for the purpose of calculating the carrier temperature when a transverse magnetic field is applied. Since E_{eff} is used in calculating the carrier temperature and the carrier temperature determines the values for μ_ℓ, μ_u and (n_ℓ/n_o), E_{eff} must also be used in calculating μ_ℓ, μ_u and (n_ℓ/n_o) in Eq. 2.2:13 instead of E. Therefore, in the presence of the magnetic field, Eq. 2.2:13 is modified to the form

$$\frac{n_\ell}{n_o} = \frac{1 + .27(E_{eff}/4.8)^3}{1 + (E_{eff}/4.8)^3} \qquad (2.2{:}16a)$$

$$\mu_\ell \begin{cases} \dfrac{n_o}{1 + (E_{eff}/4.8)^3} \text{ cm}^2/\text{V-sec} & \text{for } E_{eff} \le (2.5/.8) \text{ kV/cm} \\ 8000 \text{ cm}^2/\text{V-sec} & \text{for } E_{eff} > (2.5/.8) \text{ kV/cm} \\ 2.5/E_{eff} \text{ cm}^2/\text{V-sec} & \text{for} \end{cases} \qquad (2.2{:}16b)$$

$$\mu_{\ell B} = \frac{\mu_\ell}{1+(\mu_\ell B)^2} \qquad (2.2{:}16c)$$

$$\mu_u = 120 \text{ cm}^2/\text{V-sec} \qquad (2.2{:}16d)$$

$$\mu_{uB} = \frac{\mu_u}{1+(\mu_u B)^2} \qquad (2.2{:}16e)$$

where $E_{eff} \equiv \dfrac{E}{\sqrt{1+(\mu_{\ell o} B)^2}}$

and $\mu_{\ell o}$ represents the zero magnetic field lower valley drift mobility as defined in Eq. 2.2:13b.

Strictly speaking, the value μ_ℓ as defined in Eq. 2.2:16b should be used in the definition for E_{eff}. However, the use of $\mu_{\ell o}$ simplifies the calculations and causes negligible change in the results. The value $\mu_{\ell o}$ is therefore used in all calculations.

Equation 2.2:16, together with Eq. 2.2:12 with μ_ℓ and μ_u replaced by $\mu_{\ell B}$ and μ_{uB} to account for the presence of the magnetic field, where

$$v_d = \left\{ \mu_{\ell B} \frac{n_\ell}{n_o} + \mu_{uB} \left(1 - \frac{n_\ell}{n_o} \right) \right\} E \qquad (2.2:17)$$

allows one to calculate the v_d-E characteristic both with and without the magnetic field. However, this only accounts for the geometrical type of magnetoresistance. The results obtained by Boardman et. al. (Fig. 2.2:4), on the other hand, accounts for both geometrical as well as non-geometrical type of effects. To facilitate comparison of results, two approaches are possible. They are:

1. to eliminate the non-geometrical effect in Boardman's results, or
2. to introduce the non-geometrical effect in the present calculations.

Since Boardman's results are presented graphically,

the first approach is difficult to implement. Therefore, the second approach is chosen in which the non-geometrical effect is phenomenologically added to the present calculations. The objective is to model Boardman's graphical results analytically. By heuristically writting

$$\mu_\ell' = \mu_\ell + f(B) \qquad (2.2{:}18)$$

where $f(B) \equiv \frac{B}{4E}\left\{1 - \exp(2-2E/3.1)\right\}$

for $E > (2.5/.8)$ kV/cm,

and $f(B) \equiv 0$

for $E \leq (2.5/.8)$ kV/cm,

it is found that the desired results are obtained as comparison between Figs. 2.2:5 and 2.2:7 plotted on the same scale indicates. The choice for the form of f(B) is quite arbitrary and no special meaning is attributed to the exponential function. Replacing μ_ℓ by μ_ℓ' in Eqs. 2.2:16, 2.2:17 and 2.2:13, and calculating the v_d-E characteristic with the magnetic field as parameter demonstrates the total magnetoresistance effect. The results are plotted in Fig. 2.2:8. Comaprison of Fig. 2.2:8 and Fig. 2.2:4 shows that the results agree well quantitatively in the shift of the threshold electric field for NDC and the drift velocity reduction at low electric field values. As for the drift velocity at high electric field values, qualitative agreements are obtained. The accuracy in this case is limited by the extent to which the non-geometrical type of cooling effect has been modeled

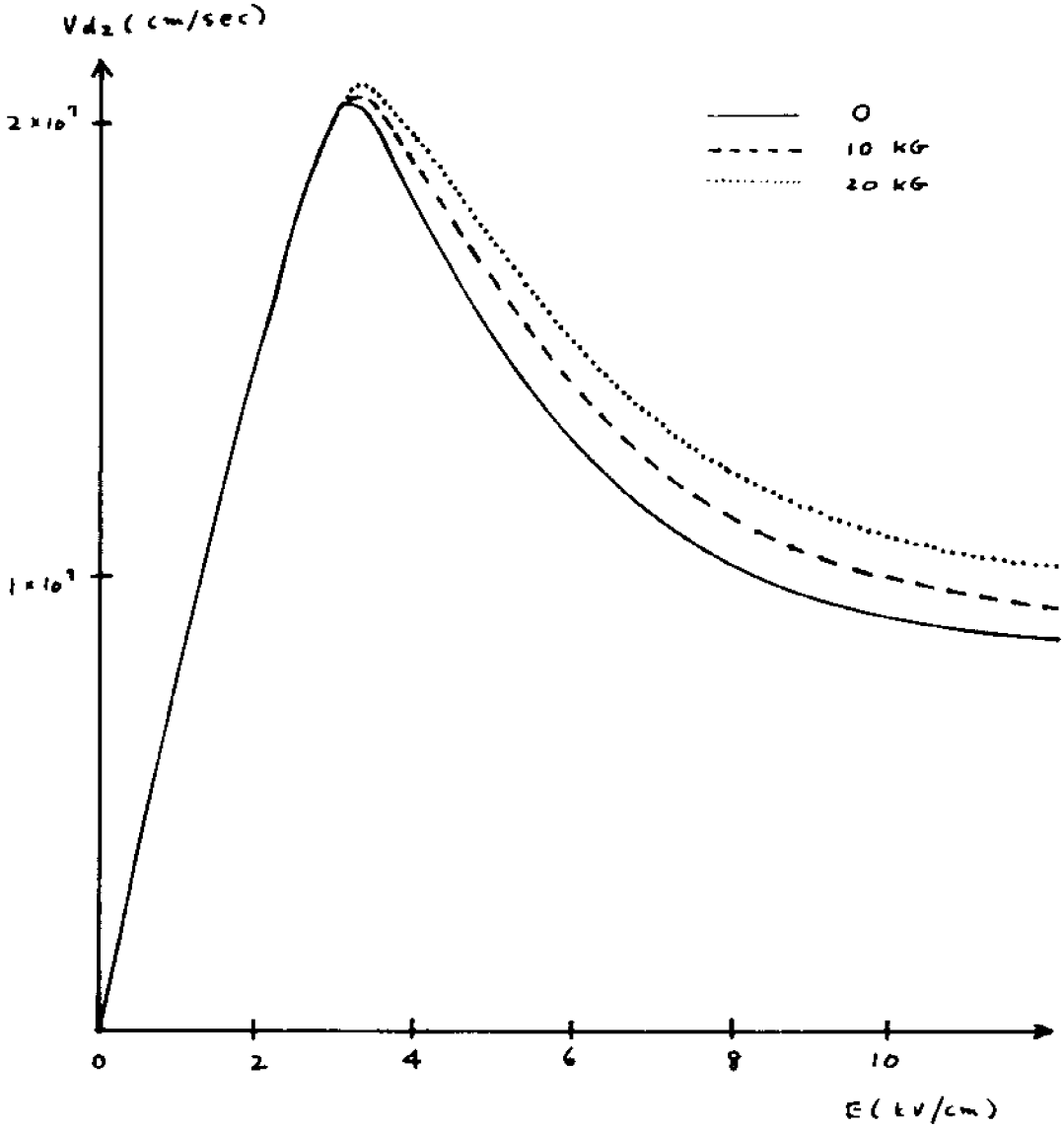

FIGURE 2.2.7 APPROXIMATION FOR NON-GEOMETRICAL TYPE OF MAGNETORESISTANCE

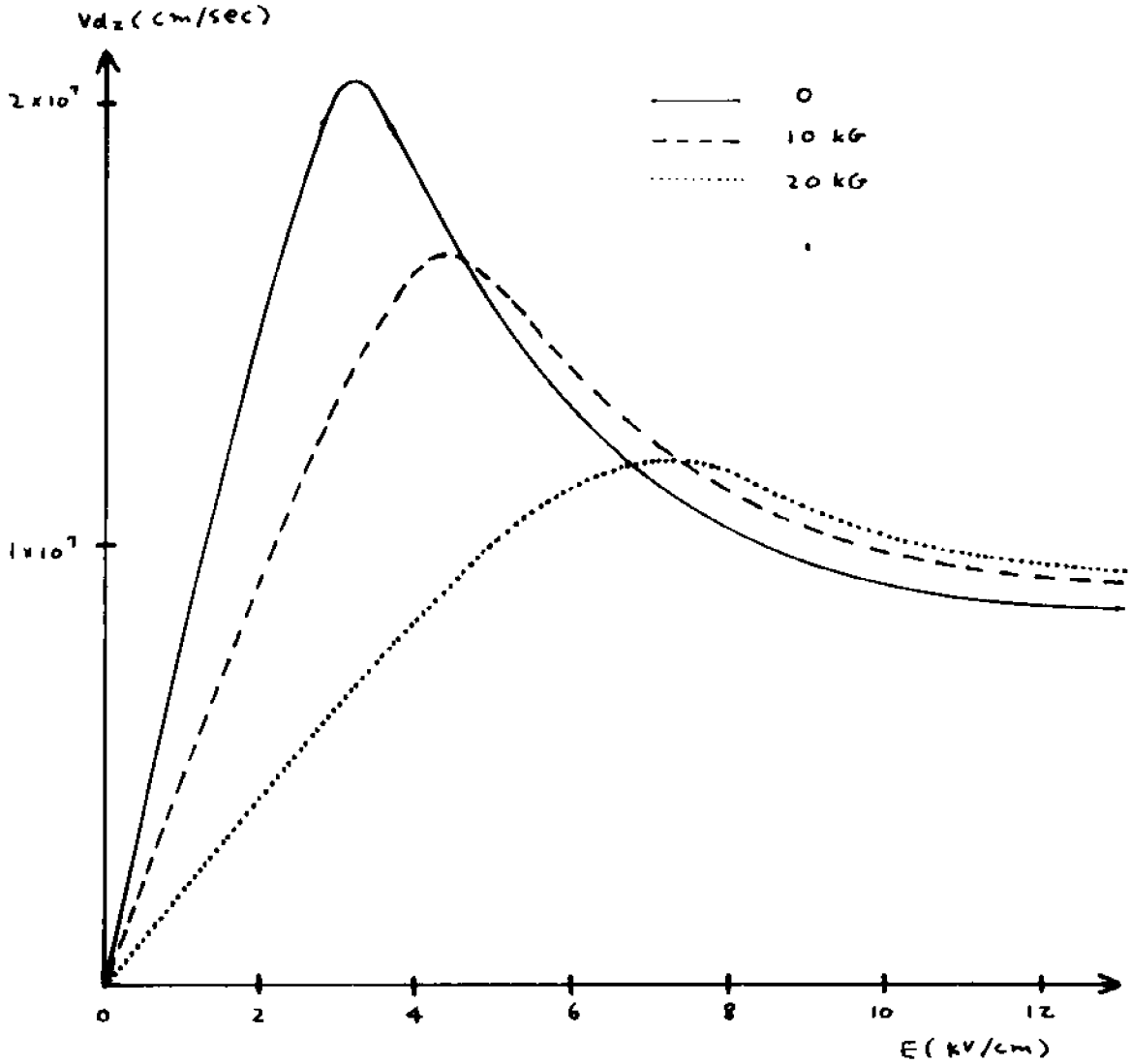

FIGURE 2.2.8 CALCULATED MAGNETORESISTANCE BY ANALYTICAL METHOD

(Eq. 2.2:18). No further attempt is made in this case to obtain better agreements since measurements (Sec. 2.3) indicate that the non-geometrical type of cooling effect is never strong enough to cause an increase in the drift velocity at high electric field.

In conclusion, by properly accounting for the dependences of the mobilities μ_ℓ, μ_u and the carrier densities n_ℓ, n_u on the magnetic field with the electric field held constant, it is possible to use a simple analytical procedure to calculate the magnetoresistance effect accurately. The validity of the method was verified by comparing the calculated results with that obtained independently by other authors.

2.3 Experimental Results on Static Magnetoresistance Measurements

The devices tested included X-band (Microwave Associate MA49157, MA 49158) and C-band (RCA) packaged Gunn diodes. Their small L/w ratios, as explained in Sec. 2.2A, allows one to calculate the geometrical type of magnetoresistance in terms of a zero Hall field. The non-geometrical type of magnetoresistance may be neglected with negligible error for calculations up to the NDC threshold as explained in Secs. 2.2B and 2.2C. It was found that the measured static zero magnetic field V-I characteristic deviates considerably from that calculated by Butcher and Fawcett [12] and that measured on semi-insulating

substrates by Ruch and Kino [11]. The difference is shown in Fig. 2.3:1. Kroemer [38], and Grubin et. al. [39] explained this effect in terms of a non-uniform electric field distribution within the sample caused by non-ohmic cathode contacts. Formulation of the non-uniform field problem requires knowledge of the cathode contact behavior. In view of the lack of exact information concerning the cathode cantact, assumptions were made by the above authors concerning the cathode. Kroemer [38] considered the cases of

1. a shallow potential barrier , and
2. a thin layer of oppositely doped semiconductor at the cathode. Grubin et. al. [39] modeled the cathode in terms of a constant cathode electric field independent of biasing. When the cathode field in Grubin's model is chosen to be well above the NDC threshold, results similar to that of Kroemer's were obtained. The major conclusion for long samples ($L \simeq 100\ \mu m$) showed that as the bias voltage is increased, a high electric field region appears near the cathode. The electric field drops off rapidly as one moves away from this region and saturates at a constant value inside the bulk. This electric field value inside the bulk is below that of the NDC threshold even when the average electric field is well above the threshold field. The situation is demonstrated graphically in Fig. 2.3:2. In the figure, the exact values for L' and E_c depends on the assumed

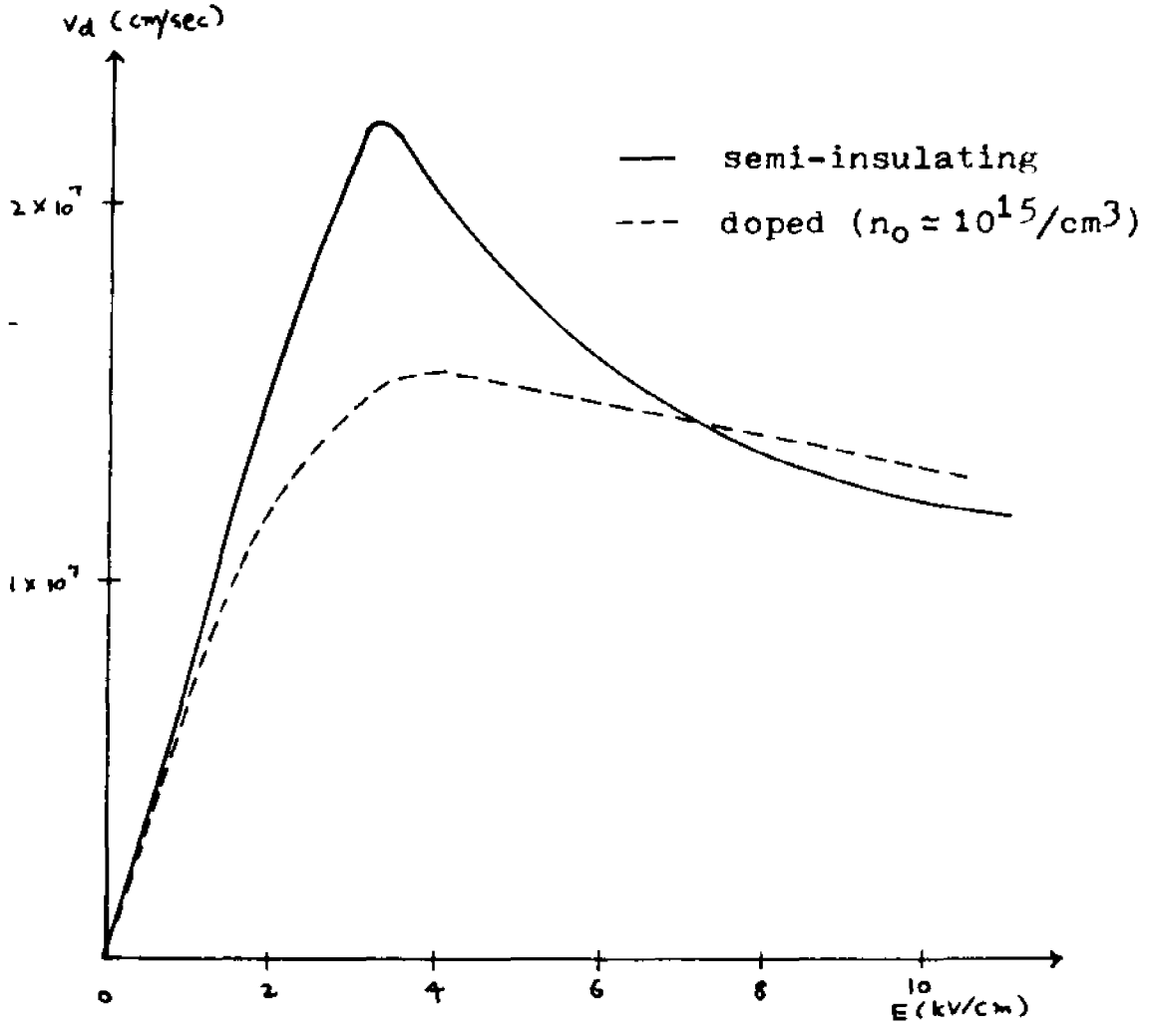

FIGURE 2.3:1 v_d-E CHARACTERISTICS FOR SEMI-INSULATING [11] AND DOPED SAMPLES

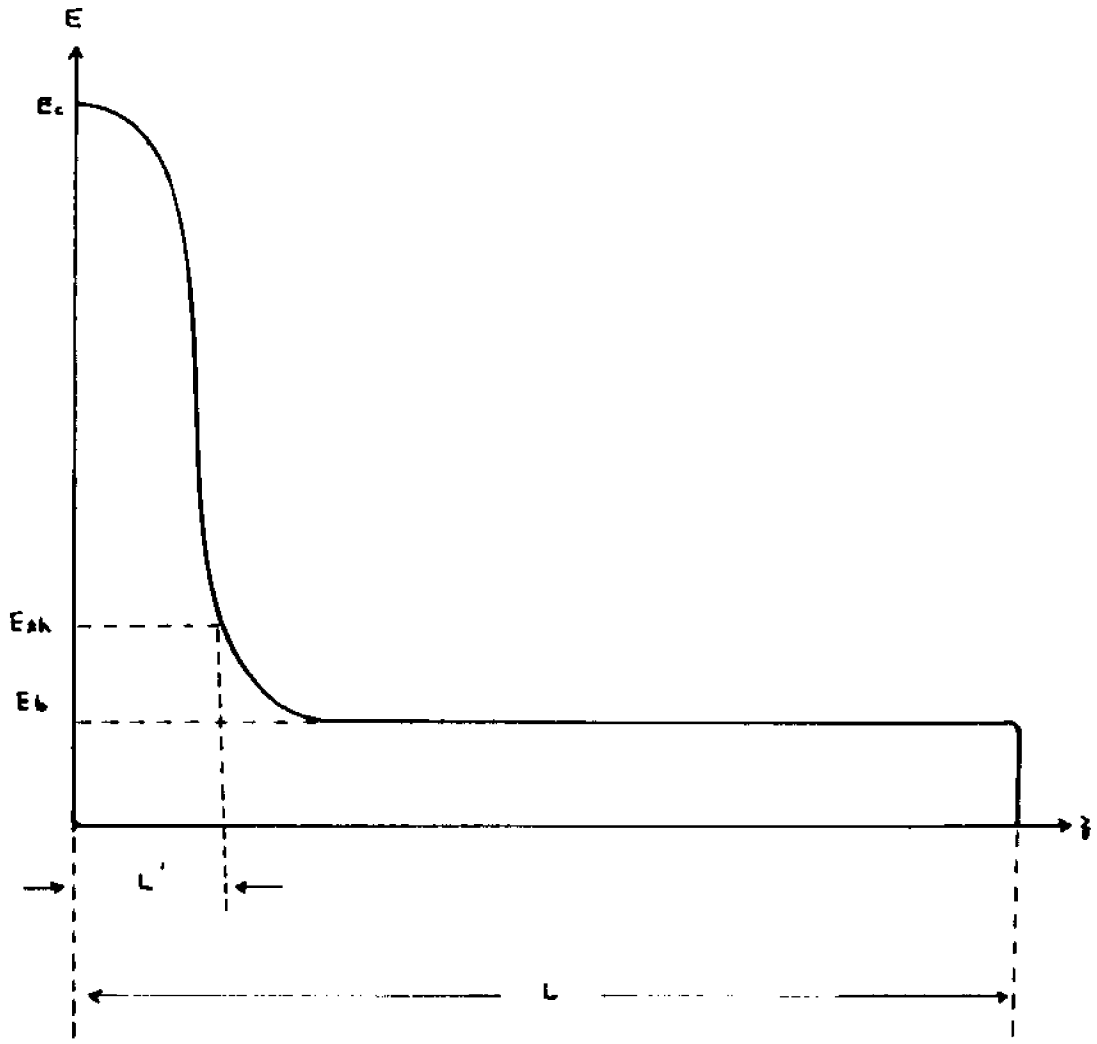

FIGURE 2.3.2 NON-UNIFORM ELECTRIC FIELD DISTRIBUTION

model for the cathode. The value L' has a strong effect on the small signal amplification properties of the device. In a recent publication, Grubin and Kaul [51] showed that L' is the effective length which determines the frequency region at which gain occurs instead of the physical length L. Experimental results (Sec. 4.2) on a-c measurements indicate that L' is close to L for the X-band Gunn diodes tested ($L \simeq 10\ \mu m$). This would preclude the possibilities of tremendous distortions in electric field distribution across the sample. In view of this and the fact that the behavior of the cathode is not known, the non-uniform field problem will not be considered in this work. Furthermore, the uniform field treatment explains well the d-c (Sec. 2.4) and a-c (Sec. 4.3) behavior of the device under the influence of a transverse magnetic field.

In the uniform field model, the deviation of the V-I characteristic from linearity is modeled as a carrier temperature dependent drift mobility. As pointed out in Sec. 2.2A, if the mobility, μ, is a function of carrier temperature, the drift velocity reduction, in the presence of a magnetic field as given by Eq. 2.2:9, with

$$v_z = \frac{v_z\big|_{B=0}}{1+(\mu B)^2} \qquad (2.2{:}9b)$$

becomes a more complicated function since μ now depends on B. The theorectical treatment of this is carried out later on in Sec. 2.4.

Static V-I characteristics with the magnetic field, B, as a parameter are measured for several Gunn diodes. Static voltage and current values are monitored by the measurement system shown in Fig. 2.3:3. The manufacturer's supplied data for the diodes tested are listed in Table 2:1.

Table 2:1 Gunn Diode Parameters

Diode	V_{th}-Volts	I_{th}-mA	
1	3.47	550	$L \simeq 10$ μm
2	3.39	644	d(diameter) ≃ 7 mils
3	3.38	616	$n_o \simeq 1.05 \times 10^{15}/cm^3$
4	3.49	592	
5	3.39	598	

With applied magnetic field, all these devices exhibit similar behavior; increase in low electric field resistance and shift of the NDC threshold to a higher bias voltage. Fig. 2.3:4 shows detailed measurements for diode #1. This is representative of all five diodes listed except for diode #2 which merits special discussion. Whereas other devices become unstable (in the form of oscillations as detected by the network analyzer) soon after the NDC threshold voltage is reached, diode #2 remains stable for a bias voltage up to twice that of the NDC threshold voltage as shown in Fig. 2.3:5. For a 10 μm device, 1 volt corresponds to an average electric field of 1 kV/cm. The theorectical threshold electric field was calculated by Butcher and Fawcett [12] to be

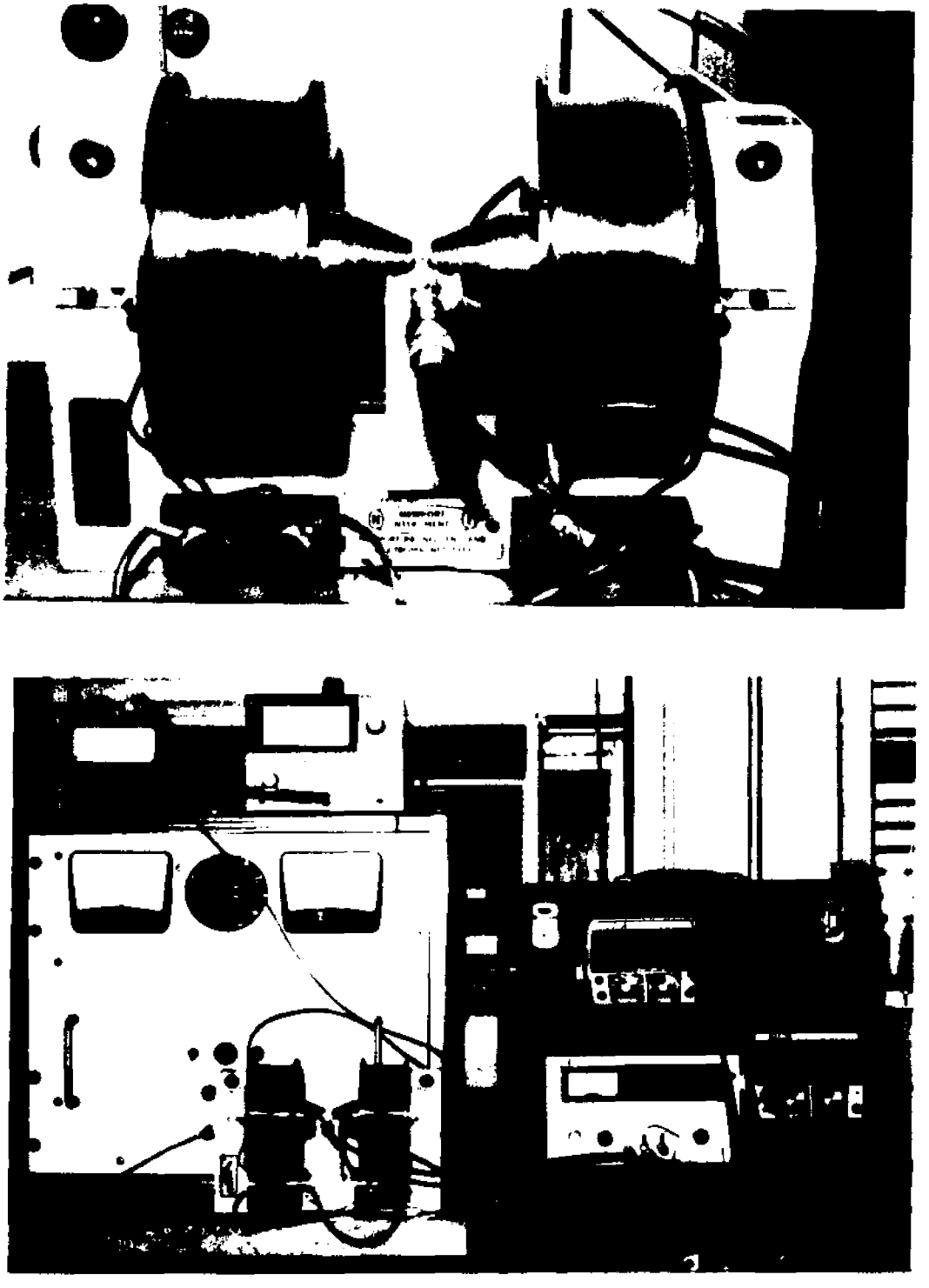

FIGURE 2.3.3 STATIC MEASUREMENT SYSTEM

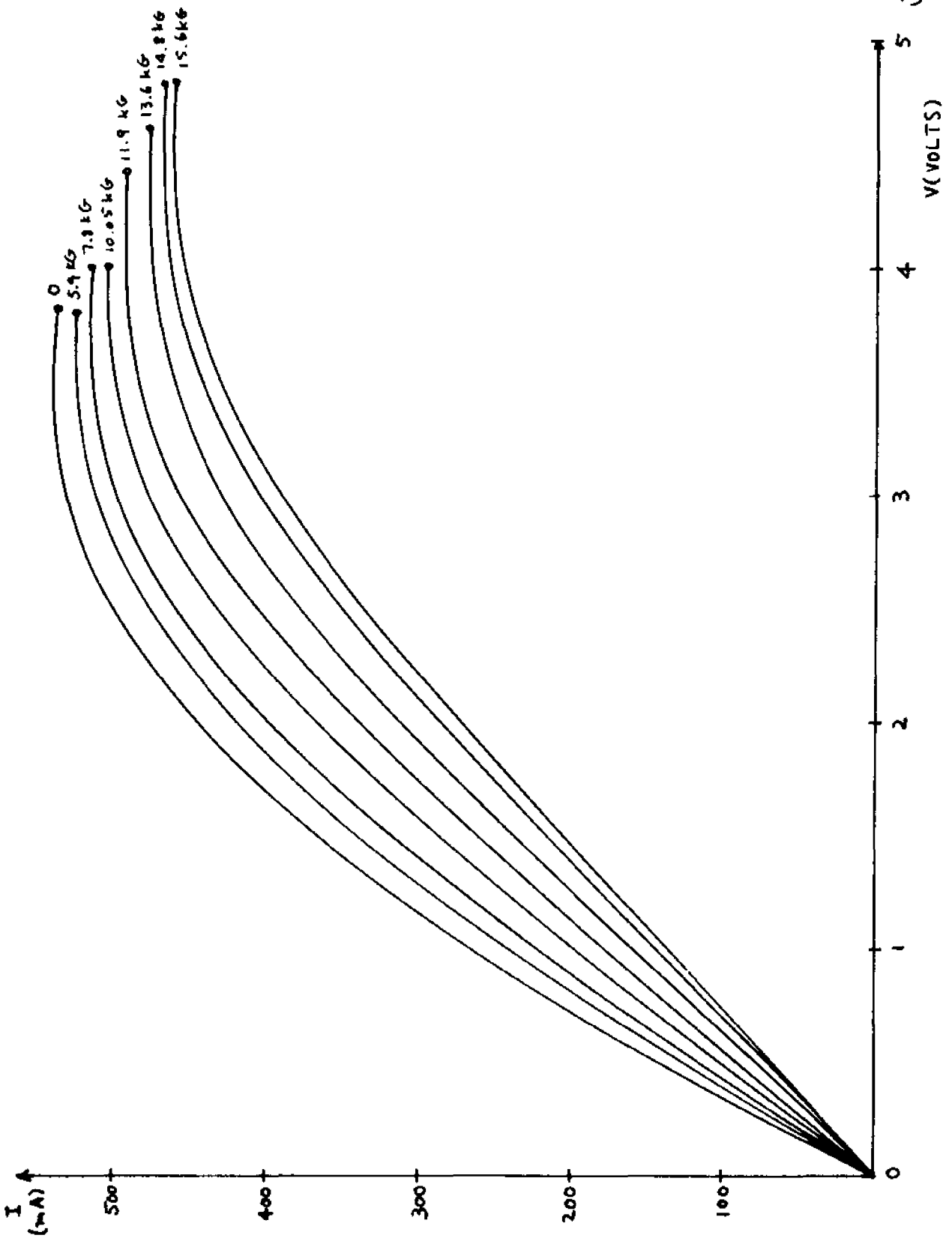

FIGURE 2.3.4 MEASURED V-I CHARACTERISTICS FOR DIODE #1 IN TABLE 2.1 WITH B AS PARAMETER

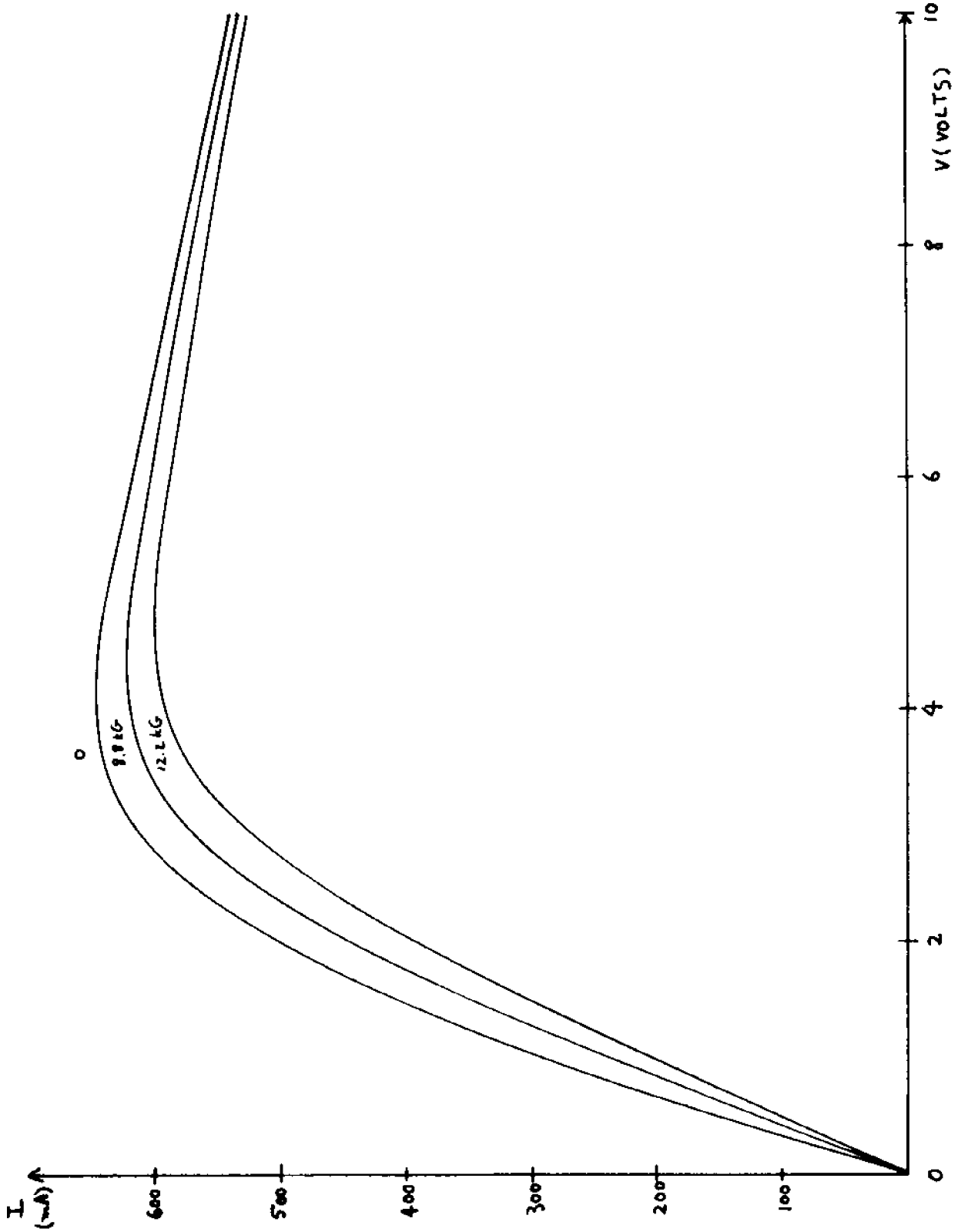

FIGURE 2.3:5 MEASURED V-I CHARACTERISTICS FOR DIODE #2 IN TABLE 2.1 WITH B AS PARAMETER

approximately 3.3 kV/cm, corresponding to a bias voltage of $V_b \sim 3.3$ volts for uniform electric field. The experimental value for V_b is found to be approximately 3.5 volts in Fig. 2.3:4. Qualitatively, the effects of the transverse magnetic field are:

1. The device resistance is increased due to mobility reduction.
2. The NDC threshold voltage is increased due to the cooling effect which reduces intervalley transfer for a given electric field value.
3. As a result of the cooling effect, the V-I characteristic becomes linear up to a higher bias voltage.
4. The cooling effect is never strong enough to cause an increase in the high electric field drift velocity.

Effects (1-3) were predicted by calculations in Sec. 2.2. Effect (4) implies that the non-geometrical type of cooling effect is not as strong as that calculated by Boardman et.al. [41]. Therefore, in view of the measured results, neglecting the non-geometrical type of magnetoresistance in all calculations is justified.

Figure 2.3:4 indicates that the V-I characteristic is linear for small bias voltages. Therefore, the mobility is independent of carrier temperature in this region. Experimentally, no deviation from linearity is detectable for measuring currents below 10 mA which is ~2% of I_{th}.

This fact is often used to measure the zero electric field mobilities of devices [46]. If the electric field within the sample is uniform, the drift velocity is related to the current through a scalar constant,

$$I = qn_oAv_d \qquad (2.3:1)$$

where $A \equiv$ cross-sectional area of sample.

Equation 2.3:1 together with Eq. 2.2:9b yields,

$$\frac{v_{zo}}{v_z} = 1+(\mu_oB)^2$$

$$= \frac{I_o}{I} \qquad (2.3:2)$$

where v_{zo} and I_o correspond to zero magnetic field quantities,

and μ_o is a constant independent of the magnetic field.

Solving Eq. 2.3:2 for μ_o results in

$$\mu_o = \frac{1}{B}\sqrt{\frac{I_o}{I} - 1} \qquad (2.3:3)$$

By accurately measuring B, I_o, and I, μ_o may then be calculated. The value for μ_o determined by this method for diode #1 is μ_o=7300 cm^2/V-sec where the measured values B=7.8 kG, I_o=10.0 mA and I=7.55 mA have been used. Other sets of data were used to check for the accuracy of μ_o. Variations of less than 5% were obtained. Measurements on other diodes listed in Table 2:1 revealed variations in μ_o of less than 10% from diode to diode. In these measurements, it was noted that the top cap of the Gunn

diodes were made of magnetic material which alters the magnetic field at the sample. A correction factor of $\sim 7\%$ was obtained when measurements were made on diode #4 with and without the top cap. Pictures of the diode with and without the top cap are shown in Fig.2.3:6. The correction factor was taken into account in calculating μ_o above.

The value for μ_o may also be calculated independently from

$$\mu_o = \frac{1}{R_o} \frac{L}{qn_oA} \qquad (2.3:4)$$

where R_o = low electric field resistance (measured),

L, A = length and cross-sectional area (manufacturer supplied),

and n_o = doping concentration (manufacturer supplied) of the sample.

For diode #1, $(1/R_o) \simeq .3125\,\mho$, $L=10\,\mu m$, $A=\pi(7/2)^2$ mil^2 and $n_o=1.05\times 10^{15}/cm^3$. The value for μ_o calculated from Eq. 2.3:4 using the above data is $\mu_o=7500$ cm^2/V-sec. This compares well with the value for μ_o obtained through magnetoresistance measurements using Eq. 2.3:3.

To facilitate comparison of results to be made in the next section, the quantity $G=(I/V)$ is calculated for each point on the V-I characteristic shown in Fig. 2.3:4. These values of G's are plotted as a function of the bias voltage in Fig. 2.3:7. These same plots, to within a scalar constant, represent the average mobility

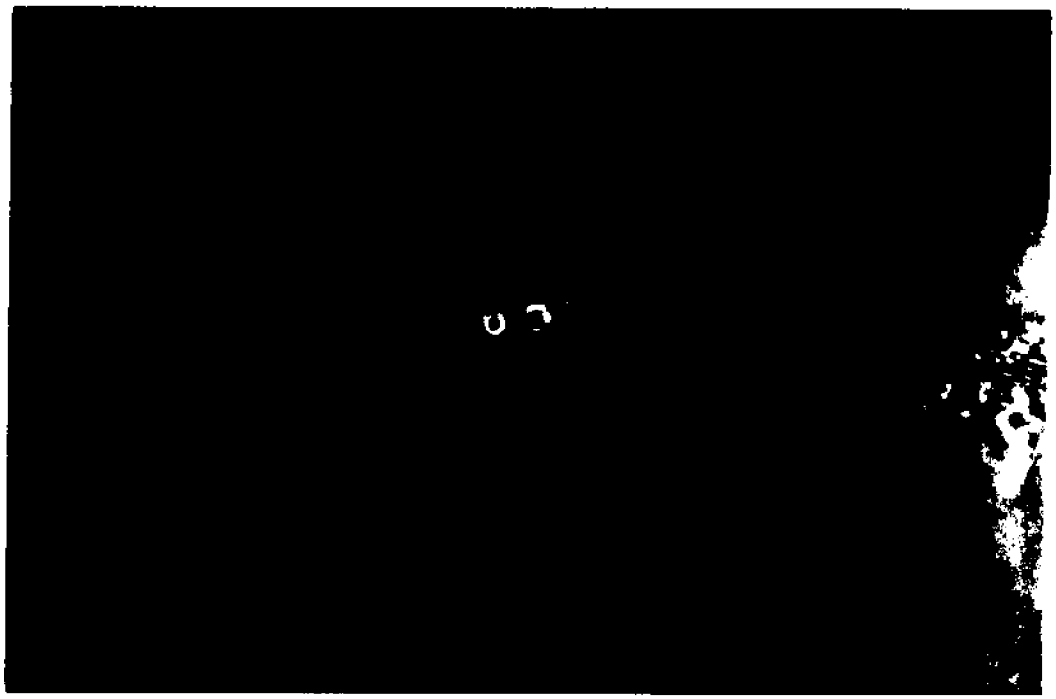

FIGURE 2.3:6 DIODE WITH AND WITHOUT TOP CAP

as a function of bias voltage since

$$\bar{\mu} = \frac{L}{qn_oA} G \qquad (2.3:5)$$

As Fig. 2.3:7 shows, the average mobility, $\bar{\mu}$, has a linear dependence on the bias voltage for zero magnetic field. With increasing magnetic field, $\bar{\mu}$ becomes less dependent on the bias voltage. It is also observed that the magnetic field has a much larger effect on the high mobility (low bias) region than the low mobility region. It should be noted that whereas the differential mobility is negative for all bias voltages, the device becomes unstable or amplifying only when a negative slope occurs in the V-I characteristic, $(dI/dV) < 0$.

2.4 Correlation of Magnetoresistance Measurements to Calculations

Having discussed in detail the measured results, it is now necessary to develop a theoretical model which will account for these effects. Qualitative discussions on this has been presented in the previous paragraphs using theoretical results from Sec. 2.2. The obstacle to a quantitative comparison was due to two different zero magnetic field characteristics; one obtained by measurement, the other used in calculations in Sec. 2.2. Therefore, it is necessary to start with a new expression for $\bar{\mu}$ as a function of bias voltage,

$$\bar{\mu} = f\{E(T)\} \qquad (2.4:1)$$

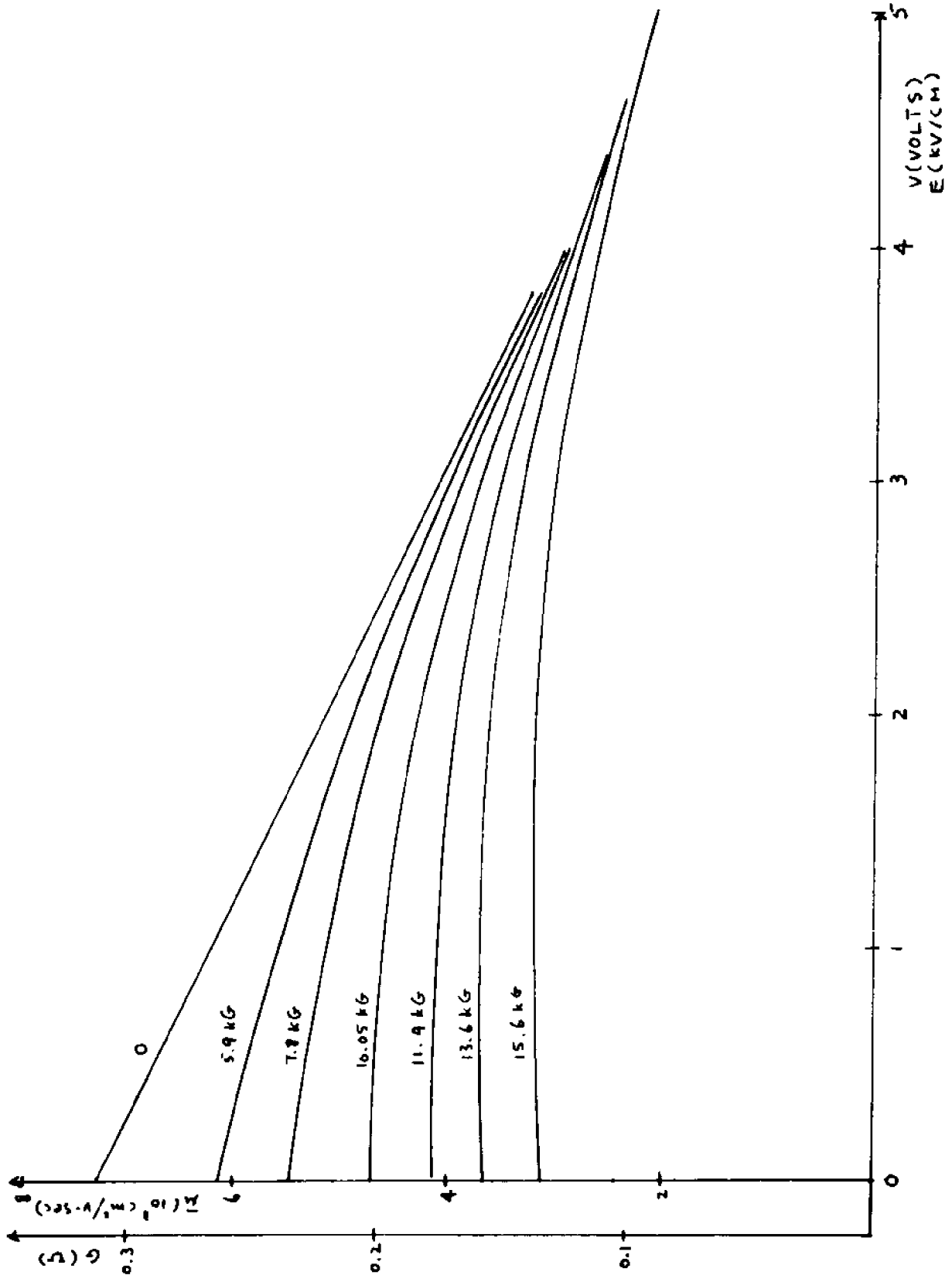

FIGURE 2.3:7 AVERAGE MOBILITY (μ) AND CONDUCTANCE (G) VERSUS ELECTRIC FIELD CHARACTERISTICS

Here, it is not possible to separate the dependence of $\overline{\mu}$ on T into a dependence of the mobility, μ, on T and a dependence of the carrier distribution, (n_ℓ/n_o), on T. Therefore, $\overline{\mu}$ is treated as a single entity which is a function of carrier temperature. The average mobility, $\overline{\mu}$, as a function of the magnetic field, B, is then obtained following steps outlined by Eqs. 2.2:9, 2.2:14 and 2.2:15. The energy transport equation in the steady state gives,

$$\frac{3}{2}\,\frac{k_B\,(T-T_o)}{\tau_e} = \frac{1}{2}\,\overline{\mu}\,E^2 \qquad (2.4:2)$$

where all parameters have been defined in Eq. 2.2:14. In the presence of the magnetic field, Eq. 2.4:2 becomes,

$$\begin{aligned}\frac{3}{2}\,\frac{k_B\,(T-T_o)}{\tau_e} &= \frac{1}{2}\,\frac{\overline{\mu}}{1+(\overline{\mu}B)^2}\,E^2 \\ &= \frac{1}{2}\,\overline{\mu}\left\{\frac{E}{\sqrt{1+(\overline{\mu}B)^2}}\right\}^2 \\ &= \frac{1}{2}\,\overline{\mu}\,E_{eff}^{\,2} \qquad (2.4:3)\end{aligned}$$

where $E_{eff} \equiv \dfrac{E}{\sqrt{1+(\overline{\mu}B)^2}}$

The term E_{eff} is again interpreted as an effective electric field for the purpose of calculating the carrier temperature. Since $\overline{\mu}$ is a function of carrier temperature, E_{eff} is to replace E to calculate $\overline{\mu}$ in Eq. 2.4:1. In Eqs. 2.4:2 and 2.4:3, it has been assumed that τ_e is not a function of the electric field. On the other hand,

if τ_e is assumed to have the same dependence on the electric field as $\bar{\mu}$, an assumption to be justified by comparing calculated and measured results, with

$$\tau_e \equiv C_1 \bar{\mu} \qquad (2.4:4)$$

where C_1 is a constant,

then, Eq. 2.4:3 becomes

$$\frac{3}{2}(T-T_o) = C_1 \bar{\mu}^2 \left\{\frac{E}{1+(\bar{\mu}B)^2}\right\}^2$$

$$= C_1 \bar{\mu}^2 E'^2_{eff} \qquad (2.4:5)$$

where $E'_{eff} \equiv \dfrac{E}{1+(\bar{\mu}B)^2}$

The term E'_{eff} should then be used to calculate $\bar{\mu}$ in Eq. 2.4:1. Before the correlation of these results with experiments are presented, a summary is made of the required calculations. The steps to be followed are:

1. Measure the V-I characteristic for B=0.
2. Calculate G=(I/V) as a function of V.
3. Divide G and V by (L/qn_oA) and L respectively to obtain the $\bar{\mu}$-E characteristic.
4. Express $\bar{\mu}$ as a function of E analytically, with, $\bar{\mu} = f(E)$.
5. Replace E by either E_{eff} or E'_{eff} (to be determined subsequently) in the $\bar{\mu} = f(E)$ expression to obtain $\bar{\mu}' = f(E_{eff})$ or $f(E'_{eff})$.
6. Calculate the effective drift mobility, $\bar{\mu}_B$.

$$\text{from } \mu_B = \frac{\mu'}{1+(\mu' B)^2} \quad .$$

7. An improvement in the results may be obtained by recalculating E_{eff} or E'_{eff} using μ' instead of μ and repeating steps (5) and (6).

Using these steps, μ_B is calculated from the zero magnetic field μ-E characteristic shown in Fig. 2.3:7. In Fig. 2.4:1, it is observed that using E_{eff} (n=1/2) provides good agreement in the low bias voltage range while using E'_{eff} (n=1) provides better agreement at the higher bias voltages. To demonstrate the necessity of the steps outlined above, direct calculations using

$$\bar{\mu}_B' = \frac{\bar{\mu}}{1+(\bar{\mu} B)^2} \qquad (2.4:6)$$

where $\bar{\mu}$ is assumed to be independent of B is plotted in Fig. 2.4:2. Graphically, it is observed that the error becomes more evident.

The same calculations and measurements were applied to diode #3. Using E_{eff} (n=1/2) for calculations over the entire bias range give resonable agreement as shown in Fig. 2.4:3. The calculation without considering the cooling effect is also shown for comparison.

2.5 Conclusions

By modeling the non-linear V-I characteristic in terms of a carrier temperature dependent average drift mobility, good agreement is obtained for calculated and

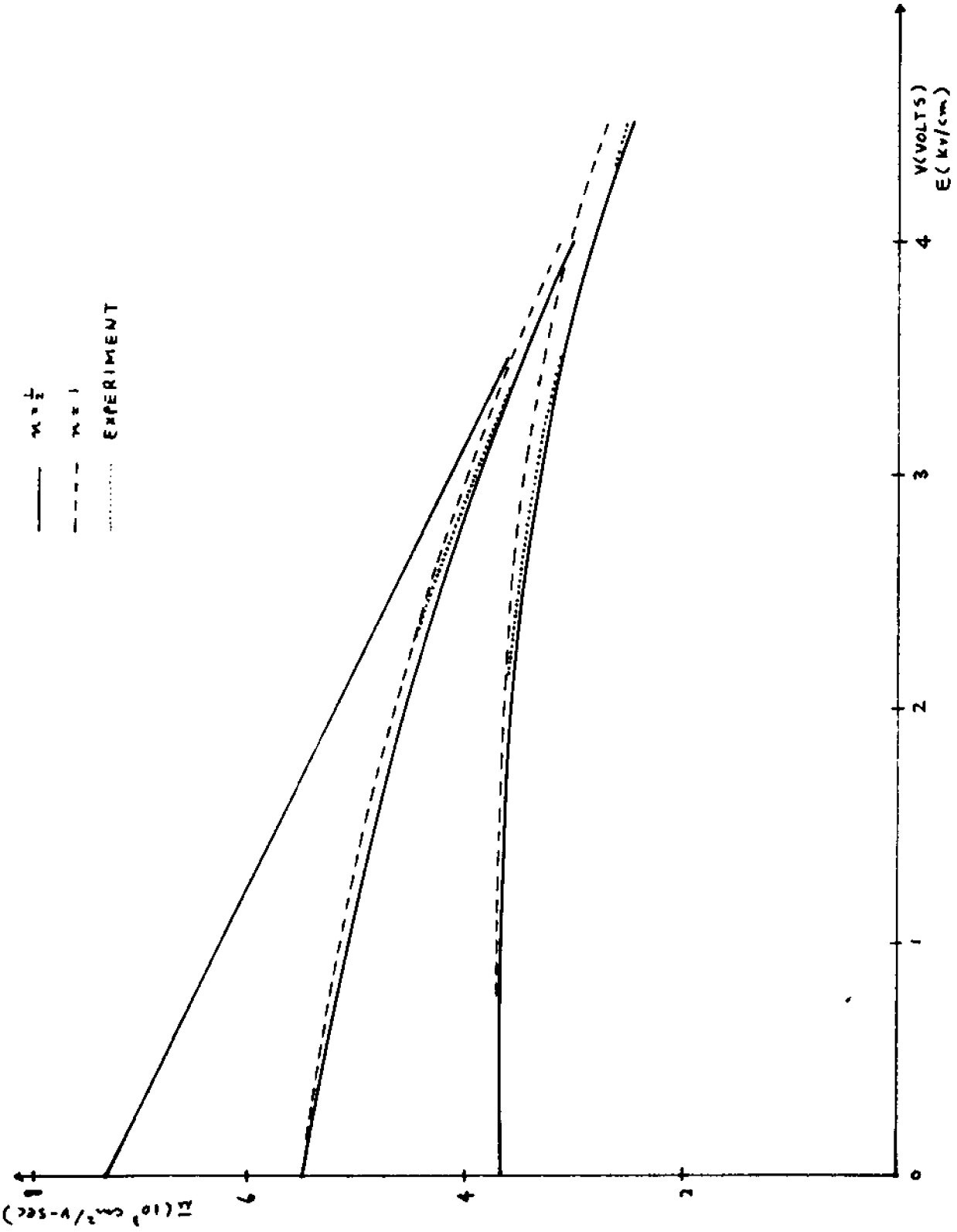

FIGURE 2.4:1 CALCULATED AND MEASURED μ-E CHARACTERISTICS WITH MAGNETIC FIELD AS PARAMETER FOR DIODE #1

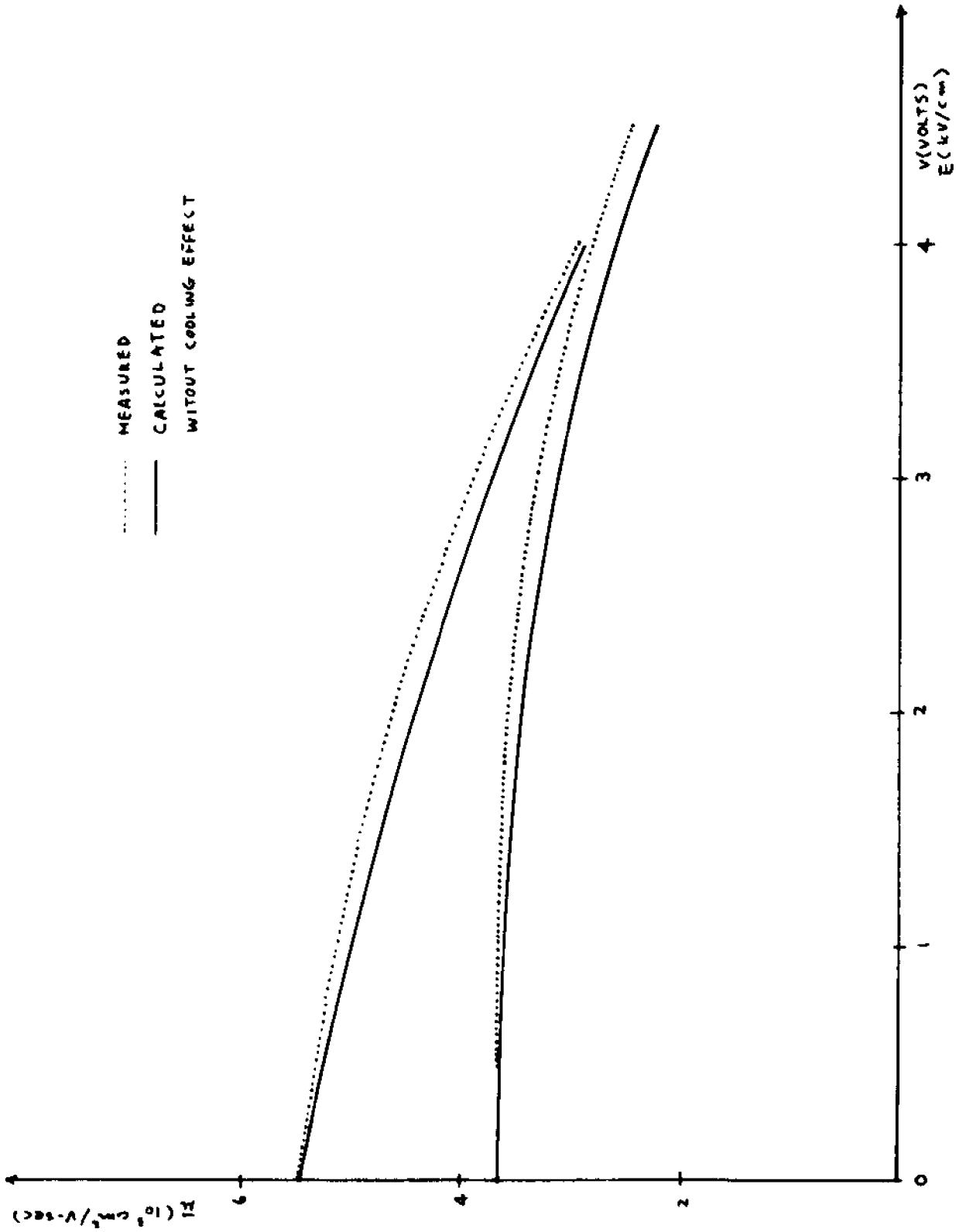

FIGURE 2.4.2 CALCULATED (WITHOUT COOLING EFFECT) AND MEASURED μ-E CHARACTERISTICS FOR DIODE #1

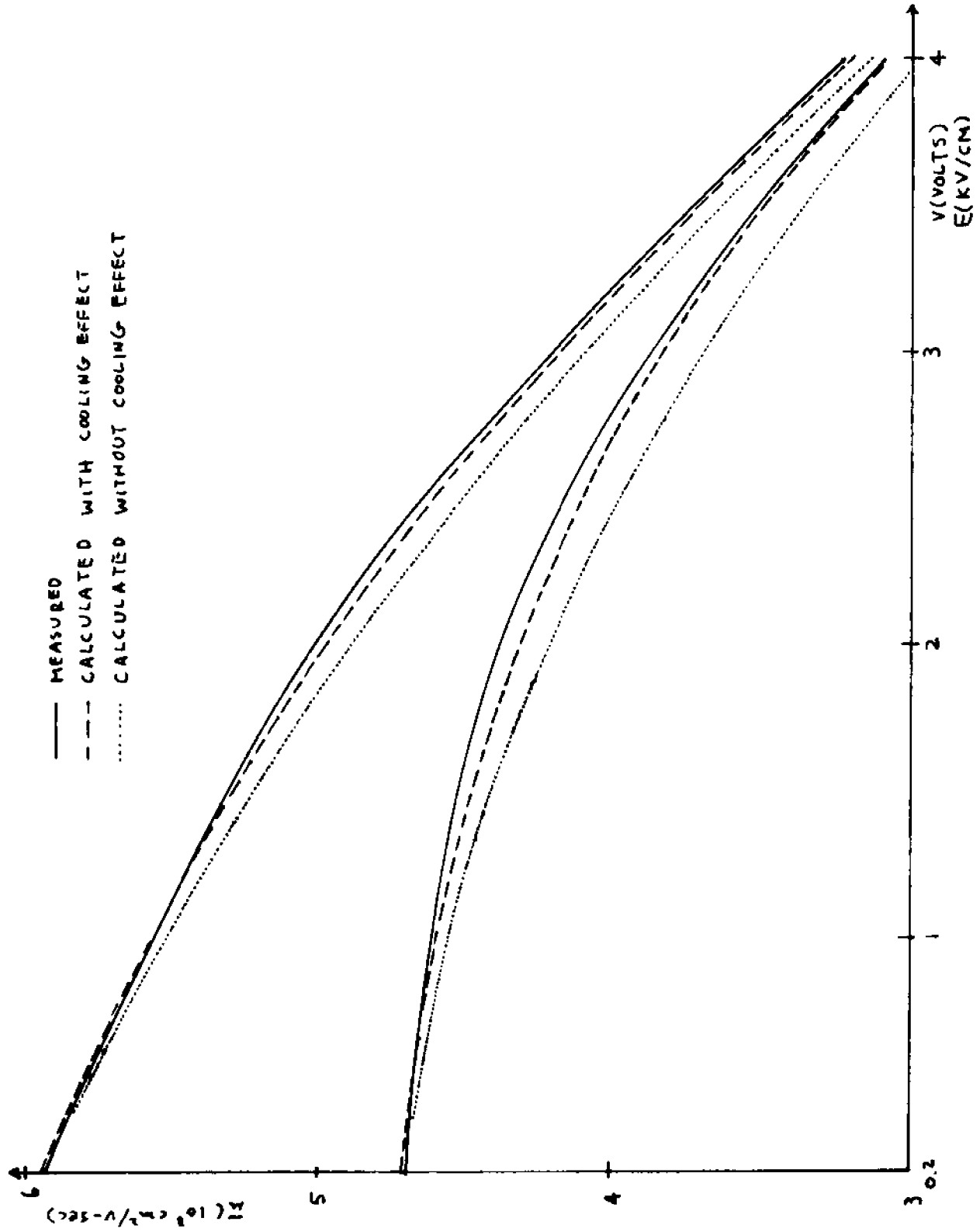

FIGURE 2.4:3 CALCULATED AND MEASURED $\bar{\mu}$-E CHARACTERISTICS WITH MAGNETIC FIELD AS PARAMETER FOR DIODE #3

measured magnetoresistance effects. It was found that whenever mobility depends on carrier temperature, inclusion of the cooling effect gives better agreement than would otherwise be obtained, Figs. 2.4:1 and 2.4:2. Magnetoresistance measurements at low bias voltages, where the V-I characteristic is linear, allows one to find the low electric field mobility of the device regardless of device parameters including length, cross-sectional area and doping concentration.

At increased bias voltages, the magnetic field causes the NDC threshold to shift to a higher bias value. This agreed with theorectical calculations in Sec. 2.2. Quantitative comparison of the shifts is difficult since the measured V-I characteristic deviates from that used in Sec. 2.2. This was circumvented by remodeling the zero magnetic field characteristic according to the experimental results. The magnetoresistance effects thus calculated gives the good agreements described.

CHAPTER 3 STABLE NEGATIVE CONDUCTANCE AMPLIFICATION

3.1 Introduction and Description of Previous Results

The reflection coefficient of a waveguide or transmission line terminated by a complex normalized load $\bar{y}_L$ is [52],

$$\bar{\Gamma} = \frac{1-\bar{y}_L}{1+\bar{y}_L} \qquad (3.1;1)$$

The magnitude of $\bar{\Gamma}$ exceeds unity when $\bar{y}_L$ has a negative real part (negative conductance). The reflected power gain for such a device is [52],

$$\text{Power Gain} = |\bar{\Gamma}|^2 = \left|\frac{1-\bar{y}_L}{1+\bar{y}_L}\right|^2 \qquad (3.1;2)$$

When the wave reflected by the load is amplified, instead of attenuated, the system is referred to as a reflection-type amplifier. The use of such an amplifier was proposed by Thim et. al. [32]. More detailed experimental results were subsequently published by Thim and Barber [19]. The circuit diagram for the amplifier used by the latter authors is shown in Fig. 3.1;1. In their experiments, n-type GaAs samples were used with n_oL products smaller than $5 \times 10^{11}/cm^2$ such that there is a range of bias voltages over which stable amplifications is possible without uncontrolled oscillations occurring. Their experimental results indicated that

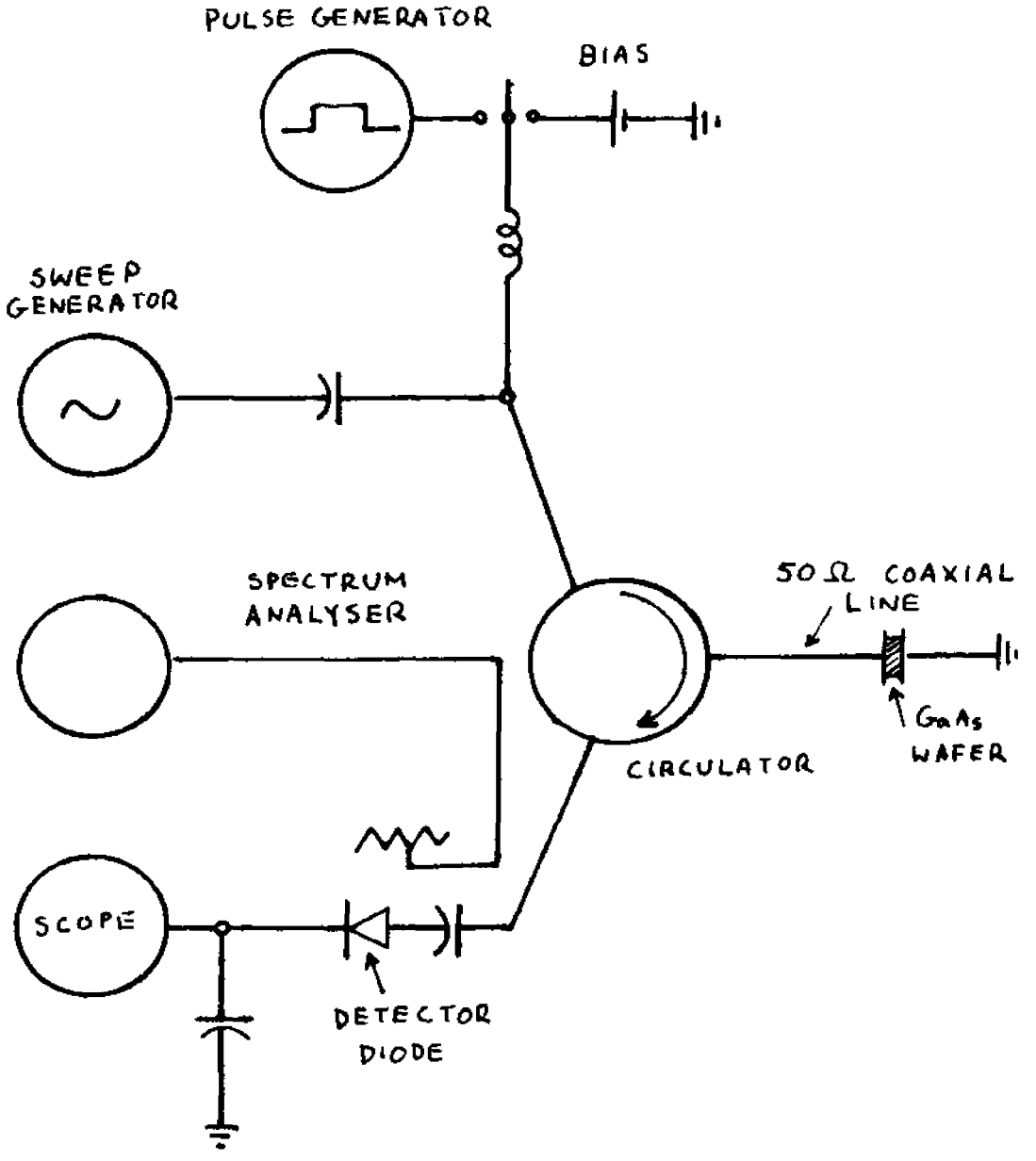

FIGURE 3.1.1 REFLECTION AMPLIFIER SYSTEM BY THIM AND BARBER [19]

> "....amplification occurred at frequencies corresponding approximately to the frequency of formation of high field domains in the oscillating condition, namely
>
> $$f = \frac{v_d}{L_{eff}} \quad ,$$
>
> where v_d is the drift velocity of the domain or approximately the drift velocity of the electrons, and L_{eff} is the effective length of the wafer. L_{eff} is always shorter than the actual sample length because of the finite thickness of the contacts and the presence of inhomogeneities."

Generally, they found that for long (100 um) samples, L_{eff} is much smaller than the physical length, L. This is due to the non-uniform electric field distribution within the sample as discussed in Sec. 3.2 where it was pointed out that as L is reduced by using shorter samples, L_{eff} (defined as L' in Sec. 2.3) approaches L. The experimental results by Thim and Barber for a 35 um sample indicated that L_{eff} is close to L. In their experiments, it was also found that the slope of the static V-I characteristic was always positive even in regions where small signal negative conductance occurred. This condition was not found to be true in the present d-c measurements of the static V-I characteristic. The possible interpretations of a measured NDC in view of Shockley's positive conductance theorem is discussed in App. 1.

Further work in this area was carried out by Hakki [29] including an expression for the small signal admittance. His theoretical and experimental results brought out the essential features of the small signal admittance when the device entered the NDC region. The development

for the small signal admittance follows the same basic steps. However, some of his assmptions will be reconsidered so that a more accurate expression may be obtained. In particular, neglecting the quadrature phase component of the conduction current with the electric field causes considerable error in the resulting small signal susceptance expression. As was shown by Rees [53], this out of phase component effectively increases the capacity of the device to approximately five times its value at zero electric field. The dispersion equation and small signal admittance was also derived by other authors [14,16,22,33]. In none of these treatments were high frequency (non-collision dominated) effects considered.

Other publications [34-37] in this area concentrated on the external microwave networks necessary to stablize the amplifier. A listing of references is found in review papers by Sterzer [54] and Perlman et. al. [55]. Recent publications on the practical application of transferred electron amplifiers include papers by Talwar and Curtice [56], and De Koning et. al. [57]. In most of these papers, theoretical treatment of the device admittance is inadequate. Since the device admittance is frequency dependent [29], a more precise expression is desirable, particularly for wide band applications.

In a most recent paper by Grubin and Kaul [51], the small signal impedence was calculated with particular attention devoted to the non-uniform electric field

problem. Their conclusions are:

1. If the electric field is highly non-uniform, Fig. 3.1:2a, the effective length of the sample is small compared to the physical length. The frequency at which negative conductance occurs is approximately 40 GHz for a 10 μm device with $n_o=10^{15}/cm^3$.
2. If the electric field becomes more uniform, Fig. 3.1:2b, the effective length approaches the physical length. For the case where the electric field over the entire physical length is above the NDC threshold, negative conductance occurs at $f \sim 8$ GHz for the same device parameters.

In the present experiments using devices with similar n_o and L values, the peak gain occurred at $f \sim 9.5$ GHz. Therefore, it is believed that the electric field across the entire sample is above the NDC threshold (case 2). Since the average electric field in the measurements is only 3500 kv/cm compared to a theoretical value of 3300 kv/cm, no large electric field non-uniformities are expected to exist. The uniform field appoximation is used in the development of the small signal admittance in Secs. 3.2 and 3.3.

3.2 Derivation of the Dispersion Equation

There are two basic models previously employed for this derivation. The two spieces (mobilities) model used

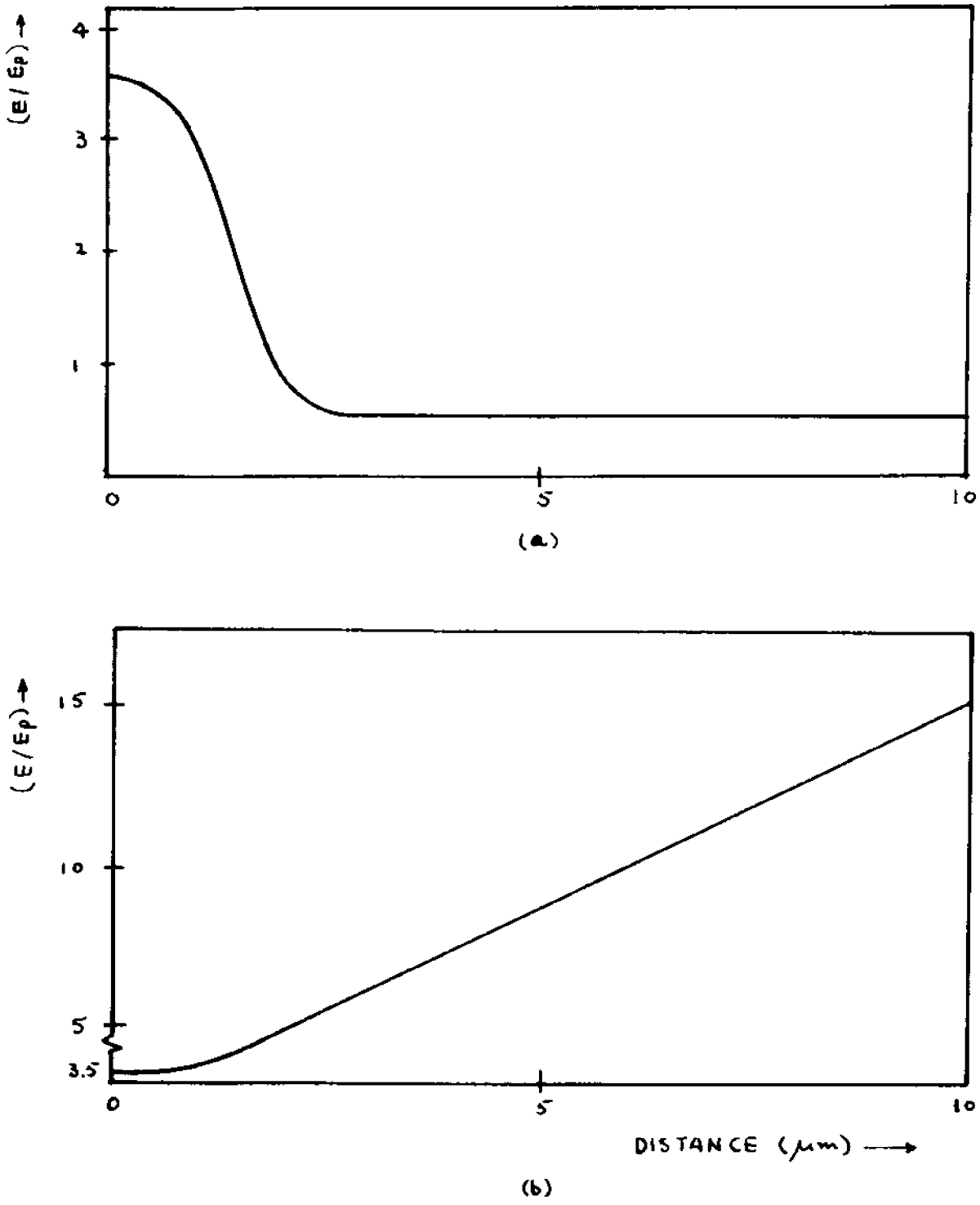

FIGURE 3.1:2 NON-UNIFORM ELECTRIC FIELD DISTRIBUTION BY GRUBIN AND KAUL [51]

by Hakki [29] expresses the carrier distribution function explicitly in terms of the electric field. The NDC obtained is a direct result of the reduction of lower valley carrier concentration. The model used by McCumber and Chynoweth [14], and Ohmi and Hauso [33] uses an average drift mobility to describe the entire system of carrier. The NDC obtained is then a result of the reduction in average carrier mobility. Whereas the two are equivalent in describing the static $\bar{v}_o$-E (previously denoted as v_d-E) characteristic, there is an important difference in the solutions to the dispersion equation using the two models. The difference is discussed in detail in App. 3. There, it is shown that the two-species model may be reduced to the average mobility model by redefining the parameter v_{ol}, the lower valley drift velocity, as $\bar{v}_o$, the average drift velocity for the entire system of carriers. On the other hand, it is difficult to interpret the results of the average mobility model in terms of the two species approach. Therefore, the two species model is used.

For n-GaAs, the two carrier species are the high mobility lower conduction valley electrons and the low mobility upper conduction valley electrons. In his formulations, Hakki treated the upper valley carriers as being essentially immobile and made the collision dominated assumption at the outset. The latter assumption becomes inaccurate [58] (1) when the operating frequency increases

to above 20 GHz or (2) below 20 GHz, when the mobility of the carriers is substantially reduced with an increase in bias voltage.

In a study of the electron distribution function in GaAs at high electric field, Rees [53] found that the speed of response to an electric field perturbation is limited by the time it takes for the drift velocity in the lower valley, and the redistribution of the carriers among the two valleys, to reach steady state. The time constant, τ, associated with both of these processes are of the order of 2×10^{-12} sec [53]. Estimates of the same order of magnitude were obtained by Conwell and Vassell [50]. For an excitation frequency of 10 GHz

$$\omega\tau = 2\pi \times 10^{10} \times 2 \times 10^{-12}$$
$$= .126 \qquad (3.2:1)$$

Even for this small value of $\omega\tau$ comared to unity, it is shown in the next section, that the collision dominated assumption substantially alters the derived small signal susceptance. In the present derivation, the collision dominated assumption will not be made at the outset. Rather, it would be applied later after the validity for such a model has been determined. As a consequence, a phase difference is allowed to exist between the a-c electric field and the time and space dependent carrier distribution. Under these conditions, the basic equations describing the behavior of a transferred electron device in the presence of a transverse magnetic field become

1. Poisson's equation

$$\epsilon \nabla \cdot \vec{E} = \text{space charge}$$

$$= \left(\sum_{s=\ell,u} \rho_s \right) - qn_o \qquad (3.2;2)$$

where $\epsilon \equiv$ the dielectric constant

$\rho \equiv$ free carrier charge density

$q \equiv$ electronic charge

$n_o \equiv$ background doping number density

and $s \equiv \ell, u$ is used to denote the upper and lower valley quantities.

2. The conduction current equation

$$\vec{J} = \sum_{s=\ell,u} \rho_s \vec{v}_s \qquad (3.2;3)$$

where $\vec{v} \equiv$ drift velocity

and $\vec{J} \equiv$ conduction current density

3. The continuity equation

$$\nabla \cdot \vec{J}_s + \frac{\partial \rho_s}{\partial t} = \left. \frac{\partial \rho_s}{\partial t} \right|_{G-R} \qquad (3.2;4)$$

where $\left. \frac{\partial \rho_s}{\partial t} \right|_{G-R} \equiv$ time rate of generation and recombination of the s-type charge densities. The process of a carrier transferring from the lower valley to the upper valley consists of simultaneously losing a lower valley carrier (recombination) and gaining an

upper valley carrier (generation).

4. The momentum transfer equation

$$\frac{d\vec{v}_s}{dt} + \nu_s\vec{v}_s = \eta_s\,(\vec{E} + \vec{v}_s \times \vec{B}) - \frac{1}{\rho_s}\nabla_r\left(\frac{\rho_s k_B T_s}{m_s^*}\right)$$

$$= \eta_s\,(\vec{E} + \vec{v}_s \times \vec{B}) - \frac{\nu_s}{\rho_s}\nabla_r\,(D_s\rho_s) \qquad (3.2;5)$$

where $\nu \equiv$ collision frequency,

$\eta \equiv$ carrier charge to effective mass ratio,

$T \equiv$ carrier temperature,

$m^* \equiv$ carrier effective mass,

$k_B \equiv$ Boltzmann's constant,

$B \equiv$ applied static magnetic field,

and $D \equiv \dfrac{k_B T}{m^*\nu}$

$\equiv$ diffusion constant.

In principle, this set of equations is not adequate to describe the system and higher order moment equations are necessary. This is due to the dependence of D_s (or T_s) on the electric field. The small signal variation in the electric field results in a small signal variation in the diffusion constant D_s. A complete non-isothermal analysis would complicate the system of equations so much that analytical solutions are difficult to obtain. It is demonstrated later on in this section that the introduction of the diffusion constant only slightly modifies the admittance function, which is the quantity of interest.

The electric field dependent properties of the diffusion constant is further investigated experimentally in Sec. 4.3 where the effect of the magnetic field on the small signal admittance is discussed. The theoretical dependence of the diffusion constant on the electric field under static conditions has been treated by Conwell and Vassell [50], and Sasaki and Tanaka [42]. For time dependent fields, there may be a phase angle between D_s and E. This phase angle can best be introduced as a phenomenological quantity and does not improve the rigor of the theory. Therefore, this quantity will be carried only in the initial steps of the derivation of the dispersion equation and is disregarded in subsequent analysis.

In the small signal analysis, the dependent variables are assumed to have the form

$$\vec{F} = \vec{F}_0 + \vec{F}_1' = \vec{F}_0 + \vec{F}_1 \exp(j\omega t + Sz) \qquad (3.2{:}6)$$

where the subscripts o and 1 denote the d-c and a-c values respectively.

The geometrical configuration being studied is shown in Fig. 3.2:1, where

$$\vec{B} = -B_0 \hat{a}_y \qquad (3.2{:}7)$$

$$\vec{E} = (E_0 + E_1)\hat{a}_z \qquad (3.2{:}8)$$

$$\vec{J} = (J_{0x} + J_{1x})\hat{a}_x + (J_{0z} + J_{1z})\hat{a}_z \qquad (3.2{:}9)$$

$$\vec{v} = (v_{0x} + v_{1x})\hat{a}_x + (v_{0z} + v_{1z})\hat{a}_z \qquad (3.2{:}10)$$

All dependent variables written in the form defined by Eq. 3.2:6 are substituted in Eqs. 3.2:2-3.2:5 and only

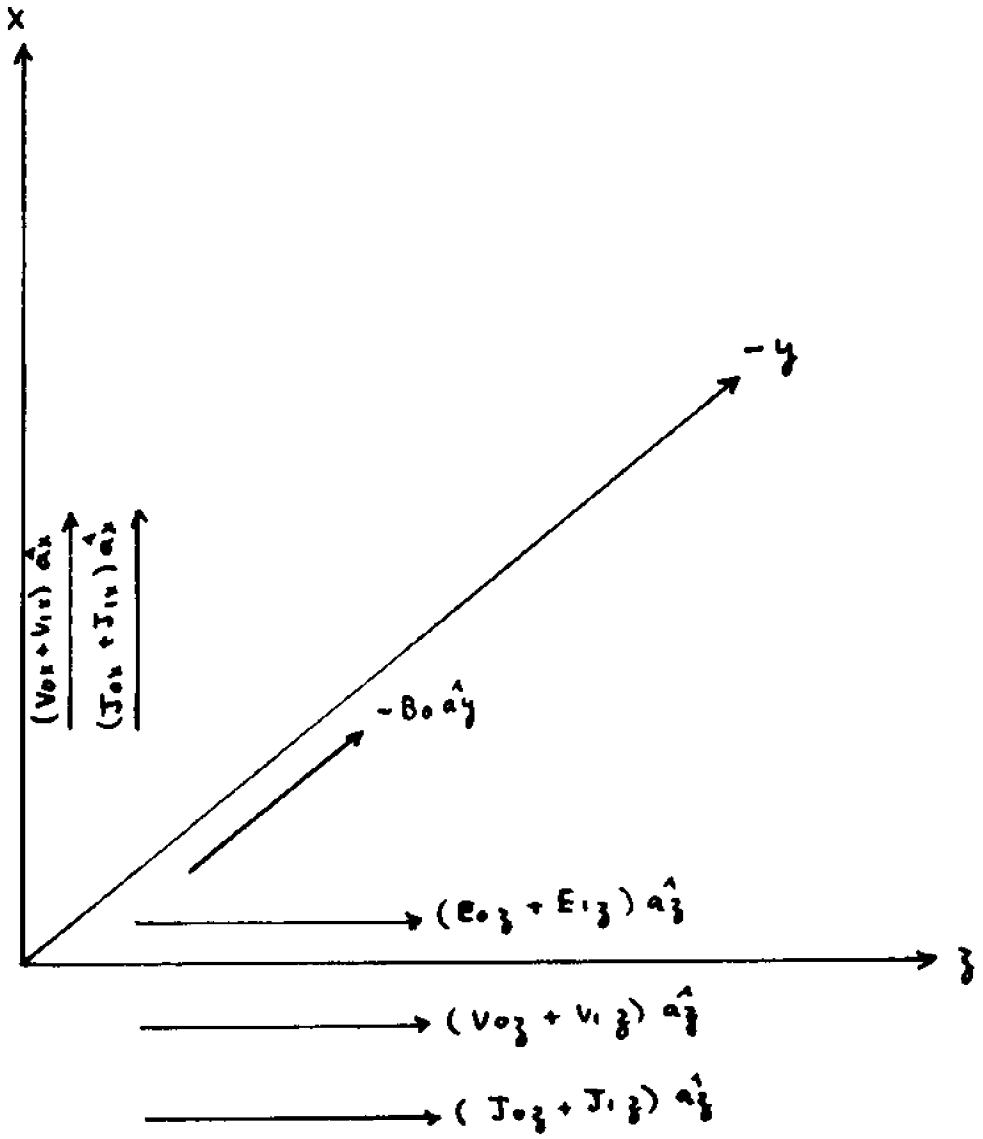

FIGURE 3.2:1 GEOMETRICAL CONFIGURATION FOR A-C CALCULATIONS

the first order terms are collected. For convenience, the subscript 'z' associated with the z-components of the vectors are dropped to give

1. Poisson's equation

$$\epsilon S E_1 = \rho_{1s} + \rho_{1u} \qquad (3.2;11)$$

2. The conduction current equation

$$J_{1s} = \rho_{os} v_{1s} + \rho_{1s} v_{os} \qquad (3.2;12)$$

3. The continuity equation

$$j\omega \rho_{1s} + S J_{1s} = j\omega \rho_{1s} \Big|_{G-R} \qquad (3.2;13)$$

where $$\rho_{1s} \Big|_{G-R} \equiv \frac{\rho_{os}}{E_o} \frac{\gamma_s}{1+j\tilde{\tau}_n(\omega+jSv_{os})} E_1$$

$$\gamma_s \equiv \frac{E_o}{\rho_{os}} \frac{\partial \rho_{os}}{\partial E_o}$$

$\tilde{\tau}_n \equiv$ intervalley relaxation time.

The term $1+j\tilde{\tau}_n(\omega+jSv_{os})$ accounts for the time and space phase between the induced charge transfer and inducing electric field. This is understood to be a phenomenological treatment, the validity of which is to be evaluated by experiment.

4. The momentum transfer equation

$$v_{1s} \left\{ (j\omega+Sv_{os}+\nu_s) + \frac{(\eta_s B_o)^2}{(j\omega+Sv_{os}+\nu_s)} \right\} =$$

$$\eta_s E_1 - S \frac{\nu_s D_{os}}{\rho_{os}} \rho_{1s} - S \frac{\nu_s D_{os}}{E_o} \frac{\beta_s}{1+j\tilde{\tau}_{es}(\omega+jSv_{os})} E_1 \qquad (3.2;14)$$

where $$\beta_s \equiv \frac{E_o}{D_{os}} \frac{\partial D_{os}}{\partial E_o}$$

and τ_e = energy relaxation time.

Equations 3.2:11-3.2:14 may be expressed in matrix form as,

$$\begin{bmatrix} 1 & 1 & -\epsilon S & 0 & 0 & 0 & 0 \\ v_{o\ell} & 0 & 0 & \rho_{o\ell} & 0 & -1 & 0 \\ 0 & v_{ou} & 0 & 0 & o_u & 0 & -1 \\ j\omega & 0 & -j\omega\alpha_\ell & 0 & 0 & S & 0 \\ 0 & j\omega & -j\omega\alpha_u & 0 & 0 & 0 & S \\ S(D_{o\ell}/\rho_{o\ell}) & 0 & -\mu_{o\ell}+S\zeta_\ell & \Omega'_\ell & 0 & 0 & 0 \\ 0 & S(D_{ou}/\rho_{ou}) & -\mu_{ou}+S\zeta_u & 0 & \Omega'_u & 0 & 0 \end{bmatrix} \begin{bmatrix} \rho_{1\ell} \\ \rho_{1u} \\ E_1 \\ v_{1\ell} \\ v_{1u} \\ J_{1\ell} \\ J_{1u} \end{bmatrix} = 0 \qquad (3.2:15)$$

where $$\alpha_s \equiv \frac{\rho_{os}}{E_o} \frac{\gamma_s}{1+j\tau_n(\omega+jSv_{os})}$$

$$\zeta_s \equiv \frac{D_{os}}{E_o} \frac{\beta_s}{1+j\tau_{es}(\omega+jSv_{os})}$$

$$\Omega_s \equiv 1 + \frac{j\omega+Sv_{os}}{\nu_s}$$

and $$\Omega'_s \equiv \Omega_s + \frac{(\mu_{os}B_o)^2}{\Omega_s}$$

Setting the determinant of the matrix equal to zero results in the dispersion equation,

$$1 - \sum_{s=\ell,u} \left\{ \frac{j(\rho_{os}/\epsilon)(\mu_{os}-S\zeta_s) + \omega(\alpha_s/S\epsilon)\left[\Omega_s+(\mu_{os}B_o)^2\right]}{(\omega-jSv_{os})\left[\Omega_s{}^2+(\mu_{os}B_o)^2\right] + jS^2\Omega_s D_{os}} \right\} = 0 \qquad (3.2:16)$$

For the special case when the electric field induced intervalley transfer of carriers and diffusion are neglected (α_s, D_{os} = 0), the dispersion equation reduces

to the one previously derived for a two species model of InSb by Robinson and Vural [59], Eq. 3.2:17.

$$1 - \sum_{s=\ell,u} \frac{\omega_{pe}^2(\omega - kv_{os} - j\nu_s)}{\{(\omega - kv_{os} - j\nu_s)^2 - \omega_{ce}^2\}(\omega - kv_{os})} = 0 \qquad (3.2:17)$$

where $\omega_{pe} \equiv (q^2 n_o/\epsilon m^*)$

$\omega_{ce} \equiv (|q| B_o/m^*)$

and the convention $S = -jk$ has been used.

To facilitate solving the dispersion equation, Eq. 3.2:16, some appropriate approximations are made:

1. The upper valley carrier drift velocity is negligibly small compared to the lower valley carrier drift velocity resulting in v_{ou}, μ_{ou}, D_{ou}, $\xi_u = 0$. This approximation is justified in view of the upper to lower valley mobility ratio, with $(\mu_{ou}/\mu_{o\ell}) \simeq (1/60)$.
2. The phase velocity of the growing mode (S1) is approximately that of the drift velocity of the carriers [14,29],

$$S1 \simeq -j(\omega/v_{o\ell}) + Re(S1) \qquad (3.2:18)$$

where Re(S1) represents the real part of S1. Hakki [29] estimated the phase velocity to exceed the drift velocity of the carriers by less than 7%. Using Eq. 3.2:18

$$1 + (j\omega + S1 v_{o\ell})/\nu_\ell \simeq 1 + (v_{o\ell}/\nu_\ell) Re(S1) \simeq 1 \qquad (3.2:19)$$

The two steps in this approximation is further

justified in Eq. 3.2:26 where the approximate form of S1 is derived.

Using these approximations, the dispersion equation, Eq. 3.2:16, reduces to

$$1 - \frac{j(\rho_{o\ell}/\epsilon)(\mu_{o\ell} - S\beta_\ell D_{o\ell}/E_o) + \omega(\gamma_\ell \rho_{o\ell}/S\epsilon E_o)}{(\omega - jSv_{o\ell}) + jS^2 D_{o\ell}} - \frac{\gamma_u \rho_{ou}}{S\epsilon E_o} = 0 \qquad (3.2:20)$$

where β_ℓ, γ_ℓ and $\gamma_u = -(\rho_{o\ell}/\rho_{ou})\gamma_\ell$ were defined in Eqs. 3.2:13 and 3.2:14. All the parameters $\rho_{o\ell}$, $\mu_{o\ell}$, $v_{o\ell}$, $D_{o\ell}$, β_ℓ and γ_ℓ are now implicit functions of the static electric and magnetic fields. Through the relationships

$$1 + \gamma_\ell = \frac{E}{\bar{v}} \frac{d\bar{v}}{dE} \qquad (3.2:21)$$

and

$$1 + \beta_\ell = \frac{E}{\bar{D}} \frac{d\bar{D}}{dE} \qquad (3.2:22)$$

where $\bar{v} \equiv (n_{o\ell}/n_o)v_{o\ell}$, and $\bar{D} \equiv (n_{o\ell}/n_o)D_{o\ell}$,

Eq. 3.2:20 is put in the form

$$S^2(-D_{o\ell}) + Sv_{o\ell}\left\{1 - \frac{\bar{\sigma}\bar{D}}{\epsilon\bar{v}^2} \frac{E}{\bar{D}} \frac{d\bar{D}}{dE}\right\} + j\omega + \frac{\sigma_{o\ell}}{\epsilon} \frac{E}{\bar{v}} \frac{d\bar{v}}{dE} = 0 \qquad (3.2:23)$$

where $\sigma_{o\ell} \equiv qn_o \mu_{o\ell}$, and $\bar{\sigma} \equiv (n_{o\ell}/n_o)\sigma_{o\ell}$.

The subscript 'o' which is used to denote static quantities has been dropped for $\bar{v}$, $\bar{D}$, E and $\bar{\sigma}$ for convenience. Multiplying Eq. 3.2:23 by $(n_{o\ell}/n_o)$ results in

$$S^2(-\bar{D}) + S\bar{v}\left\{1 - \frac{\bar{\sigma}\bar{D}}{\epsilon\bar{v}^2} \frac{E}{\bar{D}} \frac{d\bar{D}}{dE}\right\} + j\bar{\omega} + - \frac{E}{\bar{v}} \frac{d\bar{v}}{dE} = 0 \qquad (3.2:24)$$

where $\bar{\omega} \equiv (n_{o\ell}/n_o)\omega$.

Equation 3.2:24 is identical to the one Ohmi and Hasuo [33] derived using an average mobility model with $\bar{\omega}$ replaced by ω. Physically, the origin of the discrepency is best explained in terms of the difference in the modeling of the conduction mechanism in GaAs. Interaction between an electromagnetic wave and the drifting carriers occurs when the phase velocity of the wave is approximately that of the drift velocity of the carriers. In the average mobility model, the entire system of carriers is assumed to drift at a velocity $\bar{v}$. Therefore, interaction occurs when $v_{ph} \simeq \bar{v}$, where v_{ph} is the phase velocity of the electromagnetic wave. In the two species model, the lower valley carriers are assumed to drift at the velocity $v_{o\ell}$ while the upper valley carriers are assumed to be essentially immobile. Therefore, interaction occurs when $v_{ph}' \simeq v_{o\ell}$. As a result, two different phase velocities, v_{ph} and v_{ph}', are considered necessary for interactions to occur. The different phase velocities give rise to two different frequencies ω and ω', where $\omega' = (v_{ph}'/v_{ph})\omega = (v_{o\ell}/\bar{v})\omega = (n_o/n_{o\ell})\omega$, at which interactions are expected to occur. Consequently, whereas ω appears in the dispersion equation based on the average mobility model, $\bar{\omega} = (n_{o\ell}/n_o)\omega$ appears in the one based on the two species model. Further comparisons, based on the solutions to the dispersion equations are found in App. 3. Experimental evaluations of the two models are discussed in Secs. 4.2 and 4.3.

Proceeding to solve the dispersion equation, Eq. 3.2:24, the roots are,

$$S1,2 = \left(\frac{\bar{v}'}{2\bar{D}}\right) \pm \left\{\left(\frac{\bar{v}'}{2\bar{D}}\right)^2 - \frac{1}{\bar{D}}\left(j\bar{\omega} + \frac{\bar{\sigma}}{\epsilon}\frac{E}{\bar{v}}\frac{d\bar{v}}{dE}\right)\right\}^{\frac{1}{2}} \qquad (3.2:25)$$

where $\bar{v}' \equiv \bar{v} - \frac{\bar{\sigma}\bar{D}}{\epsilon\bar{v}^2}\frac{E}{\bar{v}}\frac{d\bar{v}}{dE}$.

In the limit of zero diffusion, $\bar{D} \to 0$, the S^2 term in Eq. 3.2:24 is zero; the solution is

$$S1 = -j\frac{\bar{\omega}}{\bar{v}} - \frac{\bar{\sigma}}{\epsilon\bar{v}^2}\frac{E}{\bar{v}}\frac{d\bar{v}}{dE} \qquad (3.2:26)$$

This verifies the approximation made earlier in Eq. 3.2:18 and the first step in Eq. 3.2:19 that $Im(S1) \simeq -(\omega/v_{os})$ $= -(\bar{\omega}/\bar{v})$. As for the second step in Eq. 3.2:19, it is estimated that $Re(S1) \simeq 1 \times 10^3/cm$ (Fig. 3.2:2d), (v_{os}/ν_ℓ) $\simeq (1.4 \times 10^7/.5 \times 10^{12}) = 2.8 \times 10^{-5}$, resulting in $(v_{os}/\nu_\ell)Re(S1) = .028 \ll 1$.

Returning to a discussion of the solution to the dispersion equation, Eq. 3.2:26 indicates that in the limit of zero diffusion, Re(S1) is independent of frequency and the phase velocity of the travelling wave is the same as the drift velocity of the carriers. The more accurate expression, where a finite diffusion constant is used, is plotted in Fig. 3.2:2. The static V-I characteristic used is similar to the one shown in Fig. 2.3:4. For this particular set of figures, $\bar{D} =$ 200 cm^2/sec is chosen. Other parameters for the device

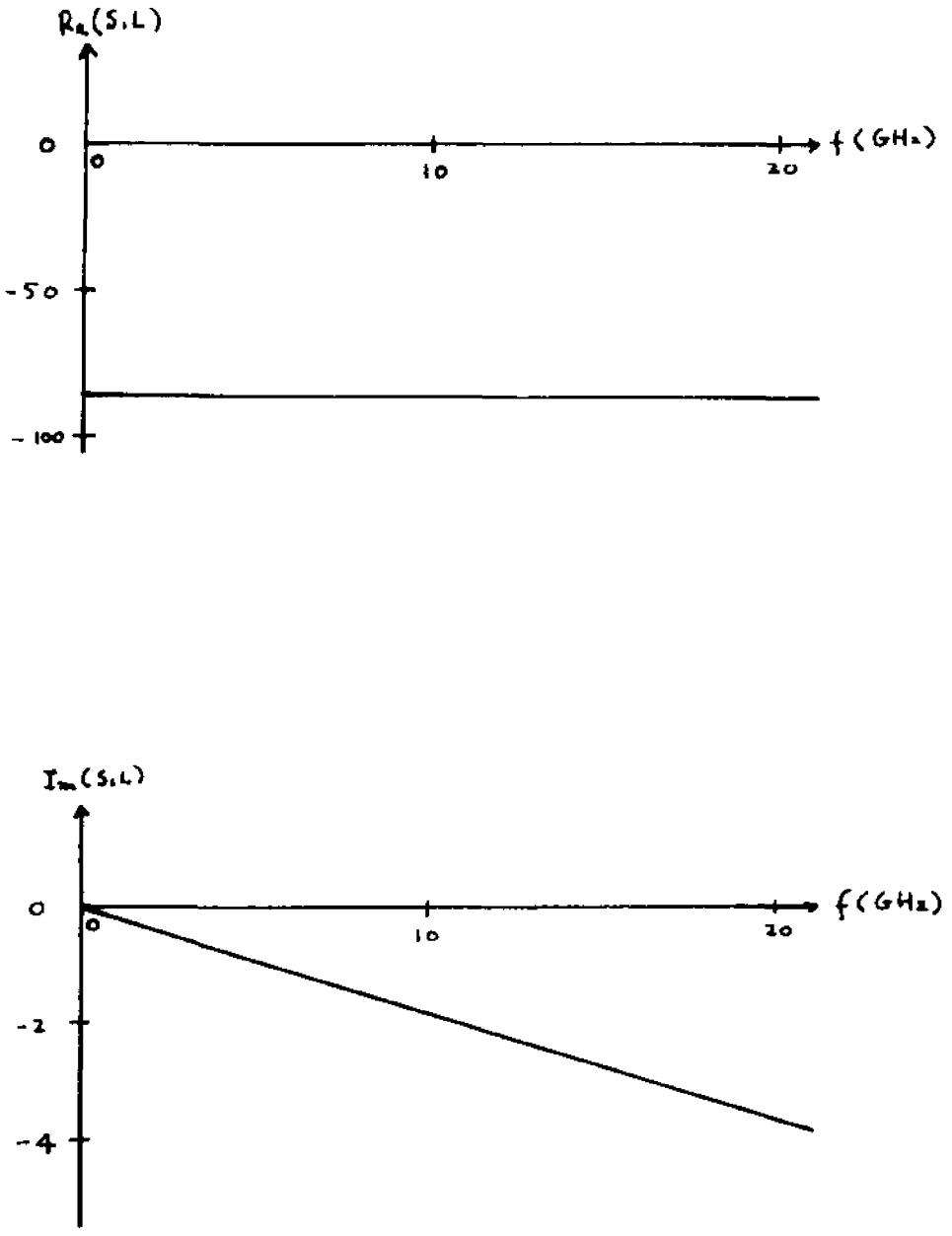

FIGURE 3.2:2a S1L PRODUCT VS. FREQUENCY V=0

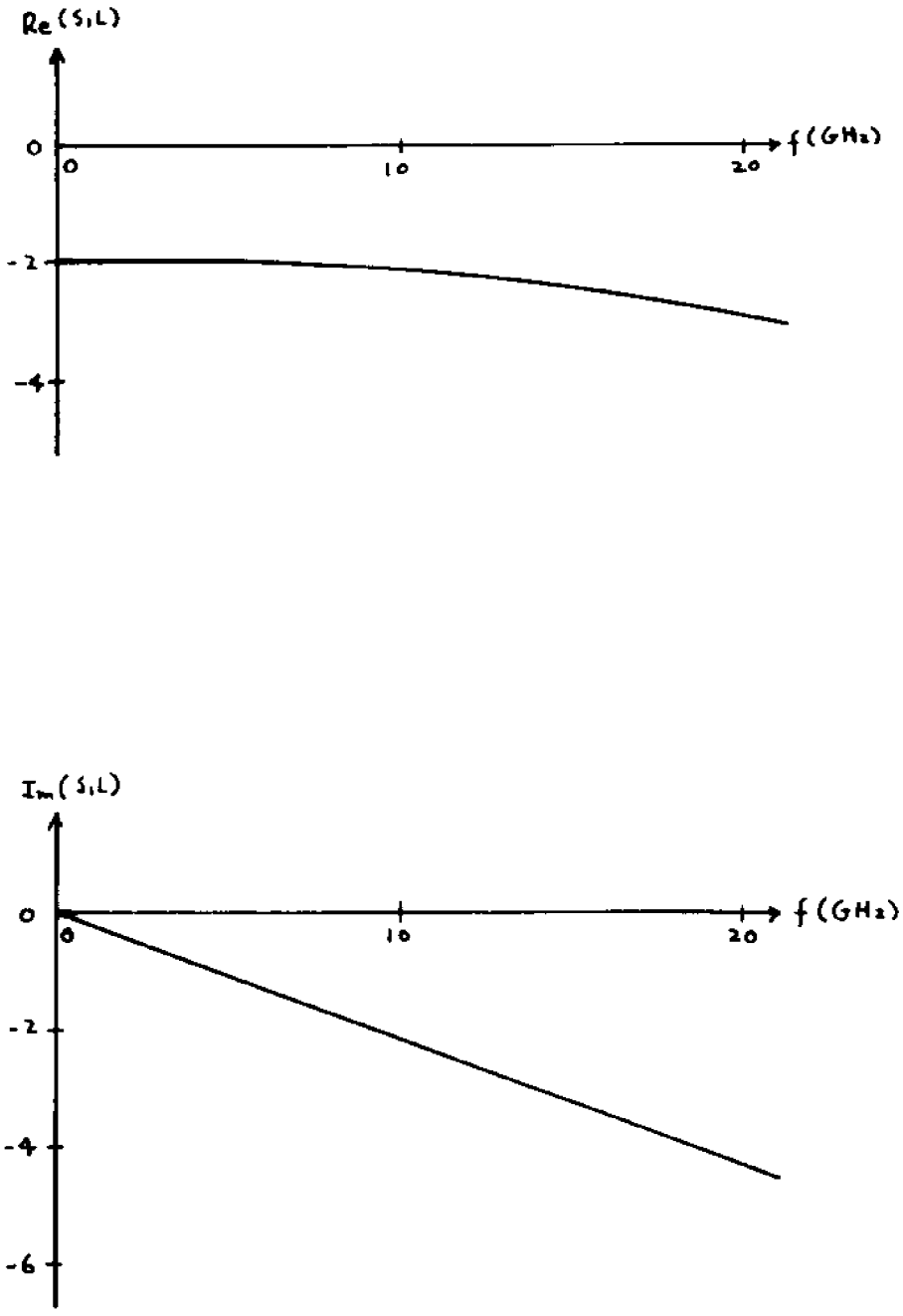

FIGURE 3.2:2b V=3.7 VOLTS

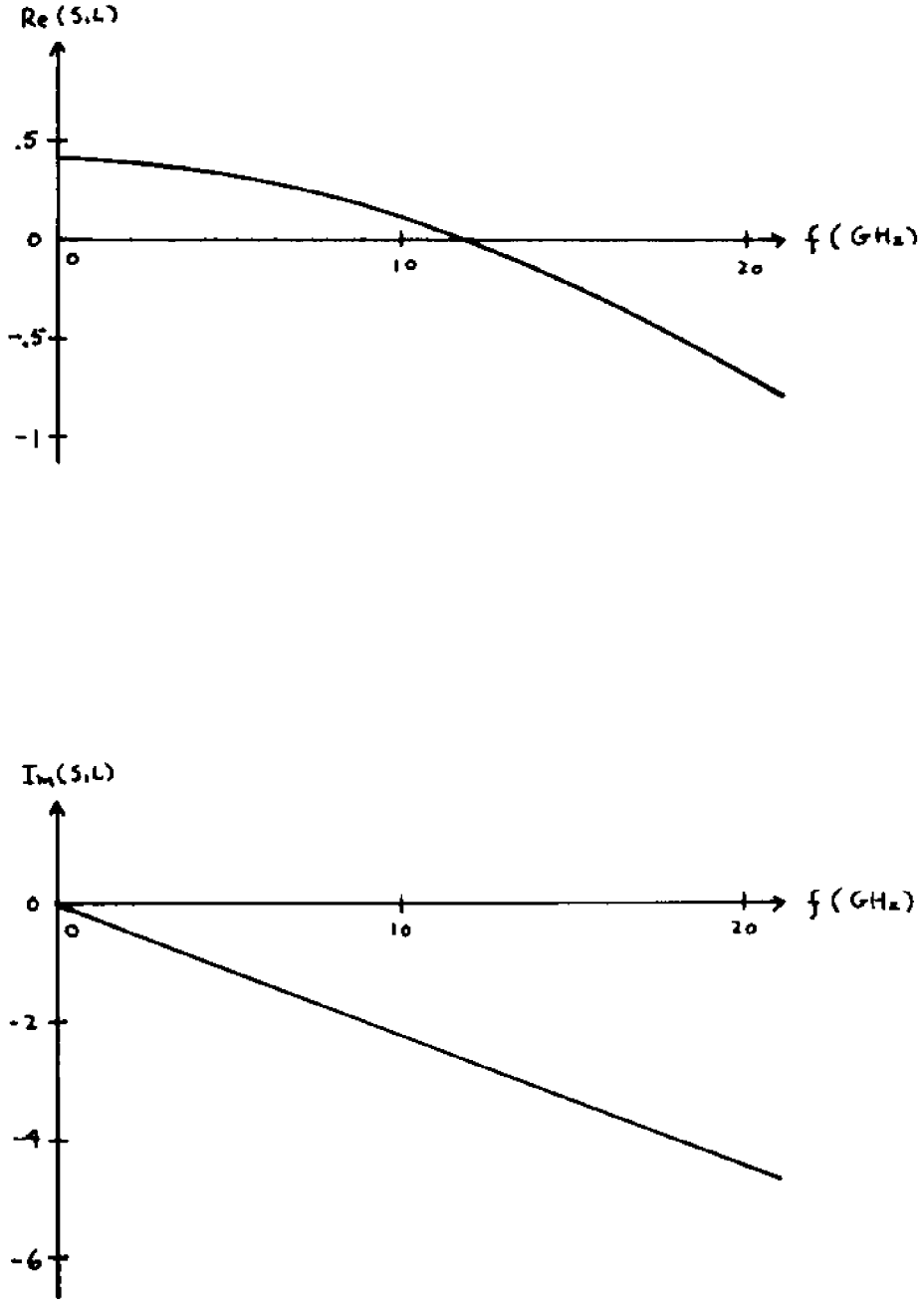

FIGURE 3.2:2c V=4.05 VOLTS

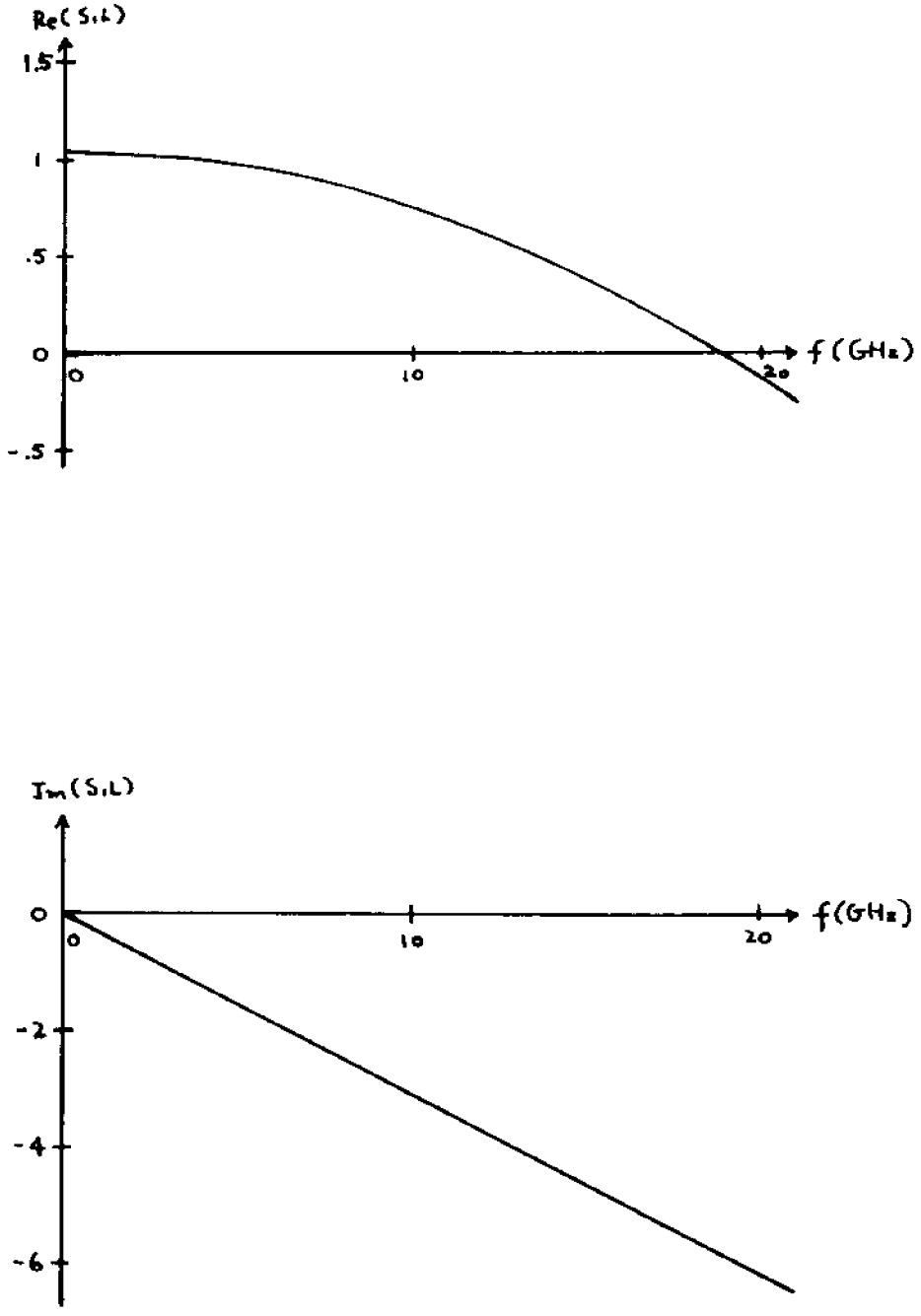

FIGURE 3.2:2d V=4.16 VOLTS

were listed in Table 2:1. As observed in Fig. 3.2:2a, S1 corresponds to a highly attenuated wave with a large negative real part at zero bias. With increasing bias voltage, it becomes less attenuating and finally attaining a positive real part, Figs. 3.2:2b,c and d. The values of S1 as a function of frequency is used in Sec. 3.3 to calculate the small signal admittance where it is shown that a negative conductance appears simultaneously with the real part of S1 becoming positive.

3.3 Derivation of the Small Signal Admittance

The total current in the device is the sum of the conduction current plus the displacement current

$$J_{total} = \sum_{n} (j\omega\epsilon E_n + \rho_o v_{1n} + \rho_{1n} v_o) \qquad (3.3:1)$$

where the summation 'n' is over all possible modes(solutions to the dispersion equation).

The subscript '1' has been dropped from the variables with the upper valley carriers assumed immobile. The determinant of the matrix, Eq. 3.2:15, from which the dispersion equation was obtained indicated that S=0 is also a solution to the dispersion equation. This becomes evident if division by S is avoided in evaluating the determinant. Therefore, the summation 'n' in Eq. 3.3:1 is for S=0 in addition to the two modes S1, S2 $\neq$ 0 obtained earlier in Eq. 3.2:25.

From Maxwell's Equation

$$\nabla \times H_1 = j\omega\epsilon E_1 + \rho_0 v_1 + \rho_1 v_0 \qquad (3.3:2)$$

Taking the divergence on both sides of Eq. 3.3:2 results in

$$\nabla \cdot (\nabla \times H_1) = \nabla \cdot (j\omega\epsilon E_1 + \rho_0 v_1 + \rho_1 v_0) \qquad (3.3:3)$$

which, for a one dimension model, becomes

$$\frac{\partial}{\partial z}(j\omega\epsilon E_1 + \rho_0 v_1 + \rho_1 v_0) = 0 \qquad (3.3:4)$$

$$\text{or } S\cdot(j\omega\epsilon E_1 + \rho_0 v_1 + \rho_1 v_0) = 0 \qquad (3.3:5)$$

For $S \neq 0$, Eq. 3.3:5 gives

$$(j\omega\epsilon E_1 + \rho_0 v_1 + \rho_1 v_0) = 0 \qquad (3.3:6)$$

Using the result of Eq. 3.3:6, the equation for total current, Eq. 3.3:1, becomes

$$J_{total} = j\omega\epsilon E_{10} + \rho_0 v_{10} + \rho_{10} v_0 \qquad (3.3:7)$$

where the second subscript in E_{10}, v_{10} and ρ_{10} indicates that it corresponds to the mode S=0.

The terms v_{10} and ρ_{10} in Eq. 3.3:7 are related to E_{10} through the momentum transfer equation (Eq. 3.2:14) and the continuity equation (Eq. 3.2:13) respectively. Substitution of Eqs. 3.2:14 and 3.2:13 into Eq. 3.3:7 for S=0 results in

$$J_{total} = j\omega\epsilon E_{10} + \rho_0\mu_{0B}\left\{\frac{1}{1+j\omega\tau_m} + \frac{\gamma_1}{1+j\omega\tau_n}\right\} \qquad (3.3:8)$$

where τ_m = momentum relaxation time

$$\mu_{oB} = \frac{\mu_o}{1+(\mu_o B)^2}$$

and the approximation $\omega\tau_m \simeq \frac{\omega}{\nu_t} \frac{1-(\mu_o B)^2}{1+(\mu_o B)^2} \ll 1$

as defined in Eq. 3.2:1 has been used.

The method for calculating μ_o in the presence of a magnetic field was presented in Sec. 2.4. Further using the approximation $\omega\tau_n \ll 1$ allows Eq. 3.3:8 to be written in the form

$$J_{total} = \left\{ j\omega\epsilon_1 + \sigma_o(1+\gamma_t) \right\} E_{1o} \qquad (3.3:9)$$

where $\sigma_o \equiv \rho_o \mu_{oB}$

and $\epsilon_1 \equiv \epsilon \left\{ 1 - (\sigma_o/\epsilon)(\tau_m + \gamma_t\tau_n) \right\}$

Measurement by Pence and Kahn [60] indicated that the value for (ϵ_1/ϵ) is in the order of 3 to 5. Similar results were obtained by Rees [53] theorectically. From the definition of ϵ_1, it implies that

$$(\tau_m + \gamma_t\tau_n) < 0 \quad . \qquad (3.3:10)$$

To lend physical insight into the problem, the relationship

$$1 + \gamma_t = \frac{E}{\bar{v}} \frac{d\bar{v}}{dE} \qquad (3.2:21)$$

is used, resulting in

$$J_{total} = \left\{ j\omega\epsilon_1 + \sigma_o \frac{E}{\bar{v}} \frac{d\bar{v}}{dE} \right\} E_{1o} \qquad (3.3:11)$$

where $\epsilon_1 \equiv \epsilon \left\{ 1 - \frac{\sigma_o}{\epsilon} \left[\tau_m + \left(\frac{E}{\bar{v}} \frac{d\bar{v}}{dE} - 1 \right) \tau_n \right] \right\}$

The last expression for ϵ_1 provides a relationship

between the effective dielectric constant and the static conductance with τ_m and τ_n as parameters. The latter could be evaluated if ϵ_1 is measured experimentally. This is considered in more detail in Sec. 4.2 where the a-c experiments are discussed.

To proceed with finding the small signal admittance, the condition of total current density continuity, $J_{ext} = J_{total}$, where J_{ext} is the external circuit current, is applied at the cathode. Using J_{total} from Eq. 3.3:11,

$$J_{ext} = \left\{ j\omega\epsilon_1 + \sigma_0 \frac{E}{\bar{v}} \frac{d\bar{v}}{dE} \right\} E_{10} \qquad (3.3:12)$$

is obtained. The second boundary condition to be applied is that of having an ohmic contact at the cathode. This requires the total a-c electric field to vanish at the cathode. Rigorously, the total electric field would include all three modes corresponding to S=0 and $S1,2 \neq 0$. However, S2 represents a heavily attenuated backward wave. Its amplitude is negligible except near the anode region. In the analysis where S2 is included in the calculation of the small signal admittance, no improvement is found when compared to the case where S2 is neglected. Therefore, in the following formulations, the effect of S2 will not be considered. Neglecting contributions from S2, the total electric field at the cathode contact, z=0, is

$$E_{total} = E_{10} + E_{11}$$

$$= 0 \qquad (3.3:13)$$

or

$$E_{11} = -E_{10} \ . \qquad (3.3:14)$$

Away from the cathode,

$$E_{total} = E_{1o} + E_{11}\exp(S1z)$$
$$= E_{1o}\left\{1 - \exp(S1z)\right\}$$
$$= \frac{J_{ext}}{j\omega\epsilon_1 + \sigma_o \frac{E}{\bar{v}}\frac{d\bar{v}}{dE}}\left\{1 - \exp(S1z)\right\} \qquad (3.3{:}15)$$

where Eqs. 3.3:11 and 3.3:12 have been used. Define the voltage across the sample as

$$V \equiv \int_o^L E_{total}\, dz \qquad (3.3{:}16)$$

and the device electronic admittance as

$$Y_d \equiv \frac{I_{ext}}{V}$$
$$= \frac{I_{ext}}{\int_o^L E_{total}\, dz} \qquad (3.3{:}17)$$

Substitution of E_{total} from Eq. 3.3:15 into Eq. 3.3:17 and evaluating the integral yields

$$Y_d = \left\{ j\omega C_1 + G_1 \right\}\left\{ \frac{S1L}{1 + S1L - \exp(S1L)} \right\} \qquad (3.3{:}18)$$

where $C_1 \equiv (\epsilon_1 A/L)$

and $G_1 \equiv (\sigma_o A/L)\ \frac{E}{\bar{v}}\frac{d\bar{v}}{dE}$

are the effective small signal capacitance and conductance respectively. Under the condition that $Re(S1L) \ll -1$, resulting in $\left\{1 + S1L - \exp(S1L)\right\} \cong S1L$, $Y_d = \left\{j\omega C_1 + G_1\right\}$ is obtained. In this case, the equivalent circuit represent-

ation for the device would simply be C_1 in parallel with G_1 as shown in Fig. 3.3:1. As expressions for C_1 and G_1 show, their values are independent of frequency. As the bias voltage is increased, Re(S1L) becomes less negative, the second term in Eq. 3.3:18 modifies the C_1 and G_1 values such that they become frequency dependent. Fig. 3.3:2 shows the plots of Y_d as a function of frequency using the values of S1 shown in Fig. 3.2:2. As observed in the figure, Y_d represents a constant conductance in parallel with a constant capacitance at zero bias (Fig. 3.3:2a). As the bias voltage is increased, the conductance is reduced while the capacitance is increased, both becoming frequency dependent (Figs. 3.3:2b, c and d). In the last figure, it is observed that G_d is negative only for a certain frequency range. The frequency at which G_d first becomes negative is at $f \simeq 13.6$ GHz. At this particular bias voltage $\bar{v} \simeq 1.39 * 10^7$cm/sec, resulting in $(\bar{v}/L) \simeq 1.39 * 10^{10}$/sec, verifying the usual statment that G_d first becomes negative at $f \simeq (\bar{v}/L)$. The value for $\bar{v}$ was calculated from

$$\bar{v} = \frac{I}{A\rho_o} \quad , \qquad (3.3:19)$$

and is the average drift velocity for the entire system of carriers.

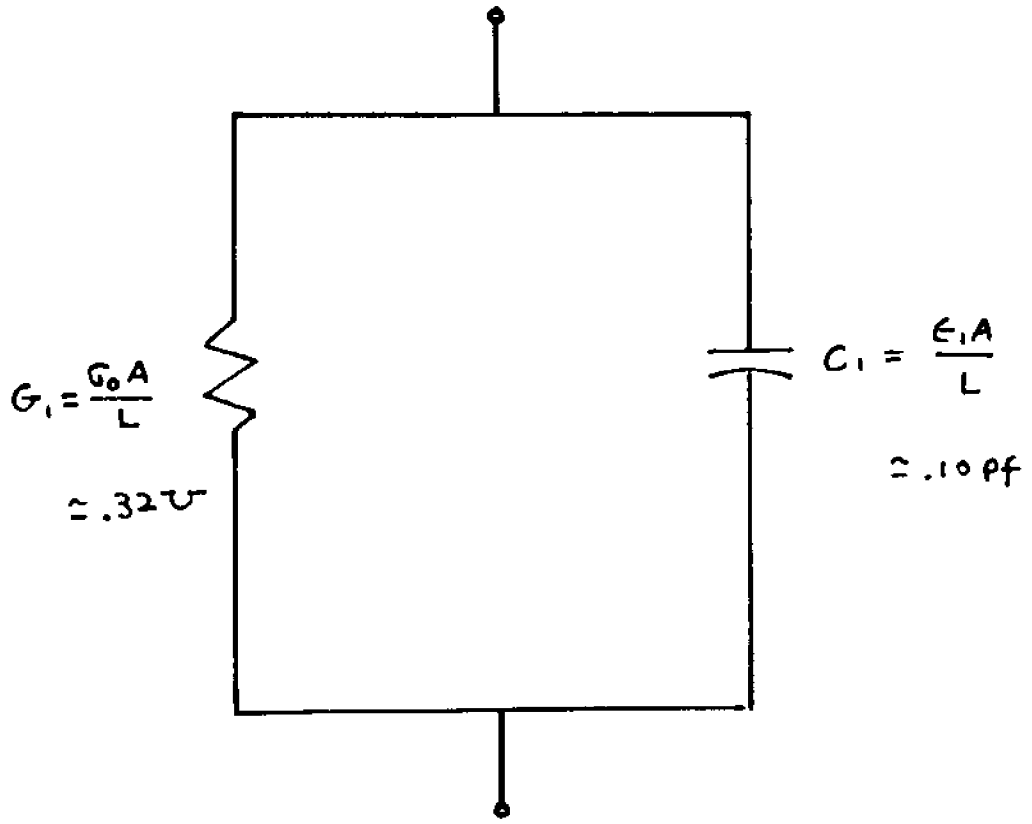

FIGURE 3.3:1 APPROXIMATE DIODE EQUIVALENT CIRCUIT AT ZERO BIAS

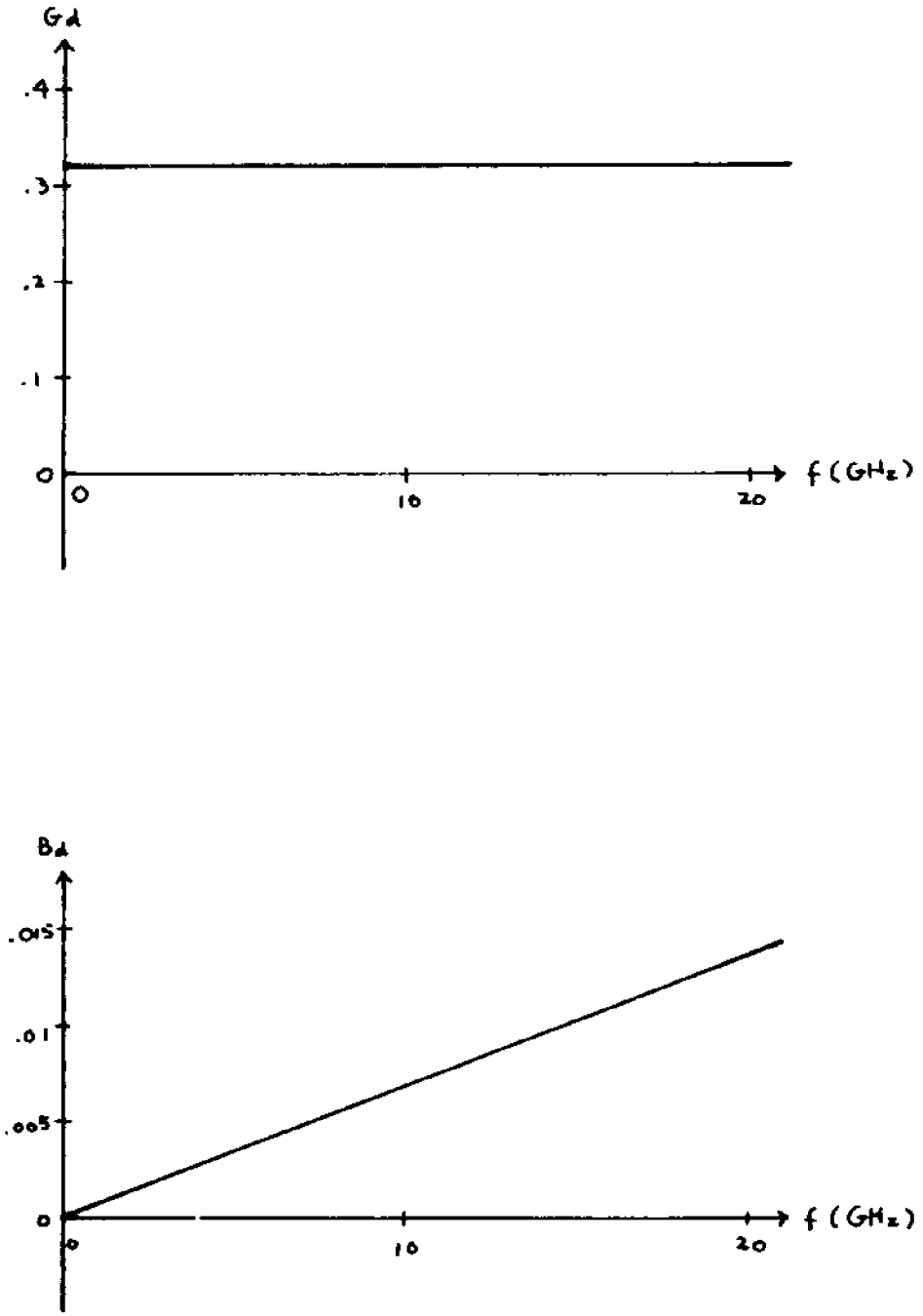

FIGURE 3.3:2a SMALL SIGNAL ADMITTANCE (Y_d) VS. FREQUENCY

V=0

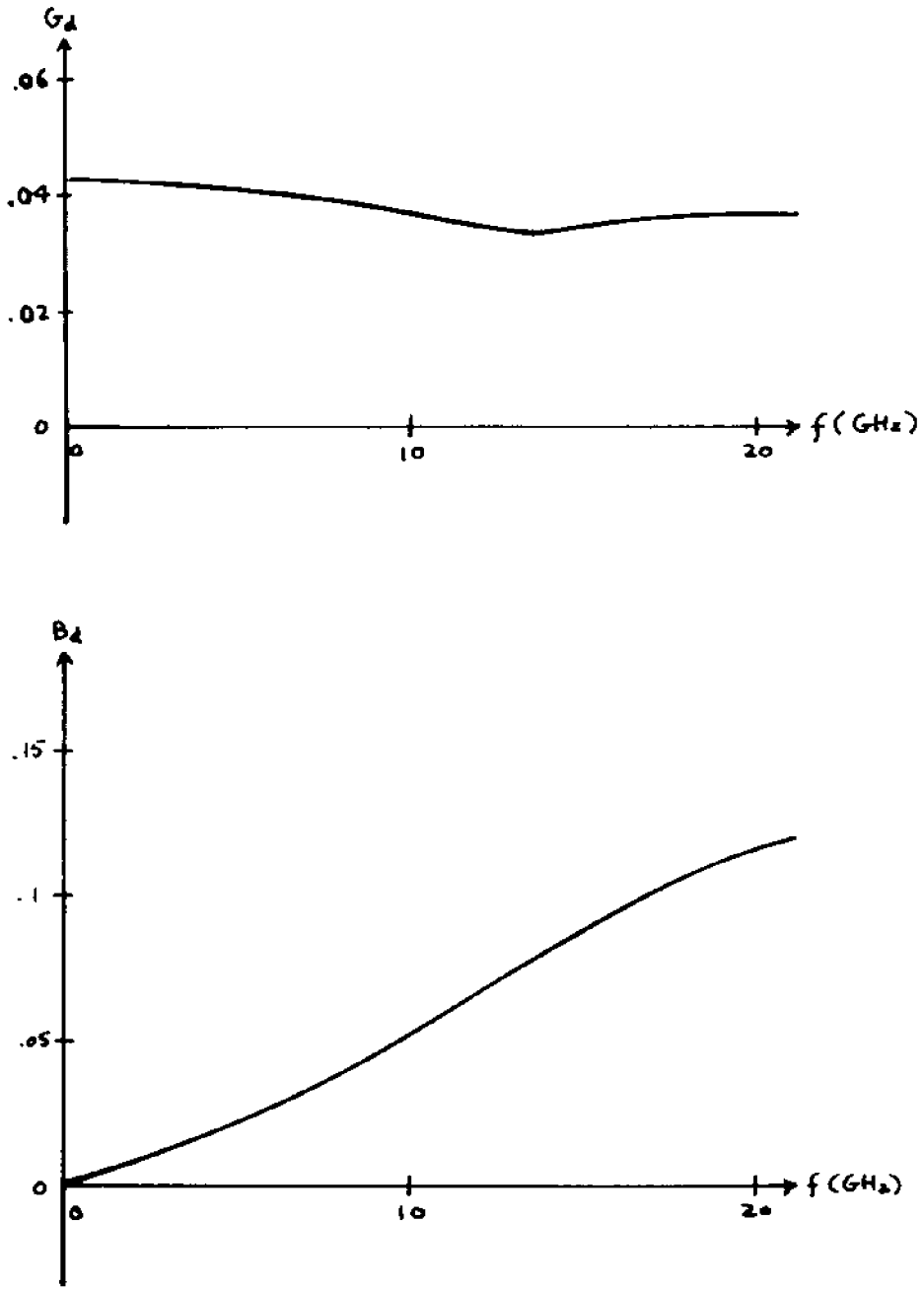

FIGURE 3.3:2b V=3.7 VOLTS

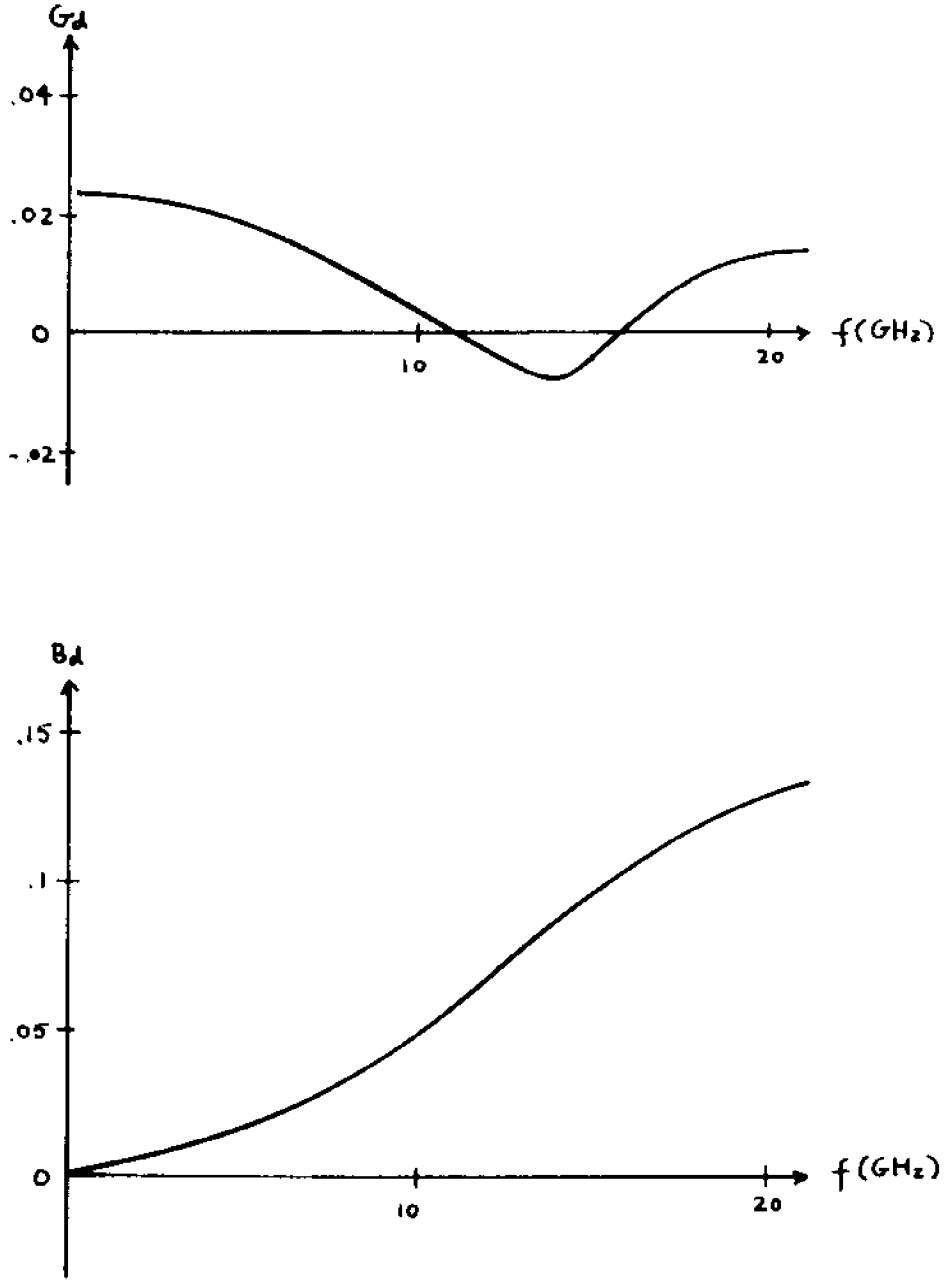

FIGURE 3.3:2c V=4.05 VOLTS

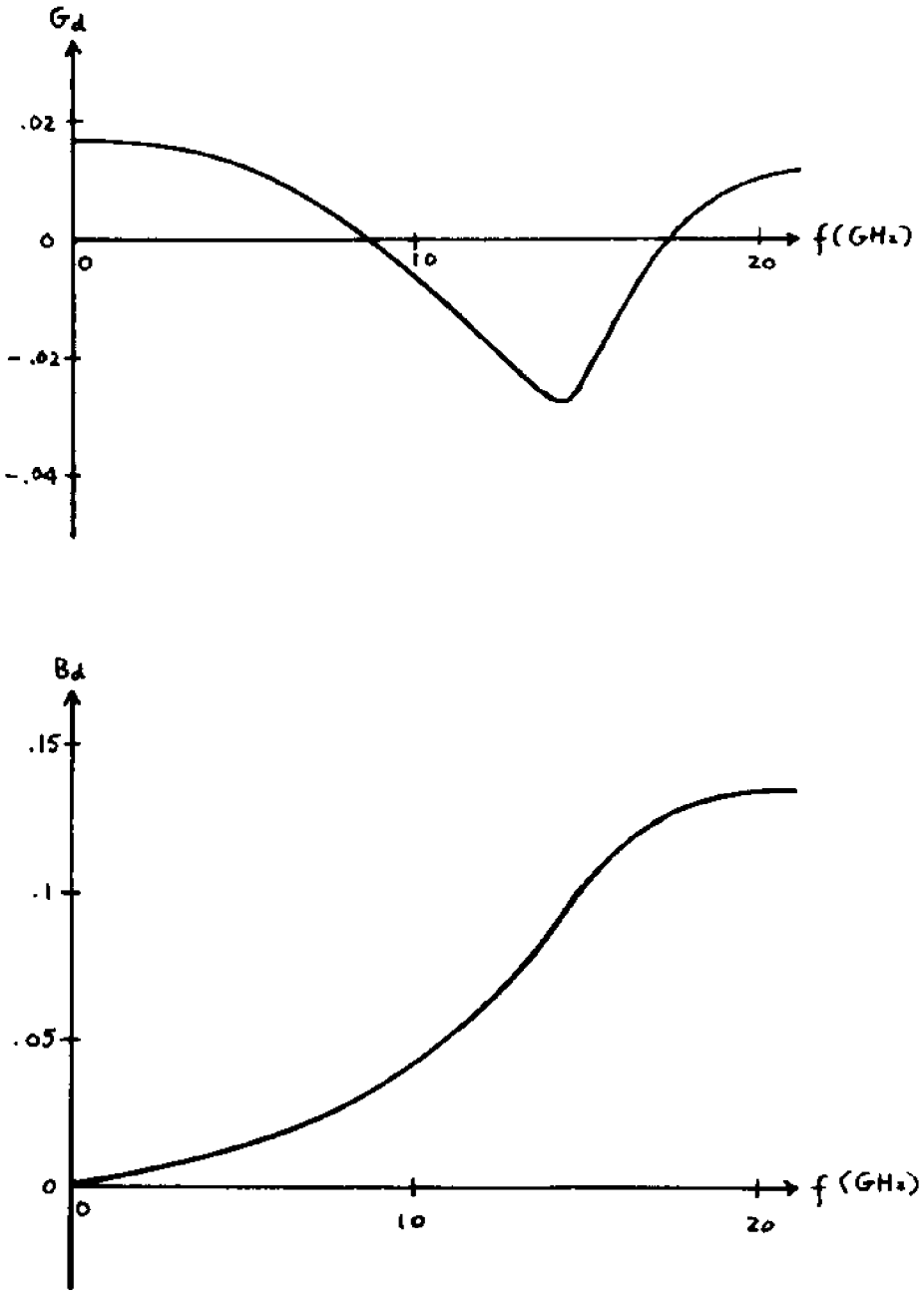

FIGURE 3.3:2d V=4.16 VOLTS

CHAPTER 4 SMALL SIGNAL AMPLIFICATION MEASUREMENTS

4.1 Modeling of the Microstrip Circuit and Package Parasitics

The structure of the microstrip circuit used to hold and bias the Gunn diodes is shown in Figs. 4.1:1a,b,c. In Fig. 4.1:1a, the 50 Ω line is coupled directly to the HP 8410-A microwave network analyzer. Other instruments in the system include the HP 8743-A reflection-transmission test unit, and the HP 8412-A (x-y) and HP 8414-A (polar) display units (Fig. 4.1:2). In Figs. 4.1:3 and 4.1:4, the cutaway views of the package and the GaAs sample itself are shown. A proposed equivalent circuit model is shown in Fig. 4.1:5. To model the packaged diode with lumped circuit elements for the X-band, it is necessary to include

1. the ribbon lead inductance L_p,
2. the ceramic capacitance C_p,
3. the phase shift inductance across the top cap L_c,
4. the capacitance between the top cap and the aluminum substrate C_c, and
5. the inductance introduced by the heat sink L_s.

The values for L_p and C_p were obtained from manufacturer's supplied data, with L_p = .3 nh, C_p = .27 pf. The series inductance introduced by the heat sink was calculated as a short section of transmission line terminated by a short

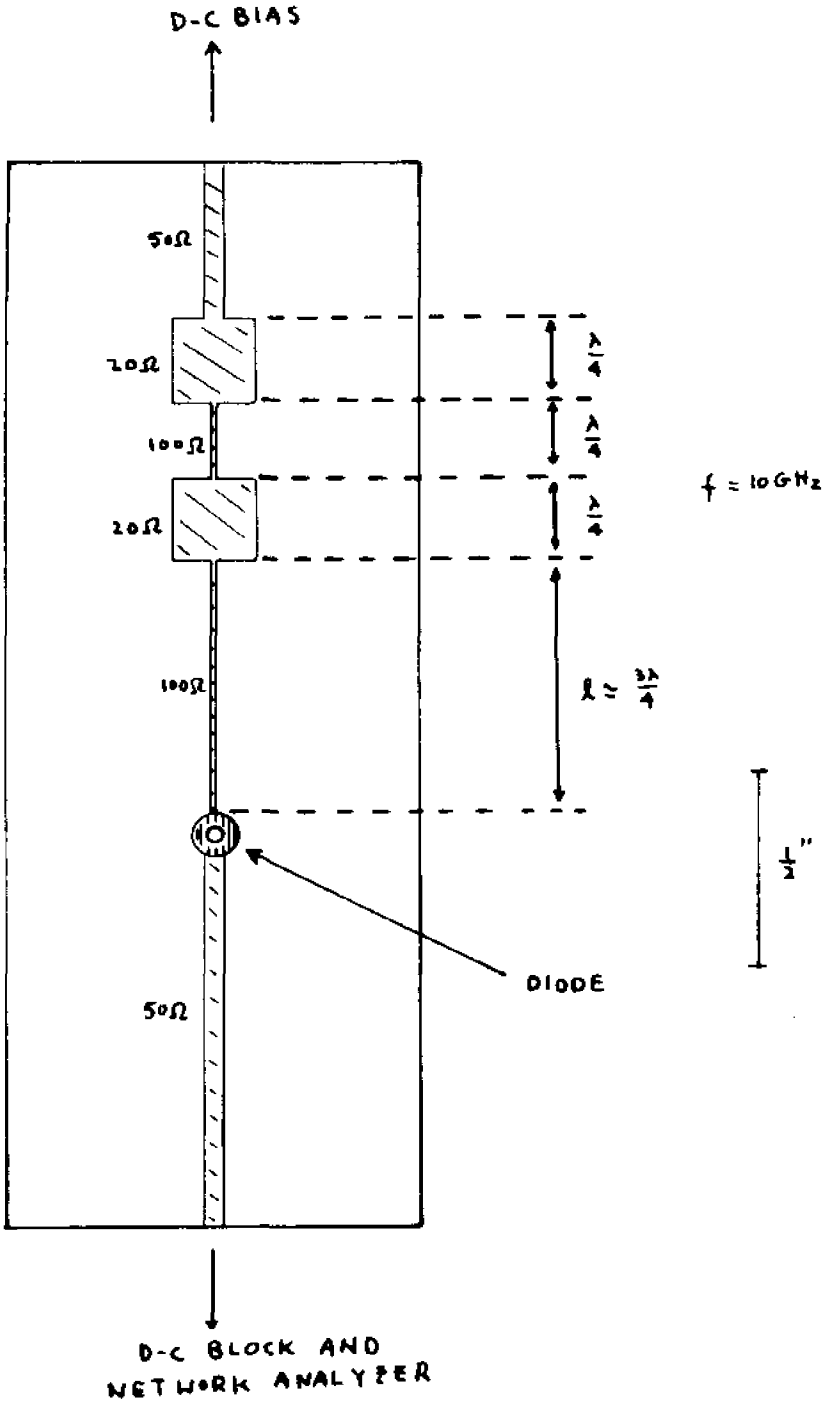

FIGURE 4.1.1a MICROSTRIP CIRCUIT

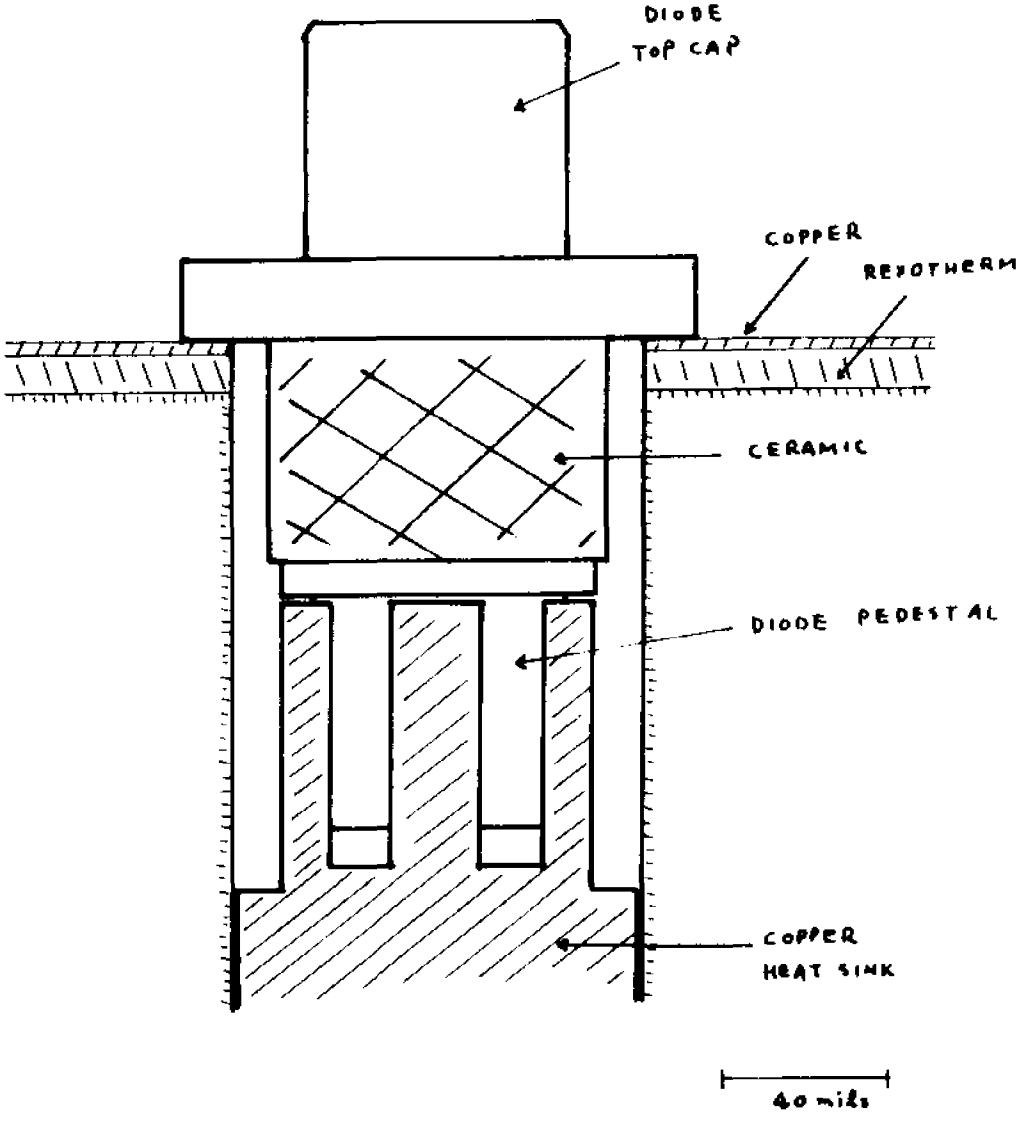

FIGURE 4.1.1b IMBEDDED GUNN DIODE

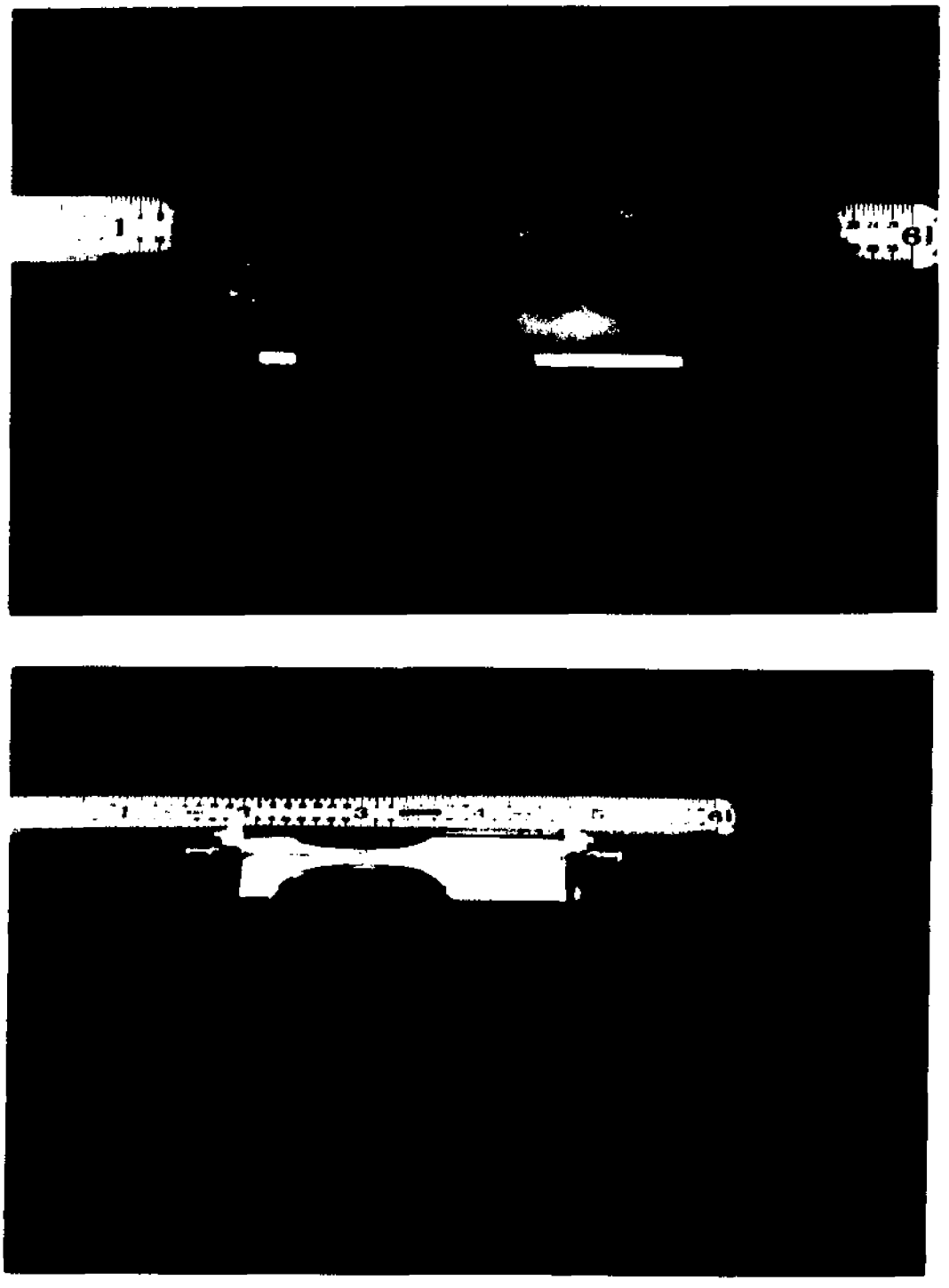

FIGURE 4.1:1c GUNN DIODE AMPLIFIER

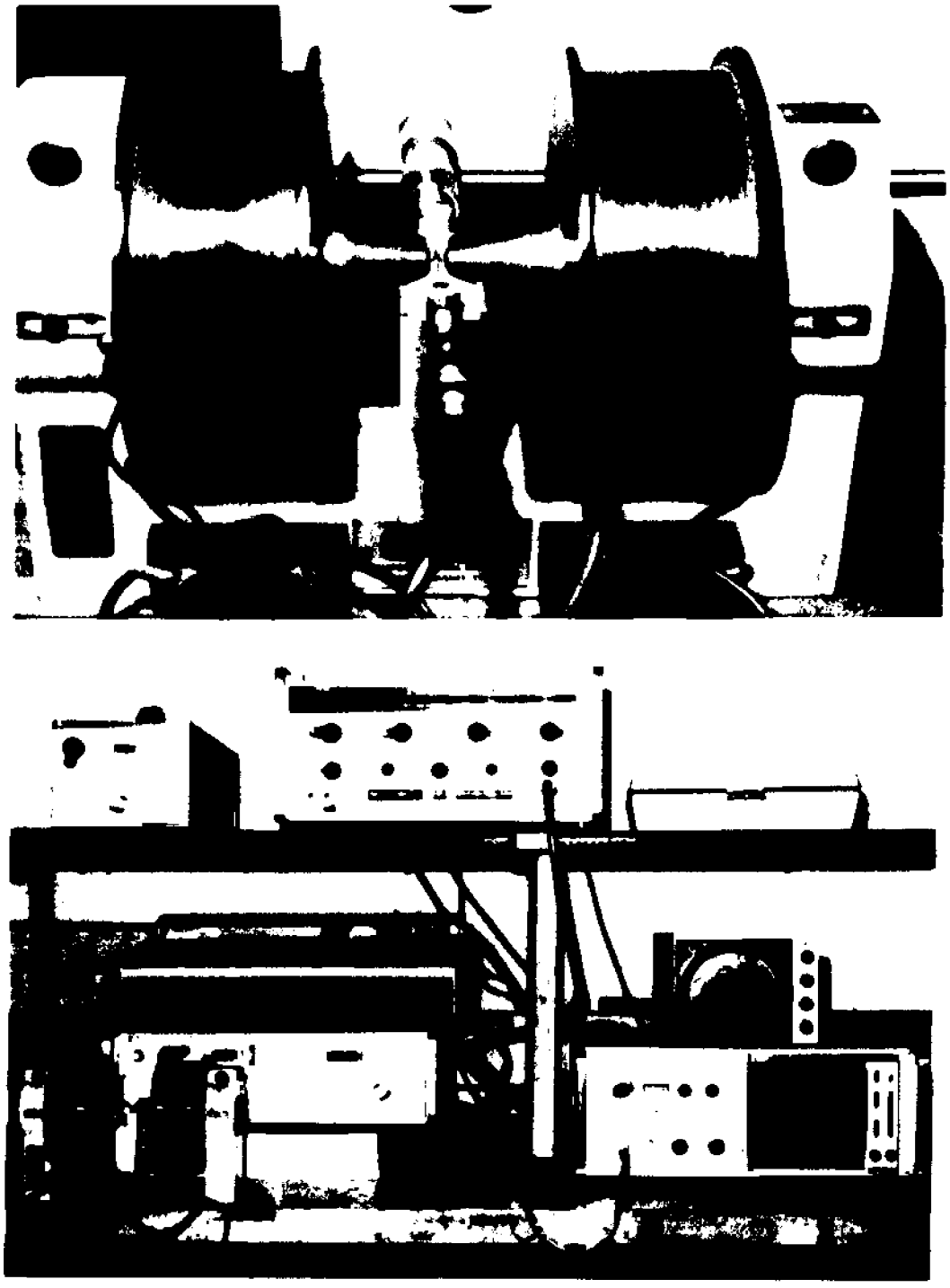

FIGURE 4.1:2 A-C MEASUREMENT SYSTEM

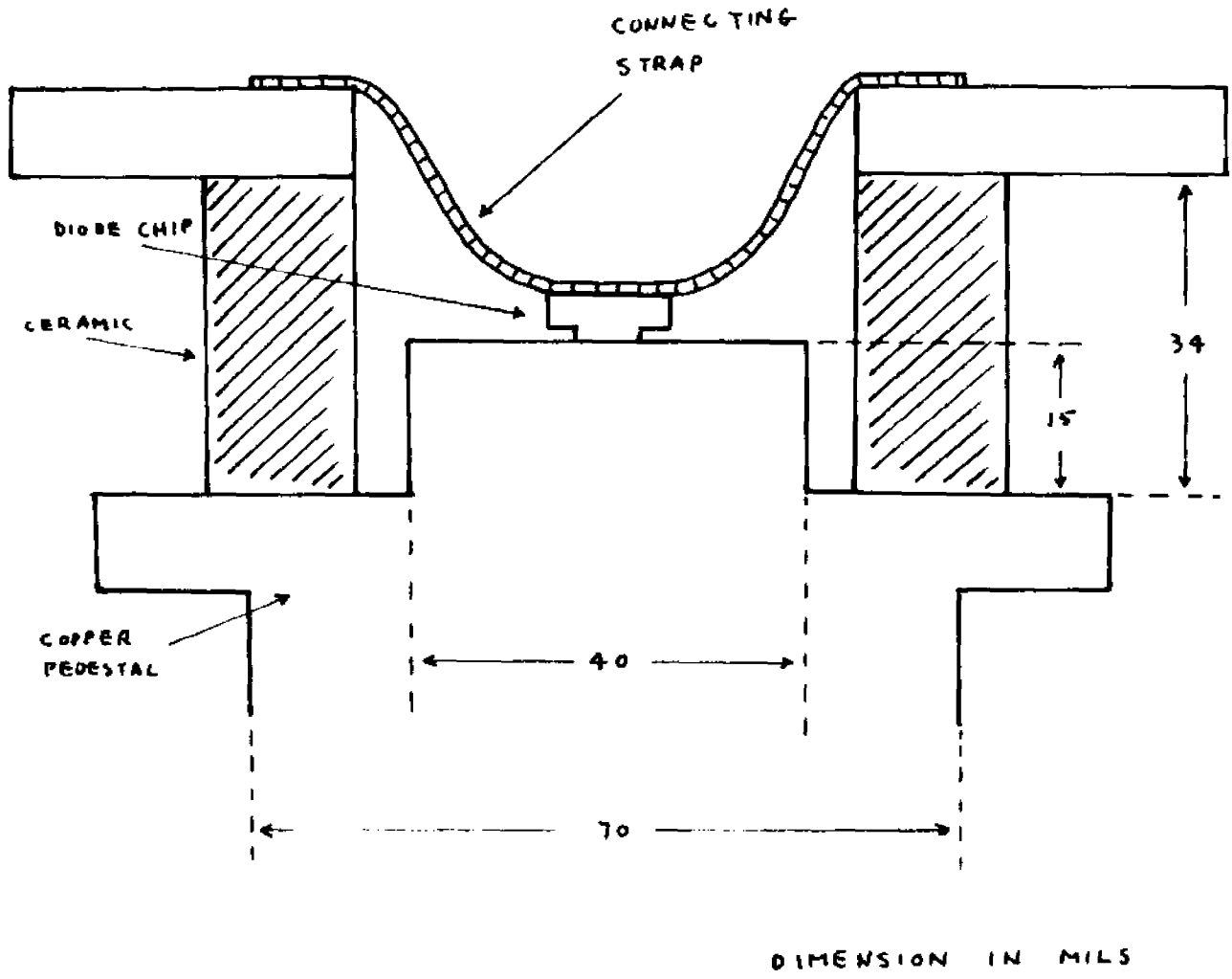

FIGURE 4.1:3 PACKAGED THERMO-COMPRESSION BONDED DIODE

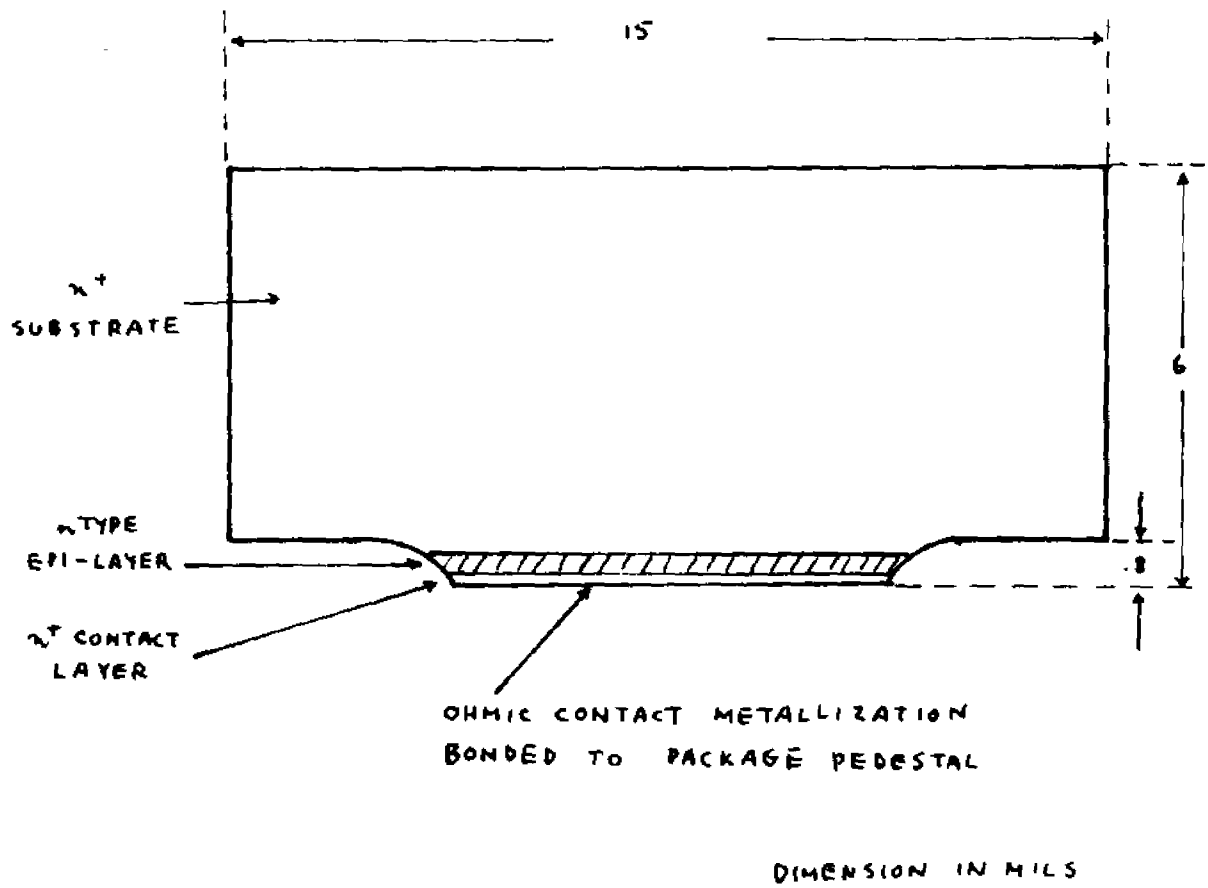

FIGURE 4.1:4 GaAs CHIP

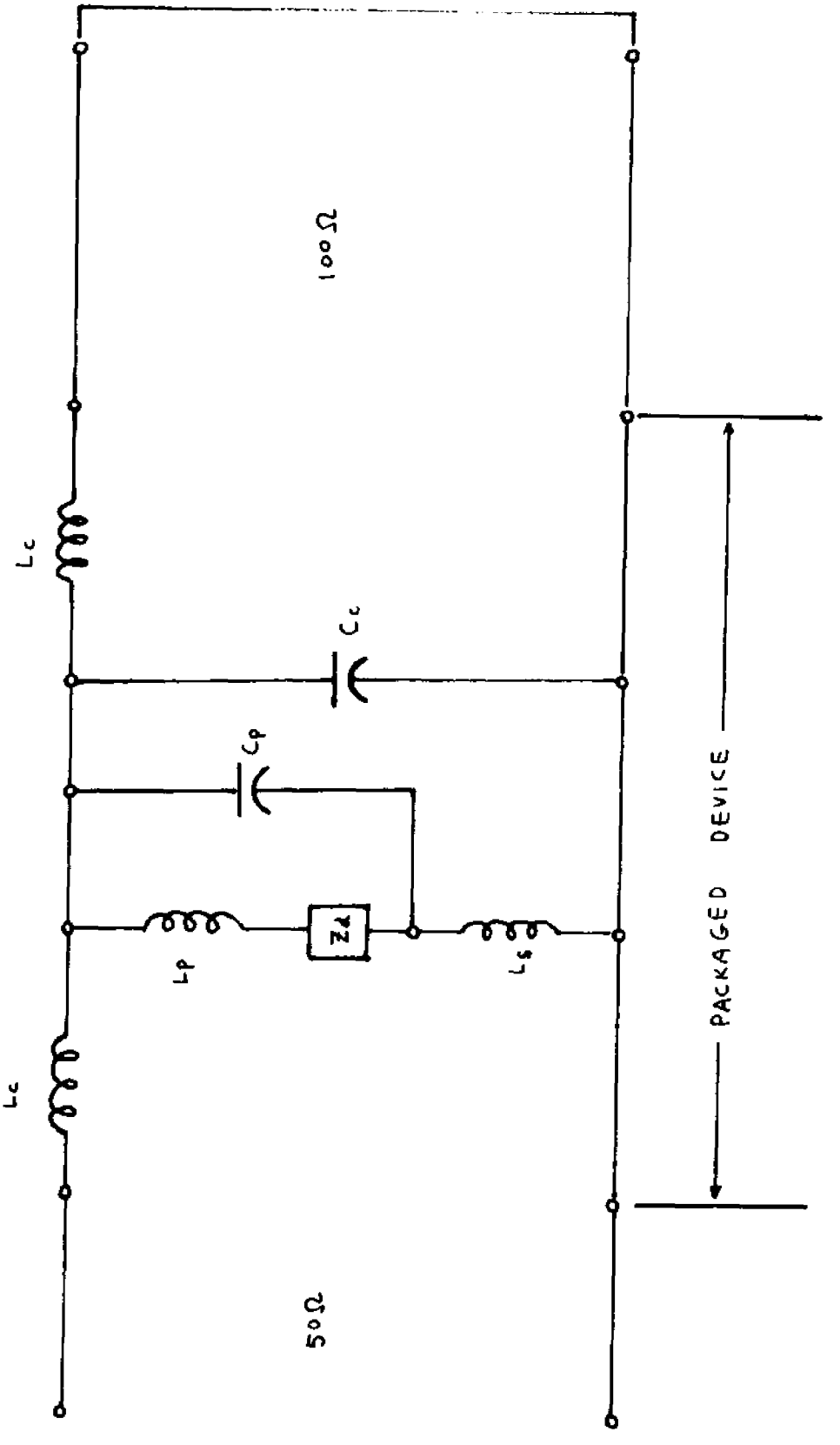

FIGURE 4.1.5 AN EQUIVALENT CIRCUIT MODEL

circuit (the aluminum substrate) [61]. The calculated value for L_s is L_s = .35 nh. Much of L_s may be eliminated by creating contact between the heat sink and the aluminum substrate all the way up to the base of the diode. Verification for the value of L_s may be obtained by measuring the packaged device impedance with and without L_s eliminated. The measured results are presented later on in this section. This leaves two parameters L_c and C_c, to be evaluated.

The short circuit is an approximation to the low impedence termination to the 100 Ω line. Experimental verification of this was obtained by measuring the admittance directly with the 50 Ω line uninterrupted by the diode. Normally, to find L_c and C_c, two measurements with

1. an open-incuited package, $Z_d \rightarrow \infty$, and
2. a short-circuited package, $Z_d \rightarrow o$

are made at each frequency. These two measured admittance (or impedance) values are substituted into the theoretical expression calculated using the lumped parameters, thus obtaining values for L_c and C_c. This must be repeated for all frequencies over the bandwidth of interest. However, calculated values for the admittance indicates that of the two resonant frequencies in X-band, C_c has a dominant effect on the parallel resonant frequency, $f_p(\angle\Gamma=0)$, and has negligible influence on the series resonant frequency, $f_s(\angle\Gamma=180^o)$; the opposite is ture for L_c. Therefore, it

is only necessary to pick C_c such that f_p agrees with the measured value and independently pick L_c to obtain agreement for f_s. Using this procedure, suitable values are found to be $L_c \simeq .12$ nh and $C_c \simeq .5$ pf. The calculated reflection coefficient using these values for L_c and C_c are plotted as a function of frequency over the entire X-band together with the measured values, Fig. 4.1:6. It is observed that resonable agreement is obtained for the frequencies of interest. Figs. 4.1:7 and 4.1:8 show the effects of varying C_c and L_c on f_p and f_s respectively. It verifies the earlier statement that varying C_c only varies f_p while varying L_c only has an effect on f_s.

The procedure outlined above allows all circuit parameters to be evaluted with a single measurement using a short-circuited package. There are two additional measurements which allows independent checks of the parameters. They are

1. measurement with the heat sink inductance shorted out which provides additional information on the value of L_s. This is shown in Fig. 4.1:9 where calculated values using L_s=0 are also displayed. The good agreement verifies the previously used value for L_s.
2. measurement with an open circuited package which provides additional verification of the model in general. This is shown in Fig. 4.1:10 together with the calculated values. The error in this

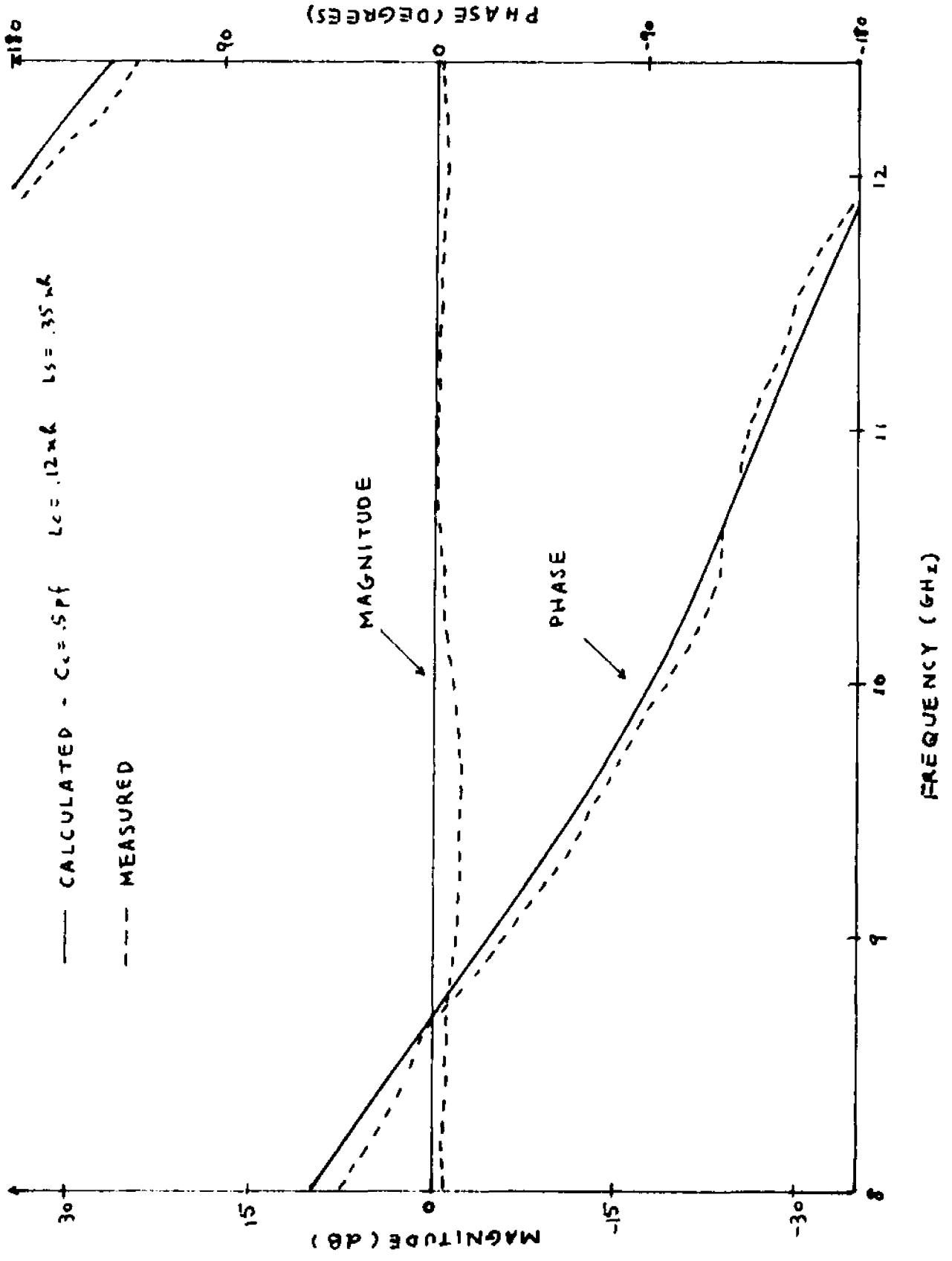

FIGURE 4.1.6 MEASURED AND CALCULATED Γ VS. FREQUENCY

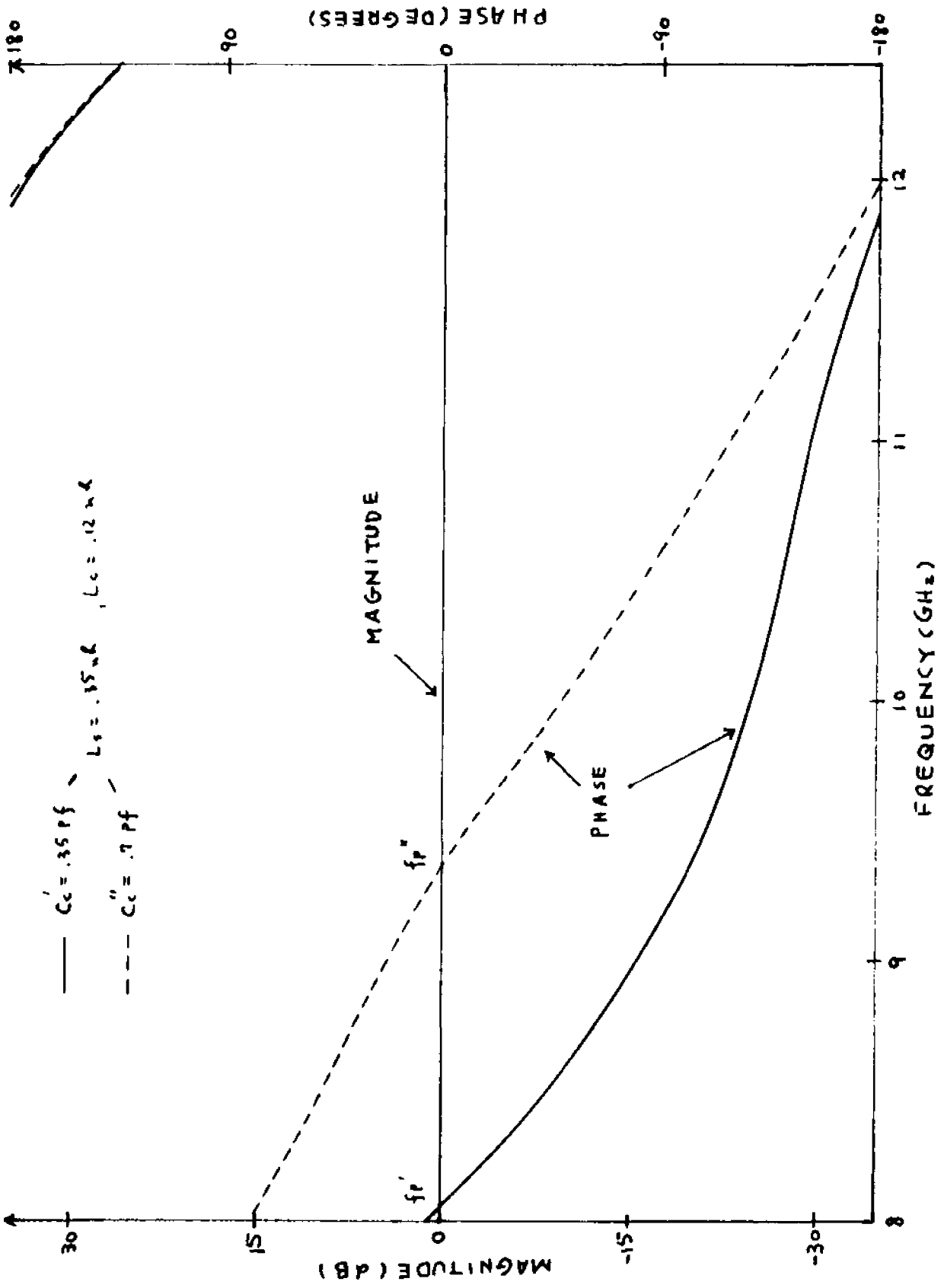

FIGURE 4.1:7 EFFECT OF C_c ON CALCULATED $\bar{T}$

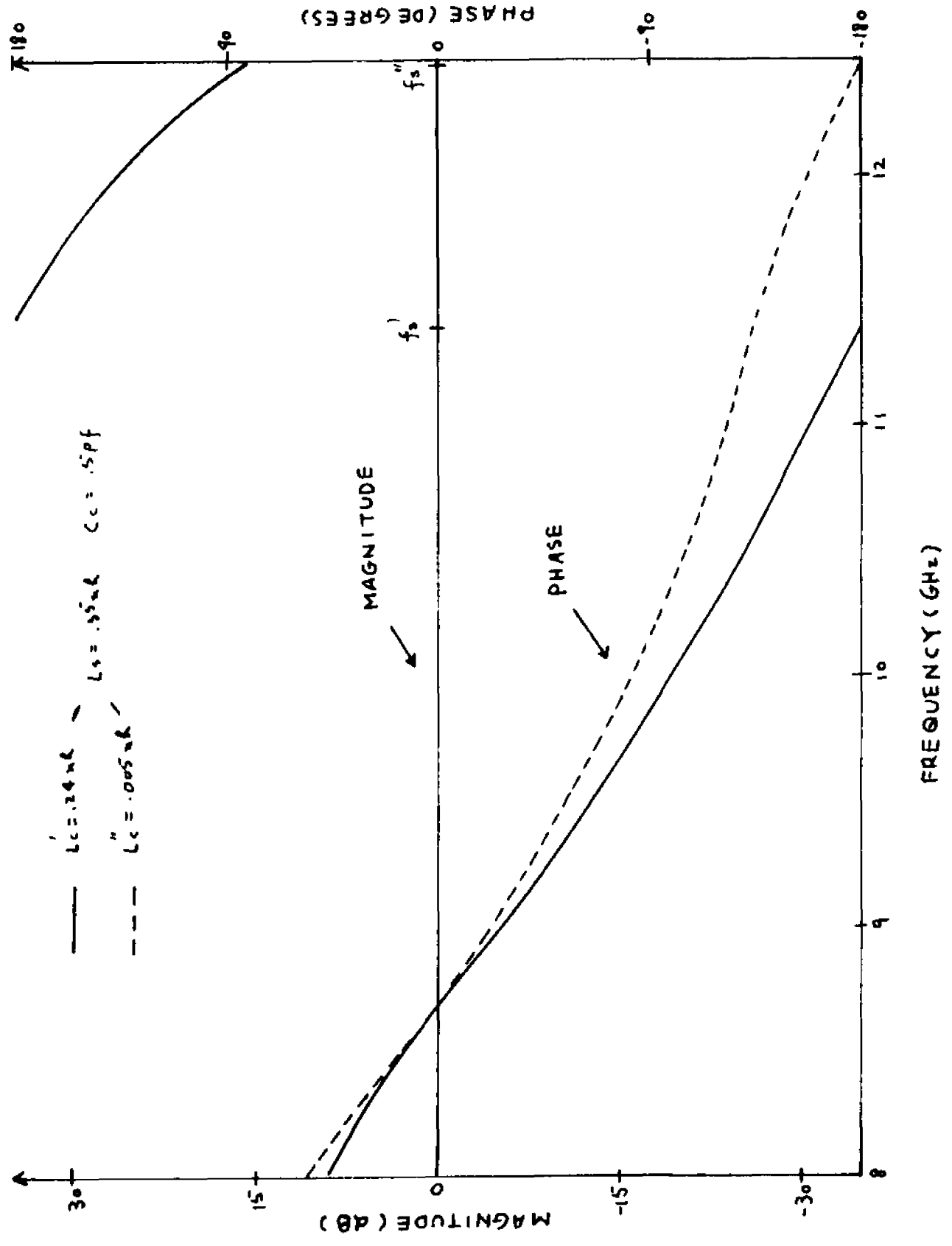

FIGURE 4.1.8 EFFECT OF L_c ON CALCULATED Γ

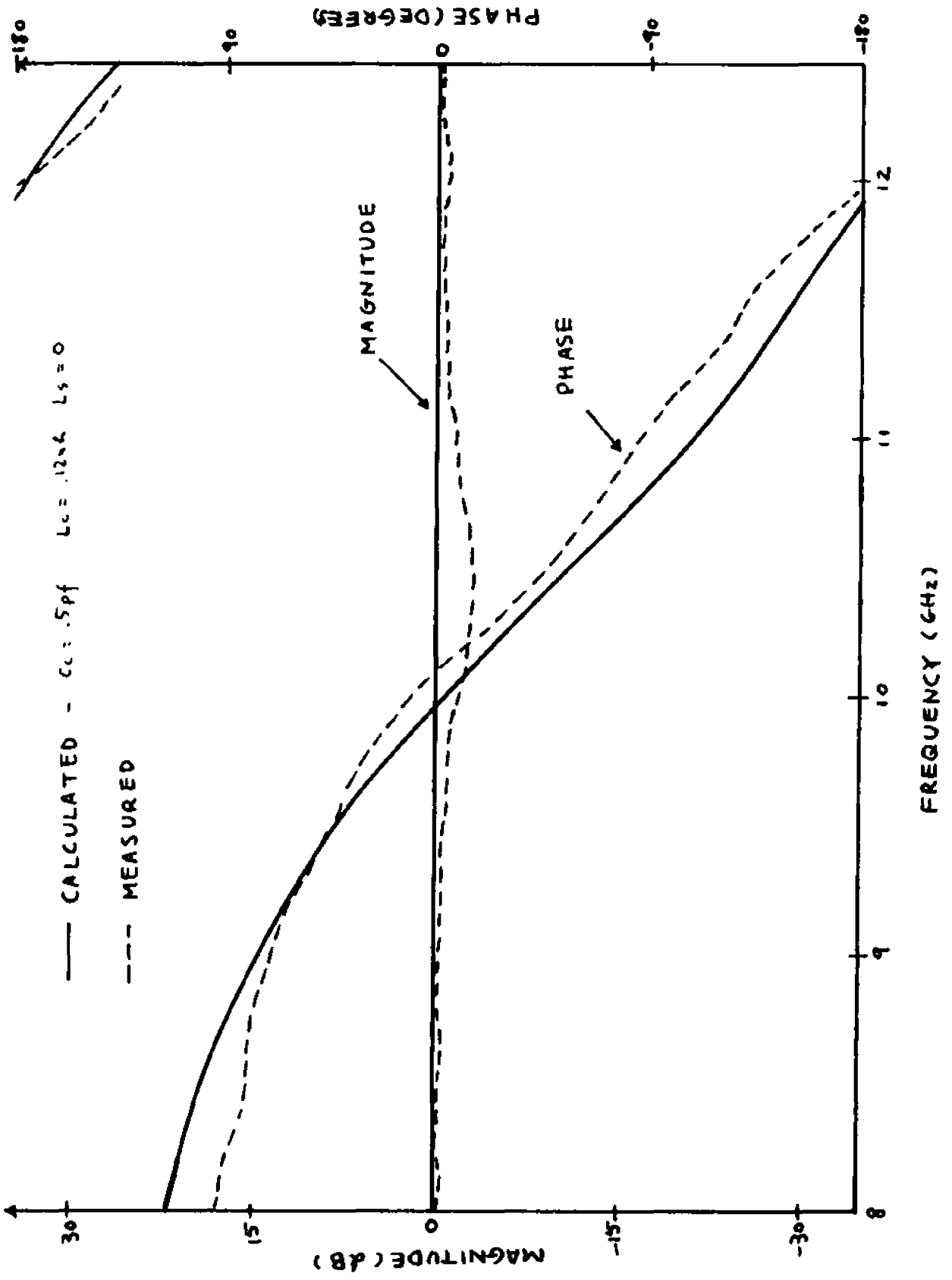

FIGURE 4.1:9 EFFECT OF REDUCING L_s ON Γ

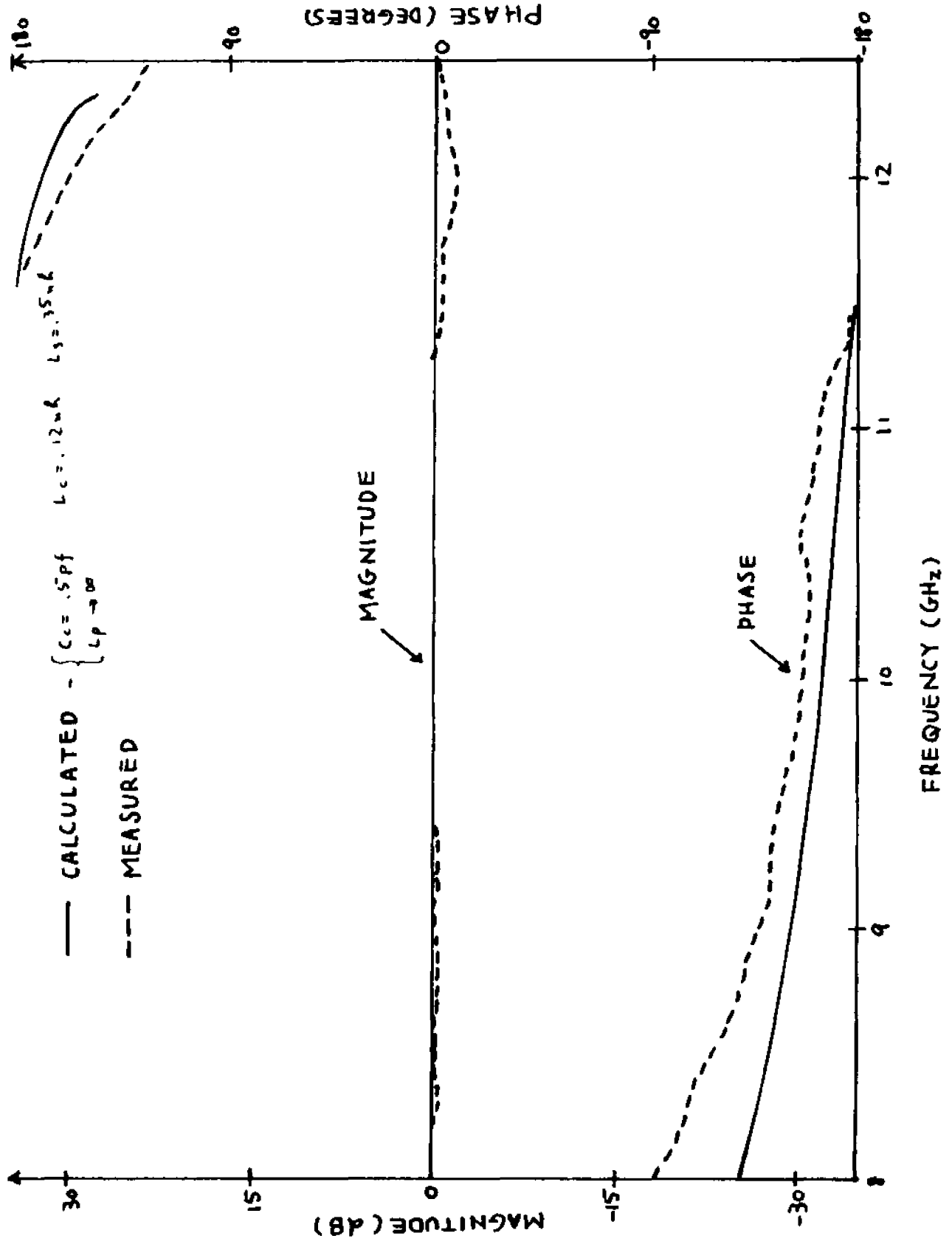

FIGURE 4.1:10 EFFECT OF ELIMINATING L_p ON $\overline{\Gamma}$ (OPEN CIRCUIT)

case is a little larger than that obtained for the measurement with the short-circuited package. However, in the actual circuit operation, the device admittance is rather low and resembles that of the short-circuited package ($Z_d \simeq 3\Omega$ at low bias). The more accurate result is believed to exist under such circumstances.

4.2 Small Signal Amplification Measurements (Zero Applied Magnetic Field)

Small signal measurements were made in the microwave circuit described and modeled in Sec. 4.2. The Gunn diode, together with the external microwave circuit, is connected as a load to the network analyzer. Since d-c voltages in excess of 3 volts may damage the test channel of the network analyzer, a d-c block in the form of a short section of X-band waveguide, is inserted to isolate the network analyzer from the d-c bias. The reflection coefficient, or its equivalent in admittance, is measured and recorded. The a-c signal, incident on and reflected by the Gunn diode, is on the order of .1 mW, which well approximates the small signal assumption. The measured results, as a function bias voltage at zero magnetic field, is first described qualitatively. At zero bias, the resistance of the diode itself is in the order of 3Ω. The measured admittance as a function of frequency resembles that obtained for a short-circuited package. Therefore, the

diode may be approximated by a short circuit, Fig. 4.2:1. As the biasing is increased, G_d decreases as revealed by the current saturation in the static V-I characteristic, Fig. 2.3:4. The susceptance B_d, which is no longer bypassed by a large G_d, becomes significant, Fig. 4.2:2. Increasing the bias voltage above the NDC threshold causes G_d to become negative, Fig. 4.2:3. If the magnitude of the NDC is small, B_d remains positive. However, $C_d=(B_d/w)$ and G_d become frequency dependent quantities. If the negative conductance becomes larger, theory predicts a resonant behavior at a frequency $f \simeq \overline{v}_o/L$ where B_d goes from positive to negative. However, this condition was never obtained in the measurements since the device supports an abolute instability (oscillations) well before the negative conductance reaches such a high value.

The measured reflection coefficients, as a function of the bias voltage, are shown in Figs. 4.2:4a, b, c and d. Calculated results, where the values of Y_d shown in Fig. 3.3:2 are used, are superimposed on the measured values which were plotted directly by an x-y recorder. The sharp variations in the measured values were introduced by the d-c block. This was confirmed by the zero bias measurements described in Sec. 4.1 where the d-c block was not employed. The device behavior, which has been described qualitatively earlier in this section are:

1. At zero or low bias, there is a parallel resonance

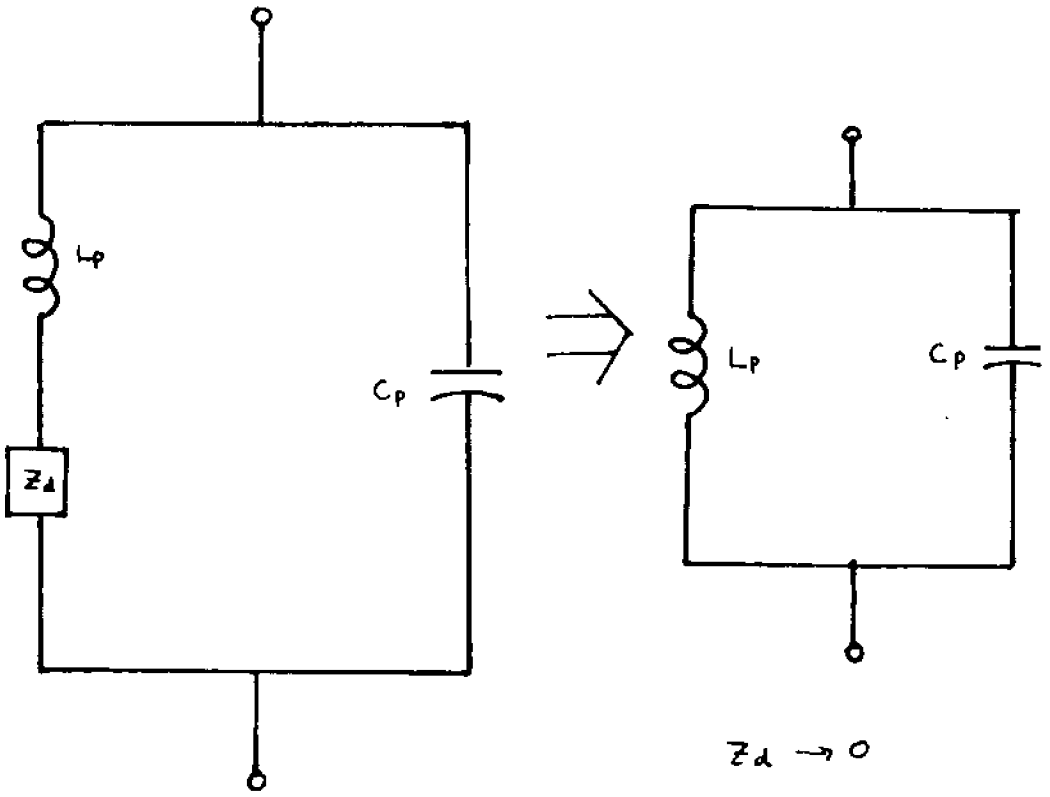

FIGURE 4.2:1 DIODE EQUIVALENT CIRCUIT AT LOW BIAS VOLTAGE (PACKAGED)

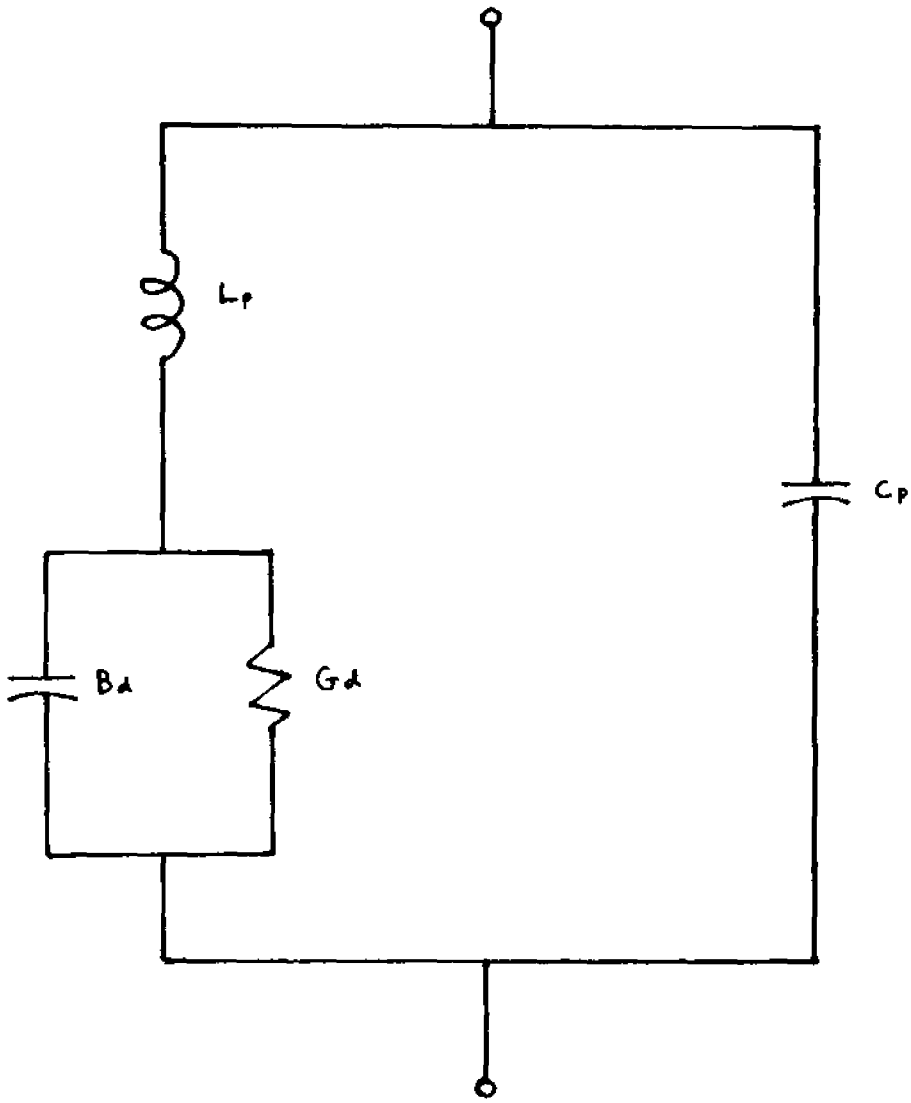

FIGURE 4.2.2 DIODE EQUIVALENT CIRCUIT AT INCREASED BIAS VOLTAGE (PACKAGED)

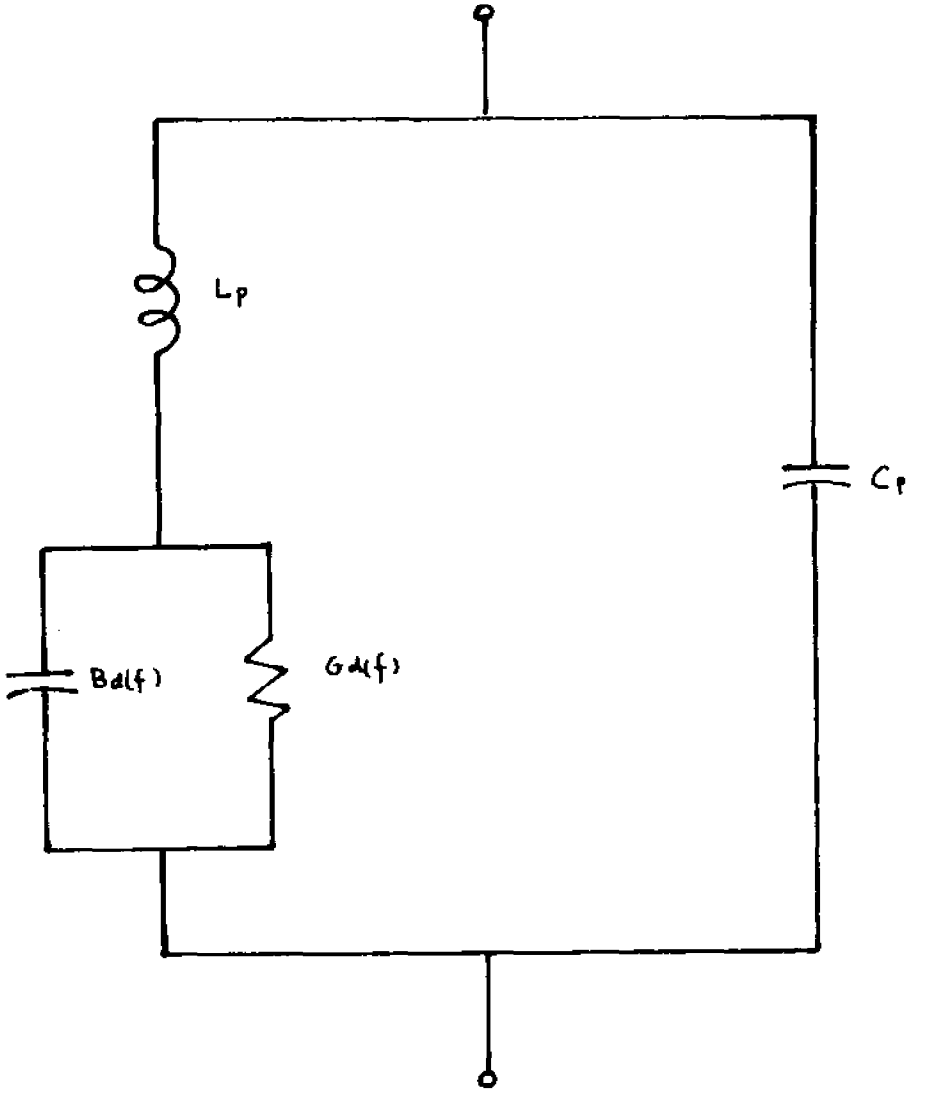

FIGURE 4.2.3 DIODE EQUIVALENT CIRCUIT AS BIAS VOLTAGE APPROACHES THE NDC THRESHOLD (PACKAGED)

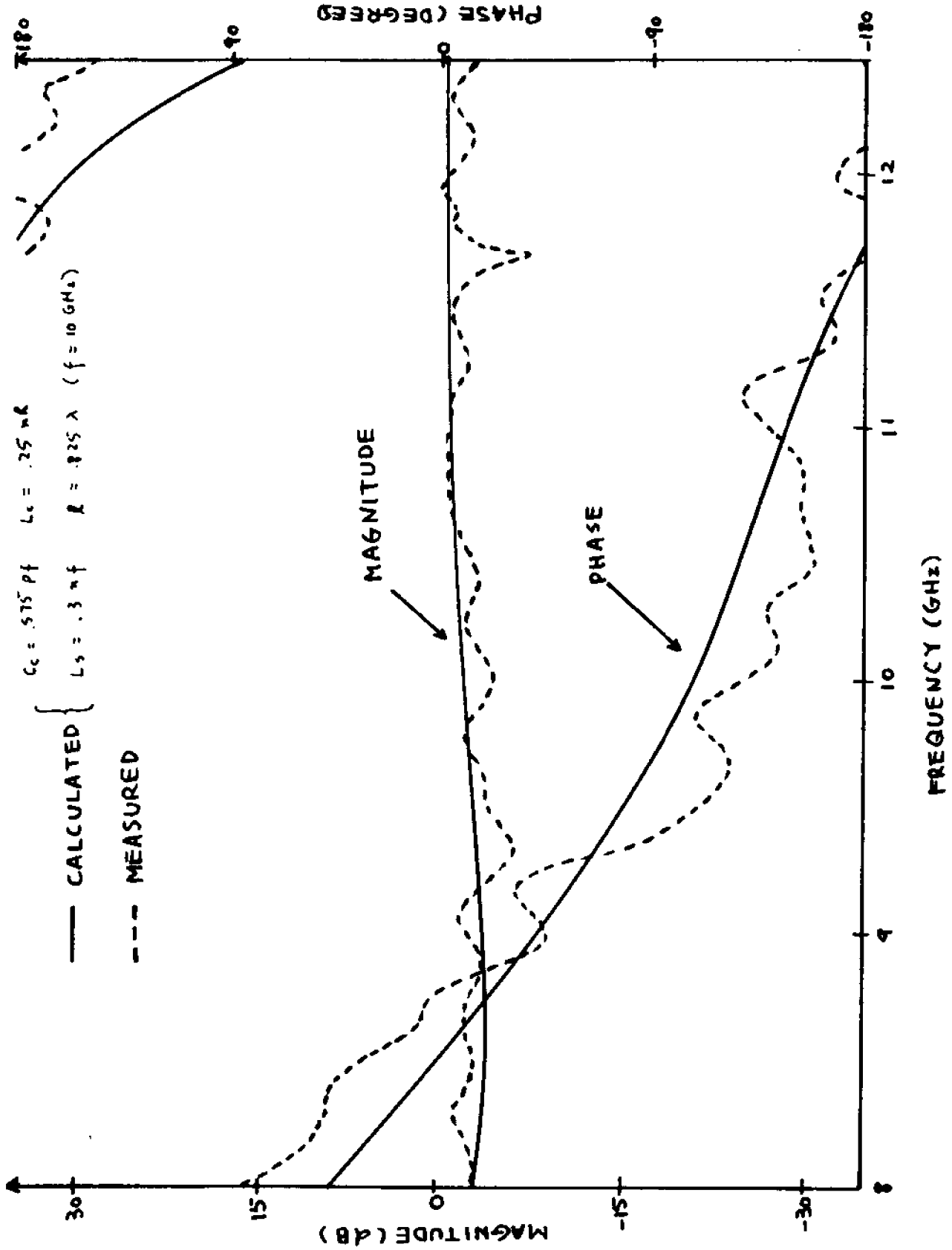

FIGURE 4.2:4a CALCULATED AND MEASURED $\overline{\Gamma}$ VS. FREQUENCY V=0

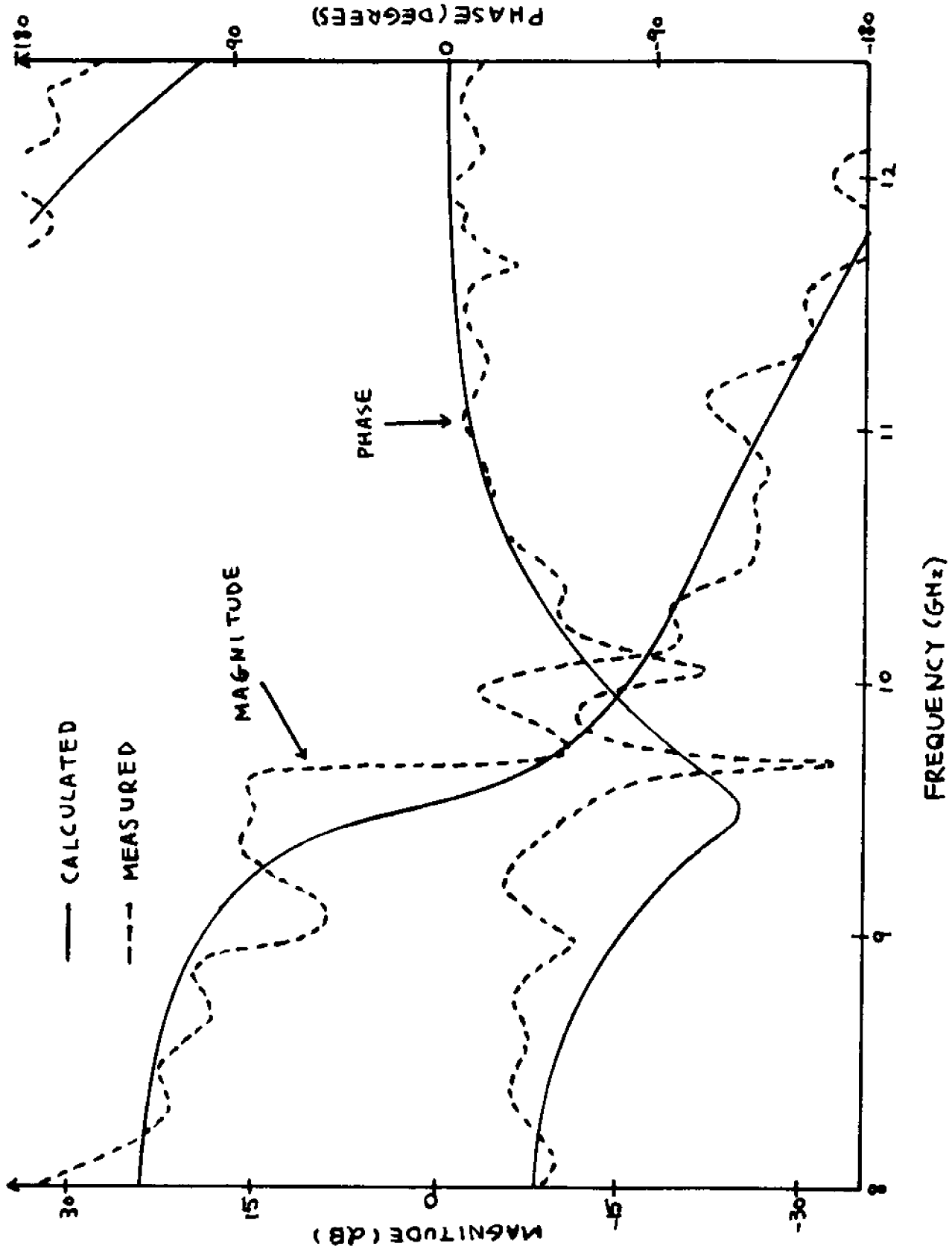

FIGURE 4.2:4b V=3.7 VOLTS

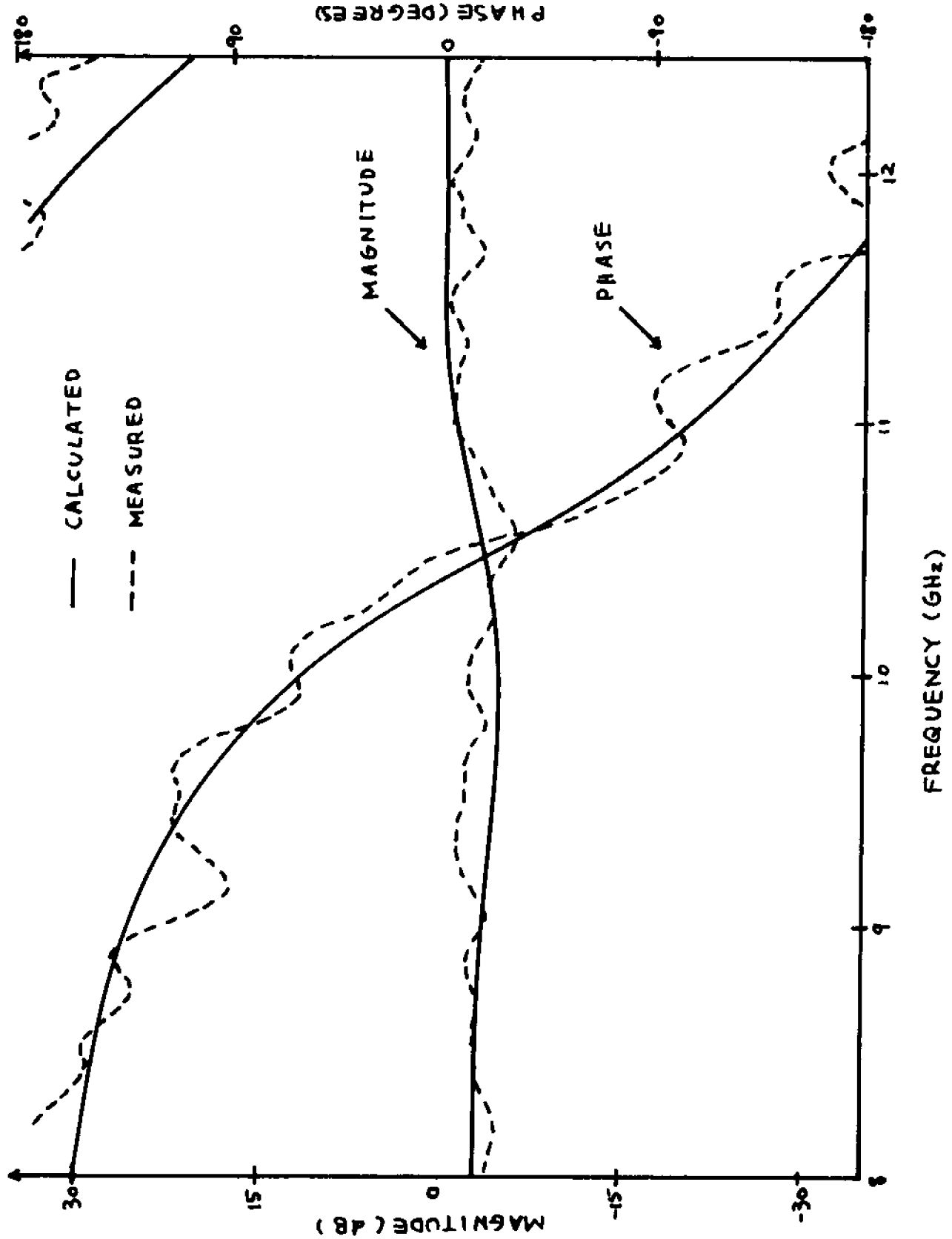

FIGURE 4.2:4c V=4.05 VOLTS

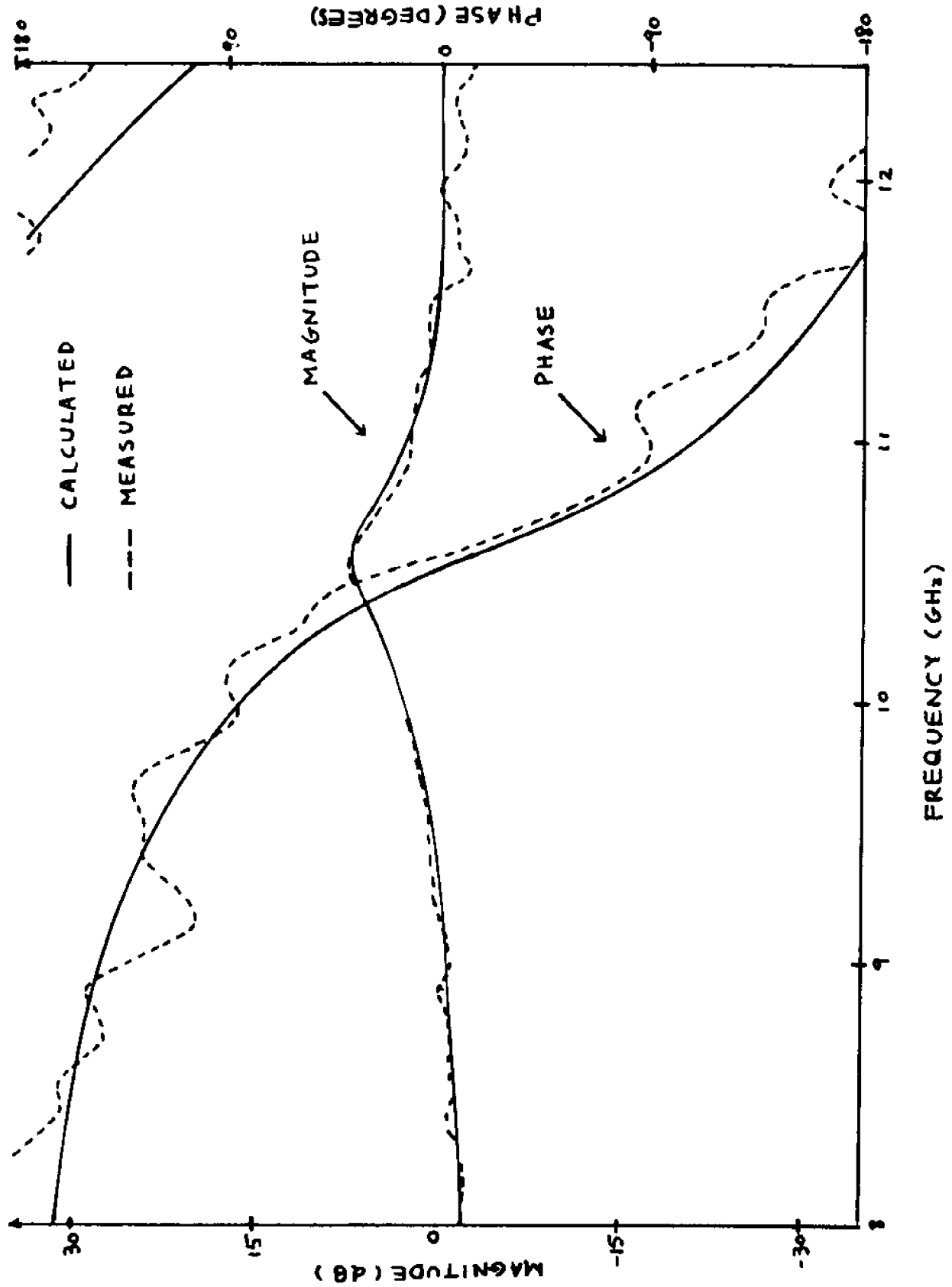

FIGURE 4.2:4d V=4.16 VOLTS

at $f \simeq 8.6$ GHz. Since the GaAs sample approximates that of a short circuit, the resonant frequency is primarily determined by the external microwave network.

2. As bias is increased, the conductance of the GaAs sample decreases while its capacitance increases. This increase in sample capacitance causes the resonant frequency to increase. This agrees with calculated variation as the figures show.
3. As the bias voltage is increased to $V \simeq 4.16$ volts, net gain occurs.

In this particular measurement, a reflection gain of only ~10 dB is obtainable before oscillations started. Another undesirable feature in this setup is that the operation becomes unstable when attempts are made to record the gain with an x-y recorder. The difficulty arises when after viewing the auto swept output on the network analyzer screen, the sweep oscillator is turned to manual sweep. The switching quite often causes oscillations to occur. A modified measuring scheme which eliminates these problems is presented following this discussion. For this particular measurement setup, only hand sketched gain curves as observed on the network analyzer screen are presented. They are shown in Fig. 4.2:5. The calculated gain curves are presented in Fig. 4.2:6 for comparison. These figures indicate that resonable agreement is obtained for gain as a function of bias and frequency.

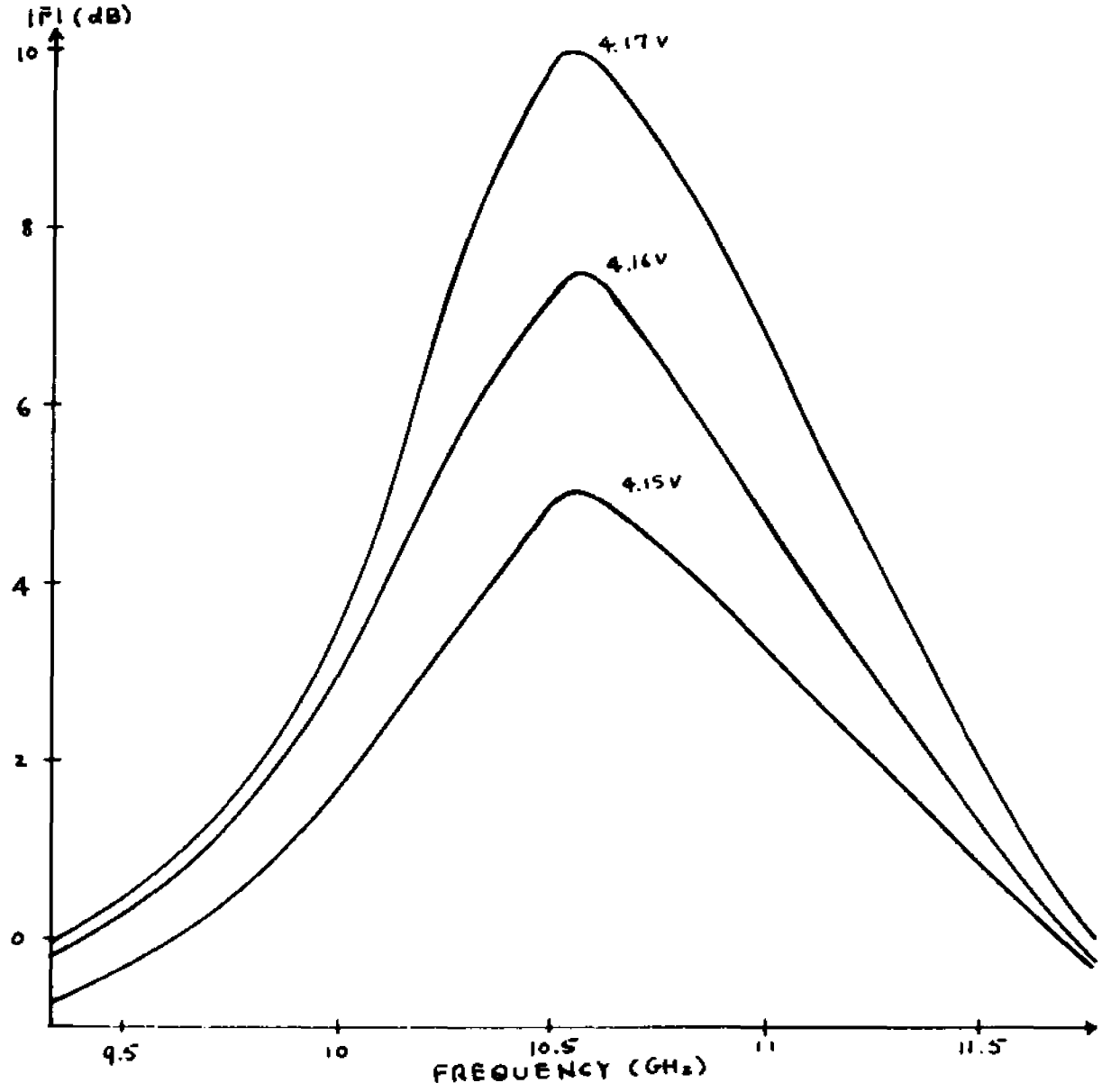

FIGURE 4.25 MEASURED $|\Gamma|$ VS. FREQUENCY WITH BIAS VOLTAGE AS PARAMETER

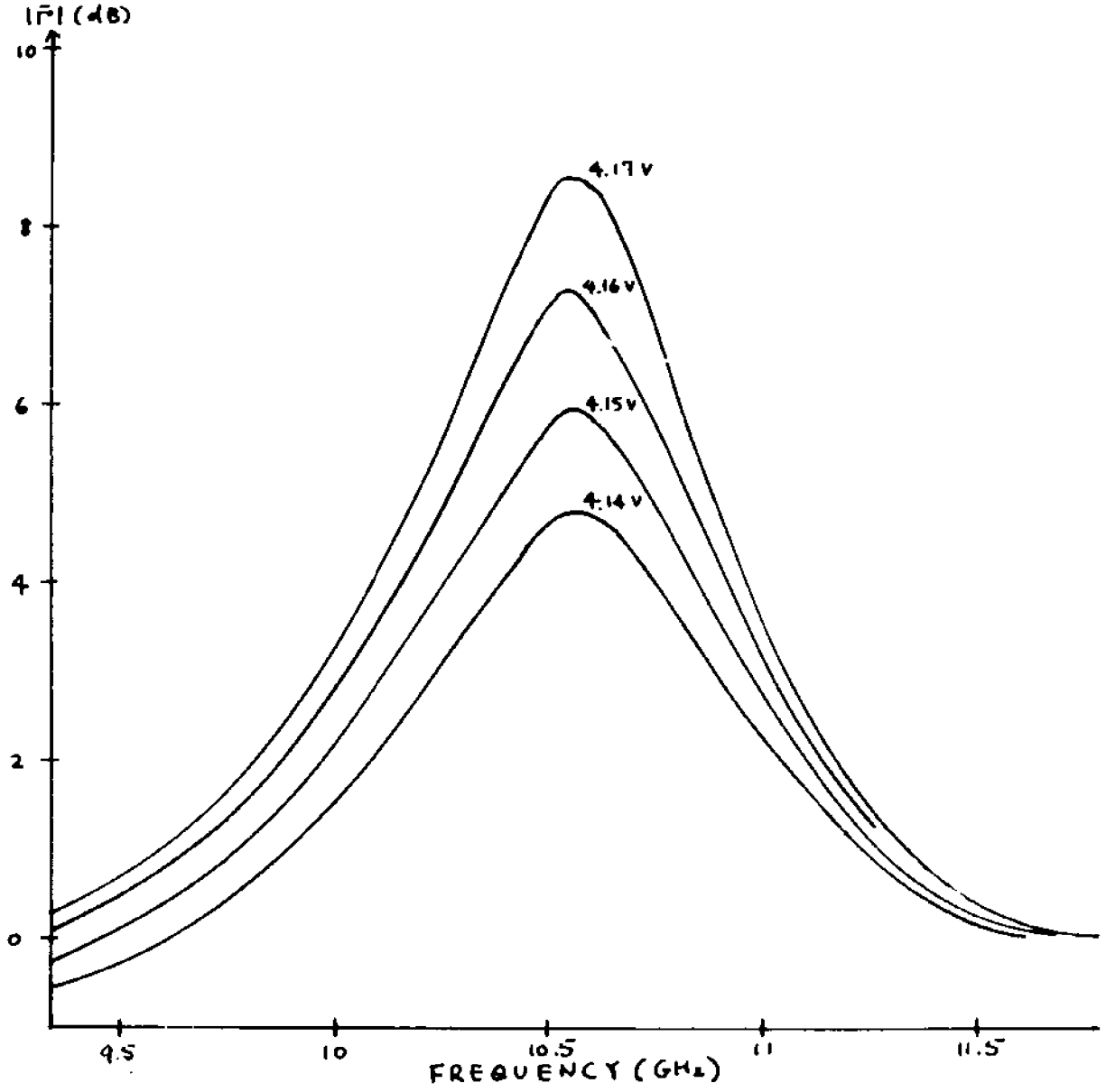

FIGURE 4.2.6 CALCULATED $|\Gamma|$ VS. FREQUENCY WITH BIAS VOLTAGE AS PARAMETER

A modified measurement system which replaces the short section of waveguide with a 10-dB attenuator alleviates the difficulties mentioned above. With the biasing not to exceed 5 volts, a 10-dB attenuation is adequate to prevent excessive d-c voltage at the network analyzer test channel. In this case, a gain of ~ 30 dB is obtained without instabilities. Furthermore, no difficulties were encountered when the x-y recorder was used to record the gain curves. The measured gain as a function of the bias voltage and frequency is shown in Fig. 4.2:7 . The calculated curves are presented in Fig. 4.2:8 . Comparison of Figs. 4.2:7 and 4.2:8 indicates that in the high gain region ($>$ 20 dB), the calculated gain curves show a sharper peak than the measured curves. This is likely to be due to large signal (non-linear) effects which has not been considered in this work. In the lower gain region ($<$ 15 dB), where the small signal (linear) analysis is more appropriate, better correlations are obtained.

In calculating the admittance, the value for $\bar{v}$ is obtained form Eq. 3.3:19

$$\bar{v} = \frac{I}{A\rho_o} \qquad (3.3:19)$$

To reconcile with the two-species model, this value of $\bar{v}$ is used as v_{oi} in the admittance expression. The agreement between theory and measurements indicates that this is a valid approach.

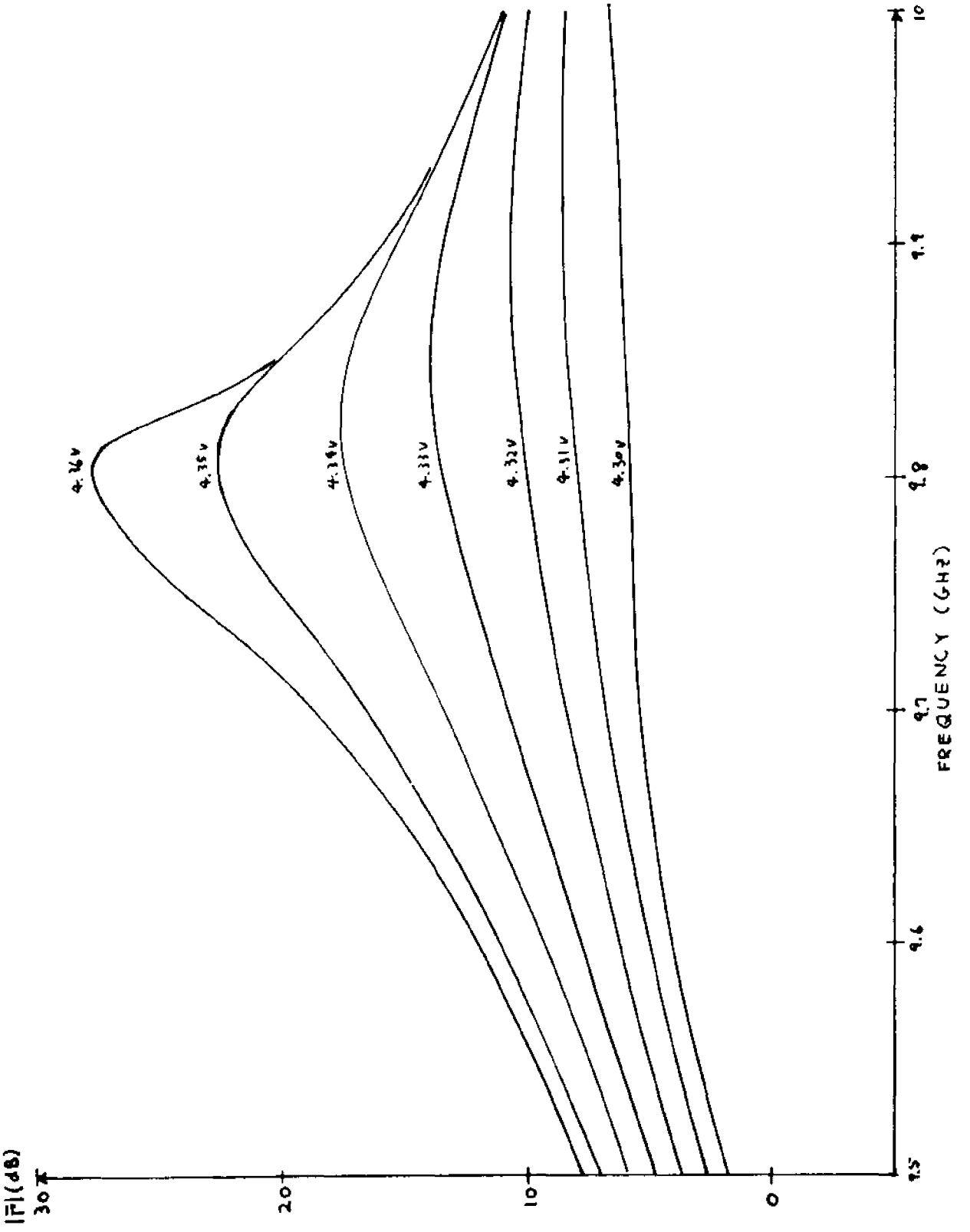

FIGURE 4.2:7 MEASURED |Γ| VS. FREQUENCY WITH BIAS VOLTAGE AS PARAMETER (WITHOUT D-C BLOCK)

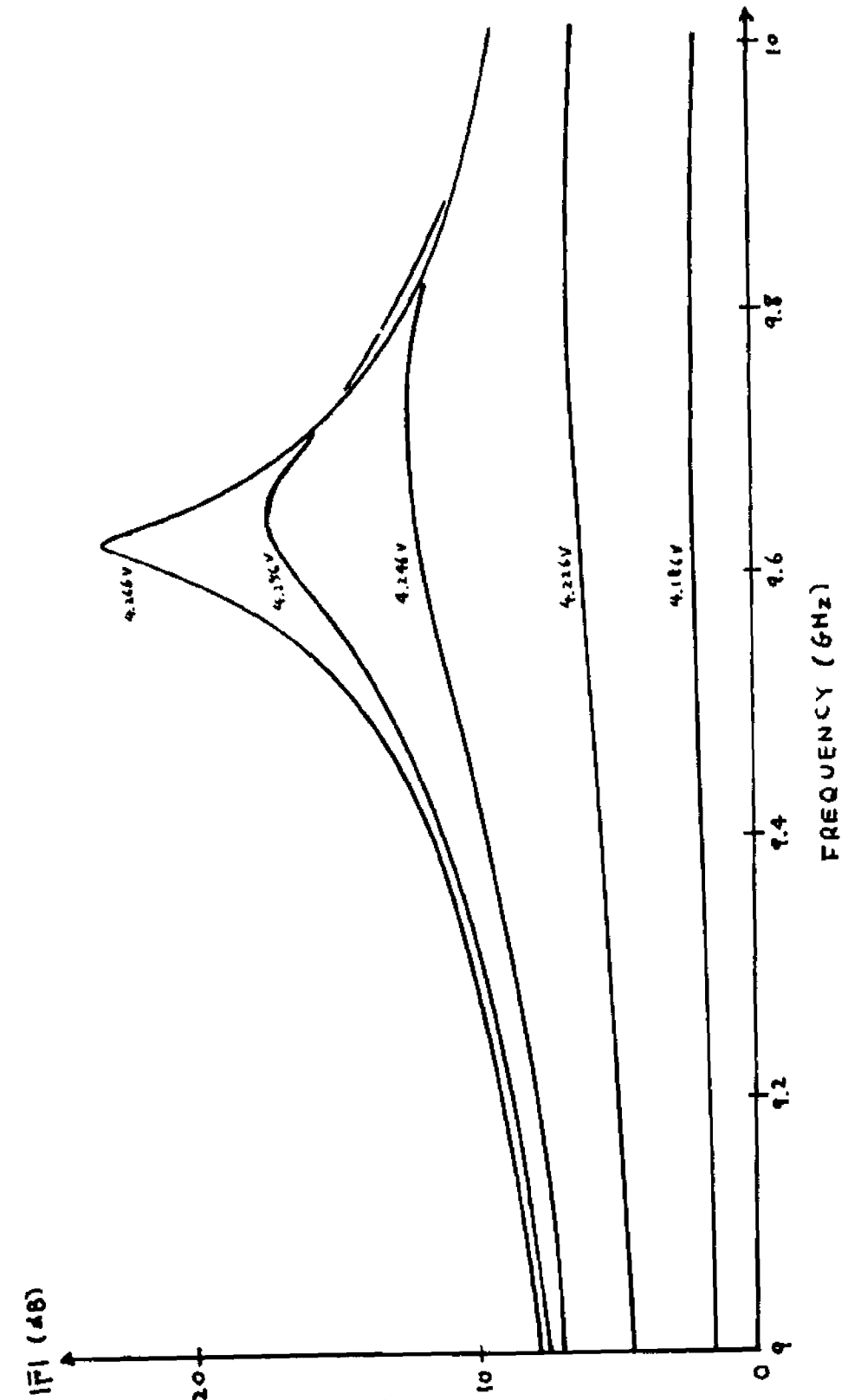

FIGURE 4.2.8 CALCULATED $|\bar{\Gamma}|$ VS. FREQUENCY WITH BIAS VOLTAGE AS PARAMETER (WITHOUT D-C BLOCK)

4.3 Small Signal Amplification Measurements (Effects of the Applied Magnetic field)

The experimental results on the static V-I characteristics for Gunn diodes presented in Sec. 2.3 showed that the application of a transverse magnetic field

1. increases the resistance, and
2. shifts the NDC threshold to a higher bias voltage (Figs. 2.2:8 and 2.3:4).

For the type of experiments discussed in Sec. 4.2 where small signal amplification occurs near the NDC threshold, the magnetic field quenches the amplification with the bias voltage kept constant. This is illustrated in Fig. 4.3:1 where it is observed that applying the magnetic field causes a device which is operating in the NDC region (B=0 curve) to operate in the positive differential conductance region (B≠0 curve). The measured results are shown in Fig. 4.3:2. It is observed in the figure that a magnetic field of 6.5 kG reduces the gain from ~27 dB to ~0 dB. The calculated results are presented in Fig. 4.3:3 for comparison. This type of measurements provides no additional insight into what is already known from the static results but serves as an introduction to another type of measurement which is more useful as a diagnostic tool. In Sec. 3.3, it was shown that the frequency, f_o, at which small signal negative conductance first occurs depends on the d-c drift velocity of the carriers at that particular bias voltage. An approximate expression of

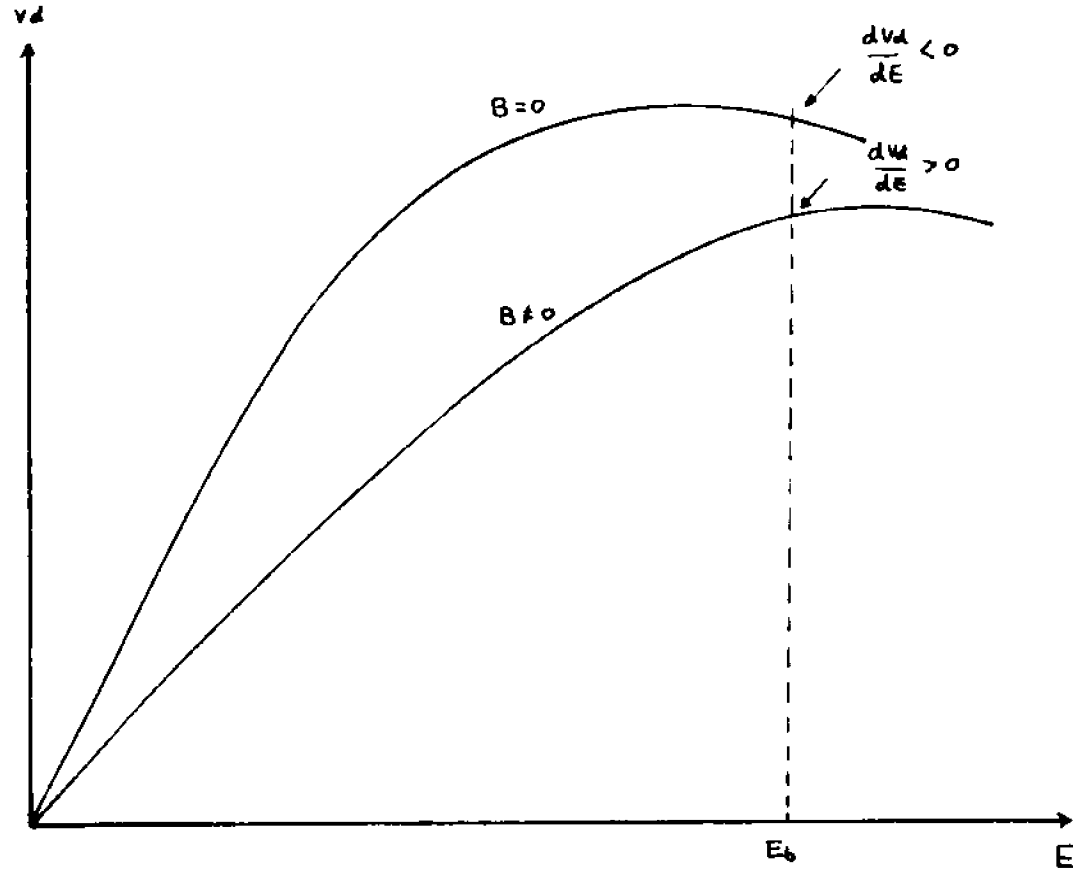

FIGURE 4.3:1 STATIC V-I CHARACTERISTICS WITH MAGNETIC FIELD AS PARAMETER

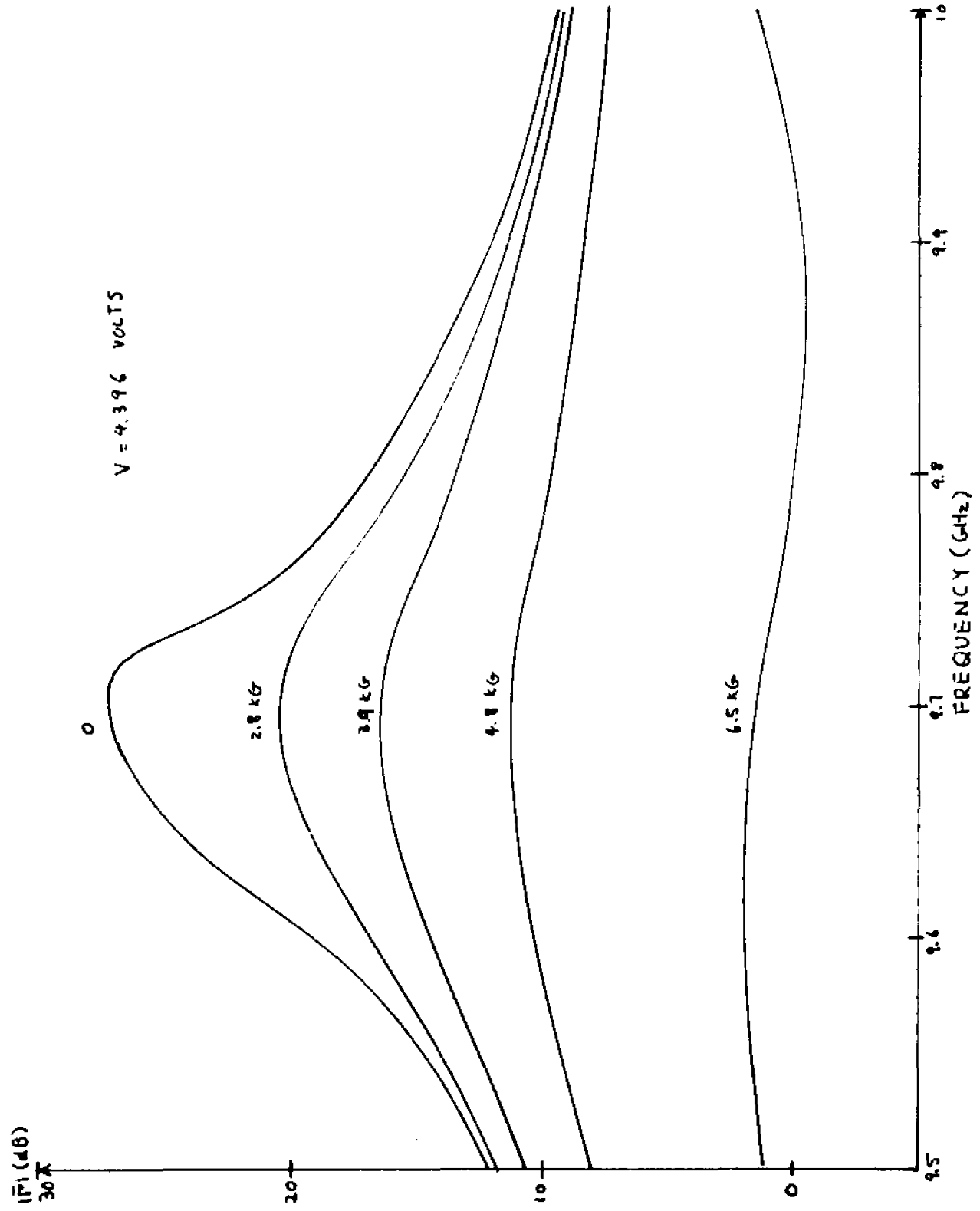

FIGURE 4.3:2 CALCULATED $|\Gamma|$ VS. FREQUENCY WITH MAGNETIC FIELD AS PARAMETER (CONSTANT BIAS VOLTAGE)

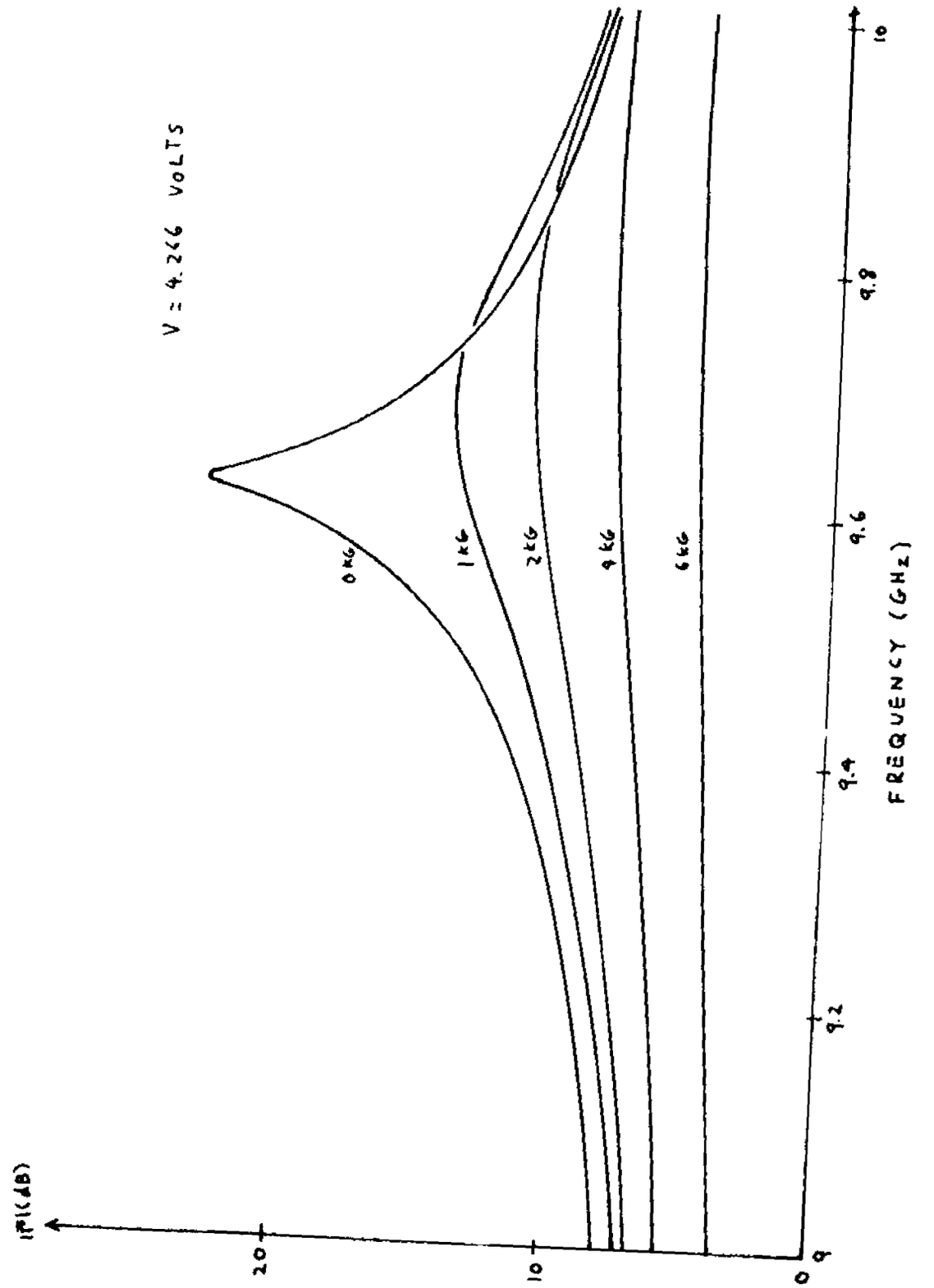

FIGURE 4.3.3 MEASURED $|\Gamma|$ VS. FREQUENCY WITH MAGNETIC FIELD AS PARAMETER (CONSTANT BIAS VOLTAGE)

the form $f_o \simeq \bar{v}_o/L$ is quite often used. However, calculation of the small signal admittance in Sec. 3.3 indicated that f_o is a more complicated function that depends as well on the diffusion constant. The more general statement which takes this into consideration is $f_o \simeq v_{ph}/L$ where v_{ph} is the phase velocity of the traveling wave; $v_{ph} \to \bar{v}_o$ in the limit of zero diffusion. The phase velocity, v_{ph}, for the forward travelling growing mode is obtained from Eq. 3.2:25 as

$$v_{ph} = - \frac{1}{\mathrm{Im}(S1)} \qquad (4.3:1)$$

Equation 4.3:1 lends little insight into the dependence of v_{ph} on the various parameters. The case for small diffusion in which

$$\bar{v}\left(1 - \frac{\bar{\sigma}\bar{D}}{\epsilon\bar{v}^2}\frac{E}{\bar{D}}\frac{d\bar{D}}{dE}\right) >> \sqrt{4\omega\bar{D}}\,,\sqrt{\frac{4\bar{D}\bar{\sigma}}{\epsilon}\frac{E}{\bar{v}}\frac{d\bar{v}}{dE}} \qquad (4.3:2)$$

allows v_{ph} to be written as

$$v_{ph} \simeq \bar{v}\left(1 - \frac{\rho_o}{\bar{v}\epsilon}\frac{d\bar{D}}{dE}\right) \qquad (4.3:3)$$

This simplified expression is only used here to illustrate the effects of diffusion on the phase velocity of the wave. The more exact expression as defined by Eq. 3.2:25 is numerically evaluated in all other calculations. Equation 4.3:3 indicates that the phase velocity may be smaller or larger than the drift velocity of the carriers depending on the sign for $(d\bar{D}/dE)$. Calculations [50] and the present

measurements indicate that $(d\bar{D}/dE)$ is positive even after the device enters the NDC region. The effects of a positive $(d\bar{D}/dE)$ on the static V-I characteristic was considered by Hauge [62]; the effects on the small signal behavior was considered by Ohmi and Hasuo [33]. To evaluate the small signal admittance, it is necessary to find the dependence of $(d\bar{D}/dE)$ on E with the magnetic field as parameter. Normally, the relationship between $\bar{D}$ and E is obtained through Einstein's relation and the energy transport equation (App. 4). However, for a system of 'hot' carriers where the distribution function is non-Maxwellian, Einstein's relation does not apply. For the lack of more precise information, the term

$$\varphi \equiv \frac{\rho_o}{\bar{v} \epsilon} \frac{d\bar{D}}{dE} \qquad (4.3;4)$$

is assumed to be a constant, with $\varphi = .175$, independent of the electric and magnetic fields. With the application of a transverse magnetic field, it is possible to evaluate the validity of the assumption. This is achieved through comparison of the measured and calculated admittance values with the magnetic field as parameter while employing the assumption that φ is a constant.

Before presenting the results, the method of measurement is first introduced. The measurement system is shown in Figs. 4.1;1 and 4.1;2. The procedure is

1. For B=0, the bias voltage V_b, is increased until the small signal gain attains a given level (gain

as high as 30 dB is possible).

2. The magnetic field, B, is increased which reduces the gain.
3. The bias voltage is increased so that the gain returns to the level for B=0.

Steps (2) and (3) are repeated for different values of B and all data are recorded. The results are shown in Fig. 4.3:4. In the figure, it is observed that a magnetic field of 16.8 kG shifts the frequency for maximun gain from 9.8 to 9.1 GHz. The peak gain is set at ~27 dB. The high peak gain is used since it produces a better defined peak than a lower peak gain. To describe the results in Fig. 4.3:4 qualitatively, the application of the magnetic field reduces the drift velocity at which maximun gain occurs. Since the frequency at which maximun gain occurs, $f_o' \simeq (\bar{v}/L)$, is proportional to the drift velocity, f_o' is also reduced. The calculated gain curves with B as parameter are shown in Fig. 4.3:5, where it is observed that a magnetic of 15 kG reduces the frequency from ~9.8 to 9.5 GHz. This is compared to the measured results of ~ 9.8 and 9.2 GHz respectively.

A more elaborate model of the device admittance is needed to better match the experimental and theoretical results. It was observed in the measurements that the small signal conductance remains positive even when the NDC region is reached. To account for possible microwave losses which are not evident in the static measurements,

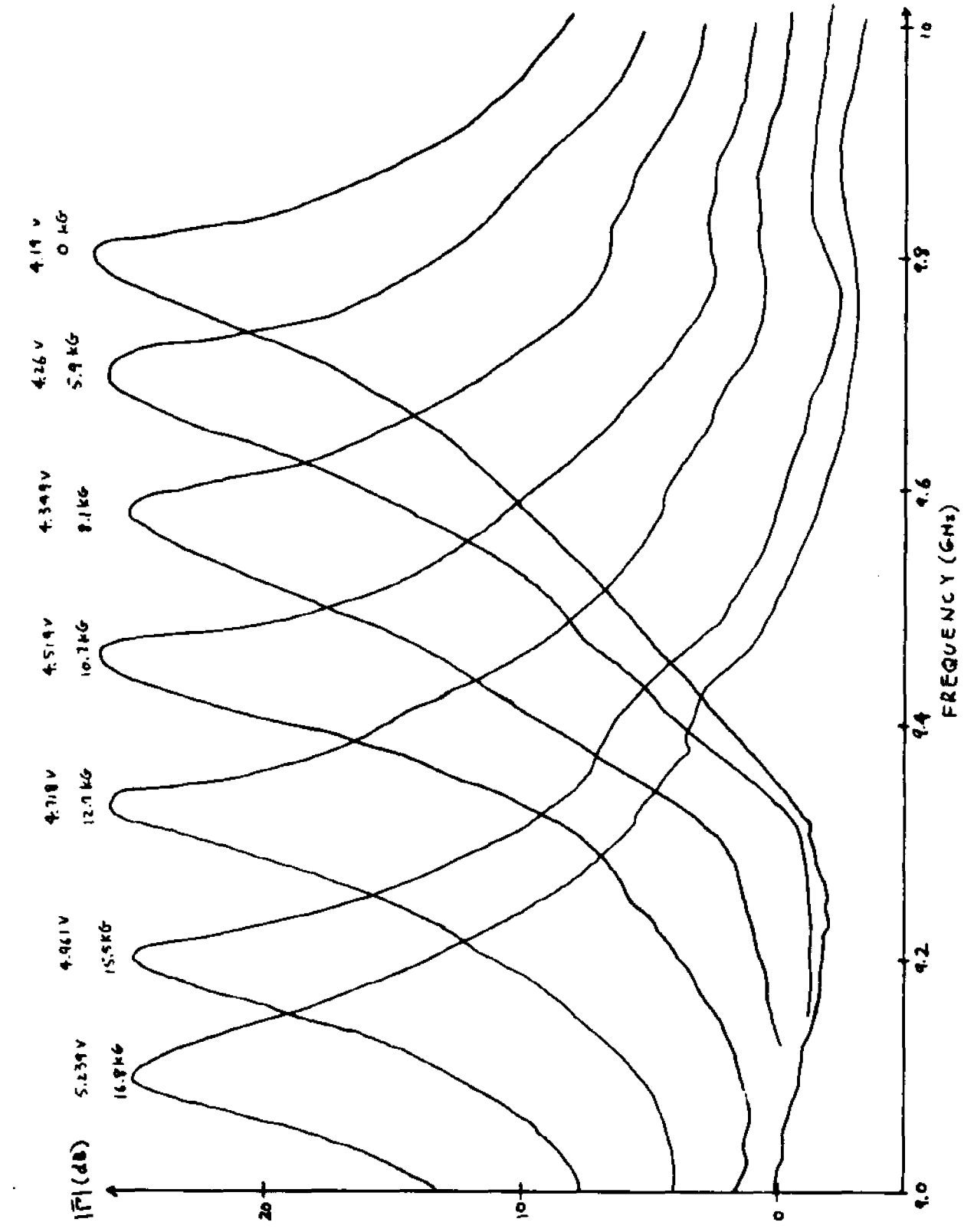

FIGURE 4.3:4 MEASURED $|\Gamma|$ VS. FREQUENCY WITH MAGNETIC FIELD AS PARAMETER (CONSTANT GAIN)

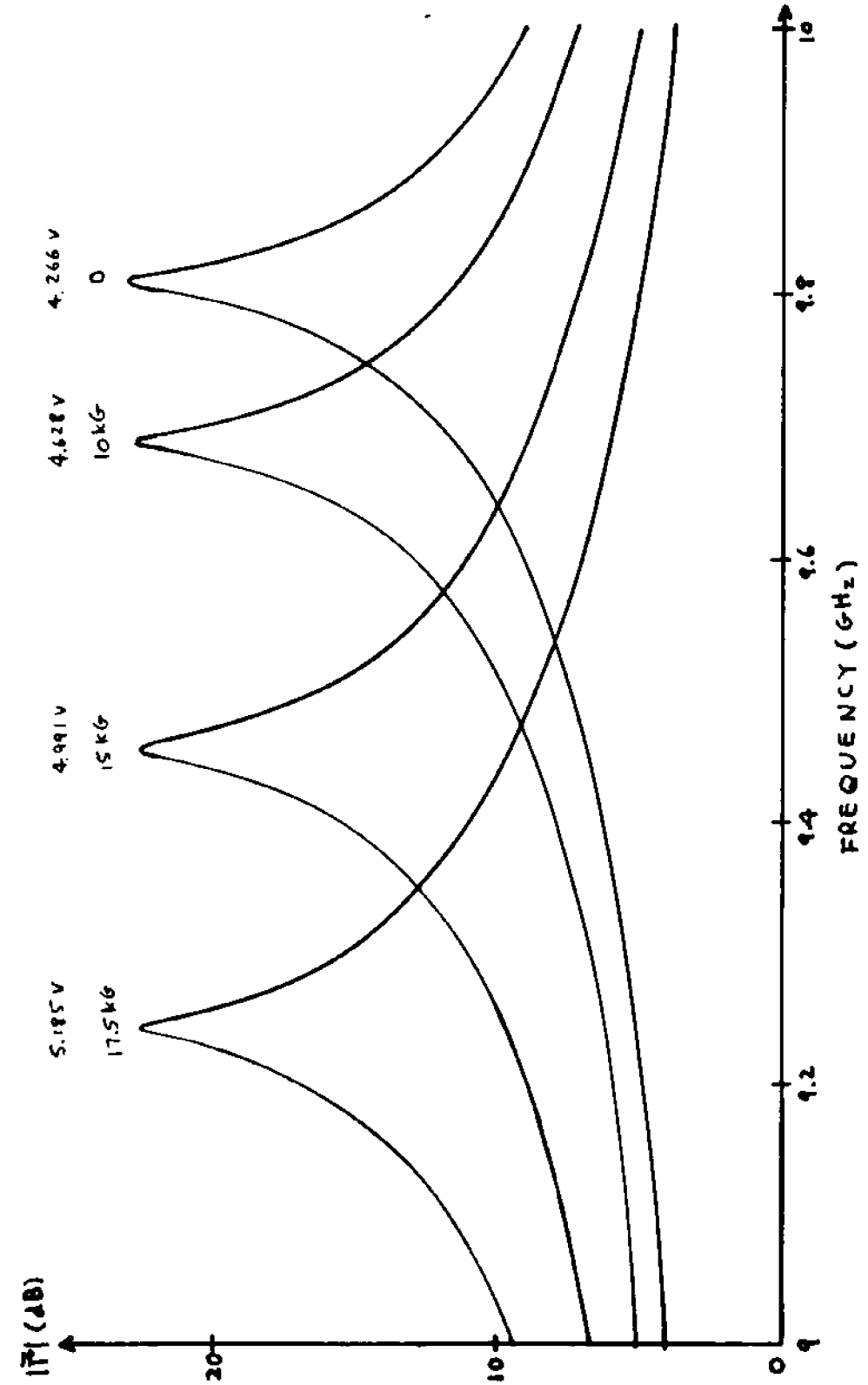

FIGURE 4.3.5 CALCULATED $|\Gamma|$ VS. FREQUENCY WITH MAGNETIC FIELD AS PARAMETER (CONSTANT GAIN)

a parallel resistive element is assumed to exist across the GaAs sample. This gives better agreement with measured results with the magnetic field. For example, placing a 100 Ω resistance in parallel with the sample shows that a magnetic field of 15 kG shifts the peak gain from 9.8 to 9.3 GHz, Fig. 4.3:6. This is in better agreement with measured results. For this measurement $\gamma = .24$ is used so that agreeements were obtained for the zero magnetic field case.

Qualitatively, there are two reasons for the different response to the magnetic field with the addition of the 100 Ω resistance. They are:

1. the value of $\gamma = .24$ used here as compared to $\gamma = .175$ prior to the addition of the resistance, and
2. the additional losses that must be overcome by the negative conductance sample in order to exhibit small signal gain.

Both of these effects act to modify the dependence of the small signal admittance on frequency, Fig. 3.3:2, and results in a different frequency response in the reflection coefficient as the magnetic field is applied.

4.4 Additional A-C Measurements

4.4A Amplification Measurements at High Bias Voltages

In Fig. 2.3:4, it is shown that diode #2 exhibited a stable V-I characteristic for bias voltages at twice

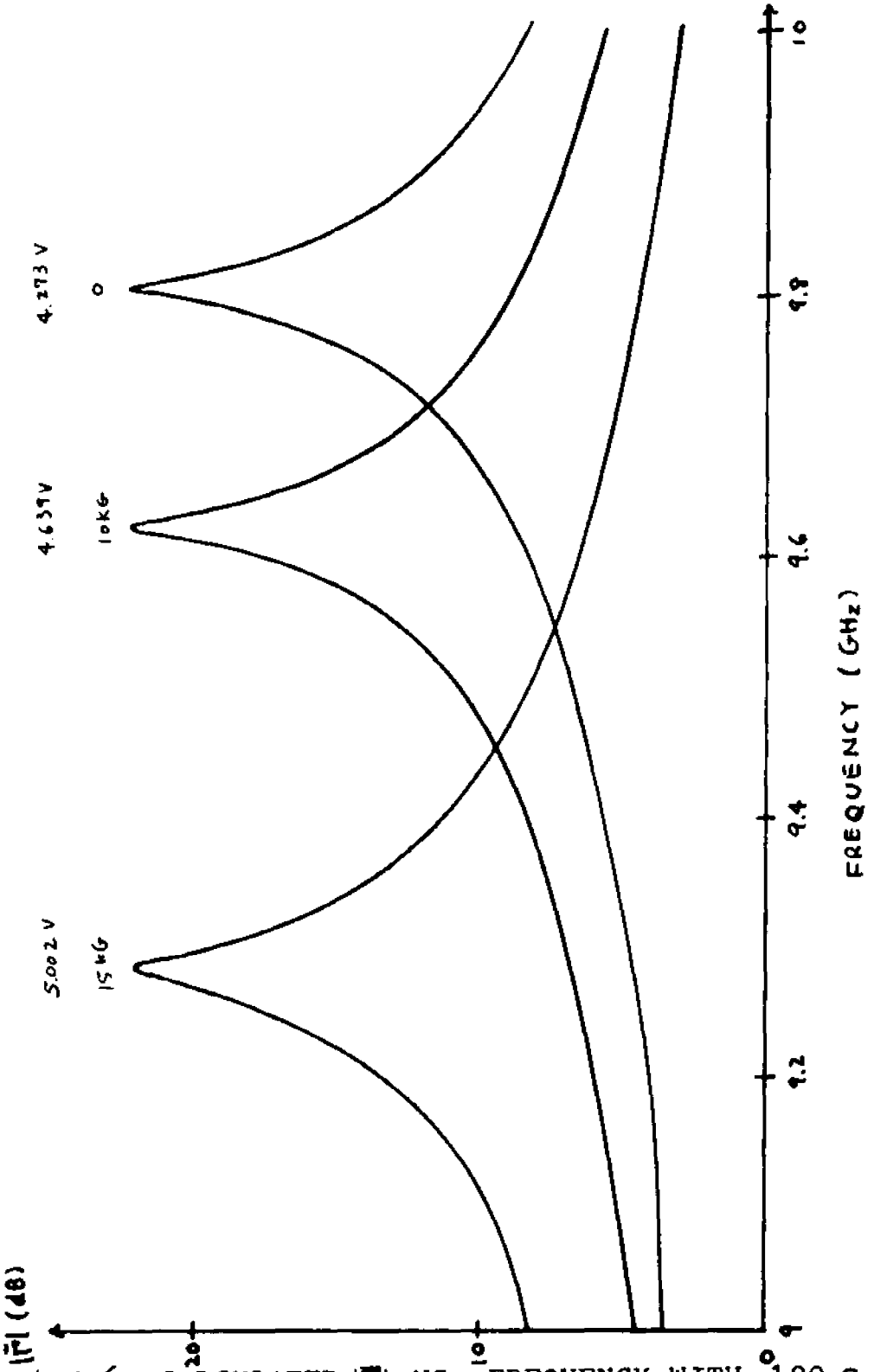

FIGURE 4.3.6 CALCULATED $|\Gamma|$ VS. FREQUENCY WITH 100 Ω RESISTANCE ADDED

the NDC threshold. Reflection gain is measured at approximately 8 volts as compared to 4 volts for the other diodes. Since the same external circuit exists for the measurements, the difference is believed to be due to differences in

1. device parameters, and
2. fabrication processes.

The parameter of particular importance is the n_oL product. However, measurements of the resistance at low electric field show that if the device geometries are assumed constant, the values of n_o varies by less than 10% from diode to diode. In terms of fabrication processes, the cathode contact behavior influences the electric field profile and therefore affects the a-c response. Another less likely reason is the difference in the v_d-E characteristic which was shown by Braslau and Hauge [13] to be somewhat dependent on the fabrication processes. The above outline does not suggest that the cause has been pinpointed. Rather, it serves as a guide to the various possibilities to be investigated more fully.

As mentioned earlier, this diode exhibits gain at approximately 8 volts. Fig. 4.4:1 shows the measured gain curves. It is observed that the peak gain occurs at $f \sim 9.656$ GHz. This is compared to $f \sim 9.8$ GHz for amplification near the threshold. Gain as a function of frequency is also similar to that obtained for amplification near the threshold. However, variation in gain as a function

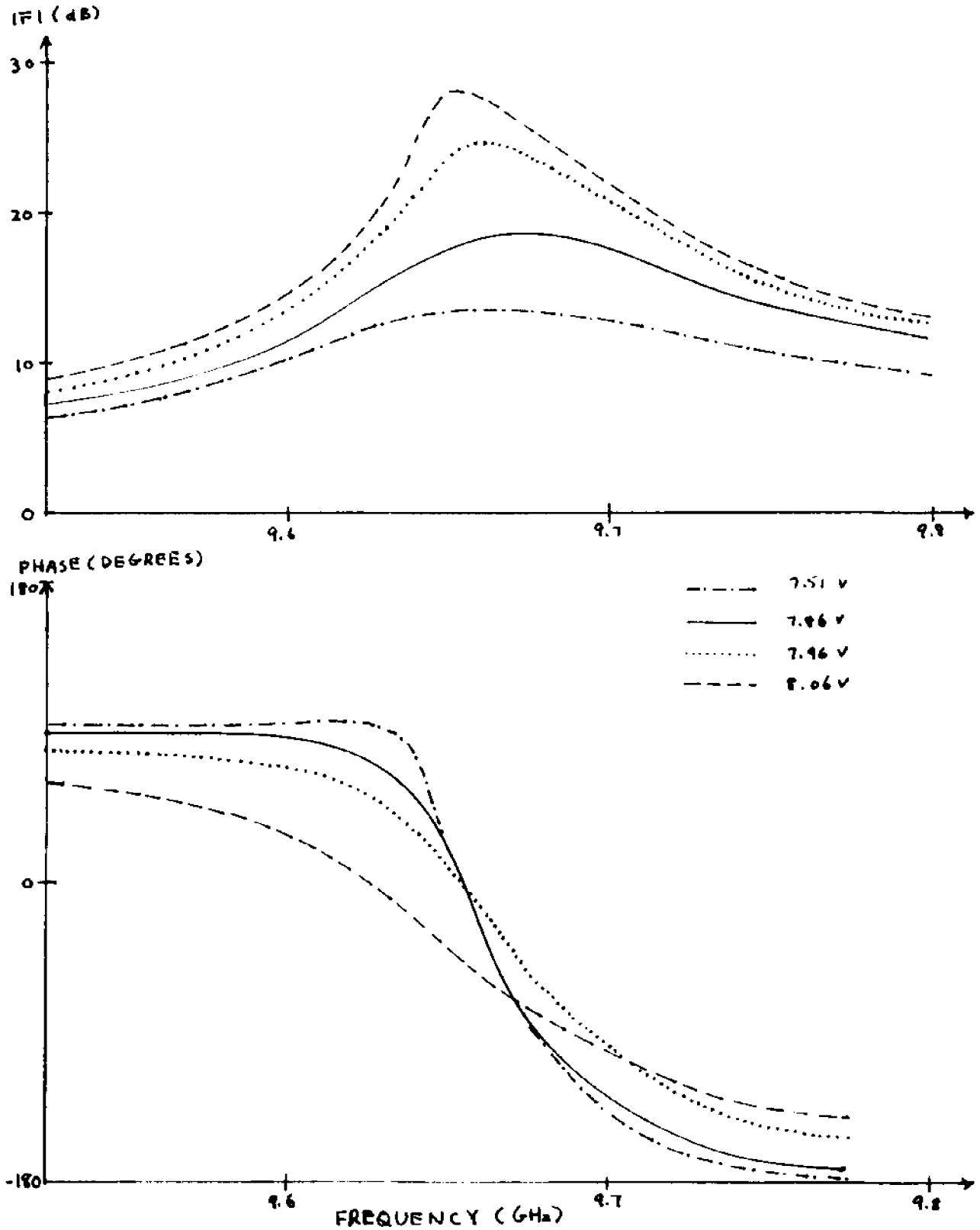

FIGURE 4.1.1 MEASURED Γ VS. FREQUENCY WITH BIAS VOLTAGE AS PARAMETER (DIODE #2)

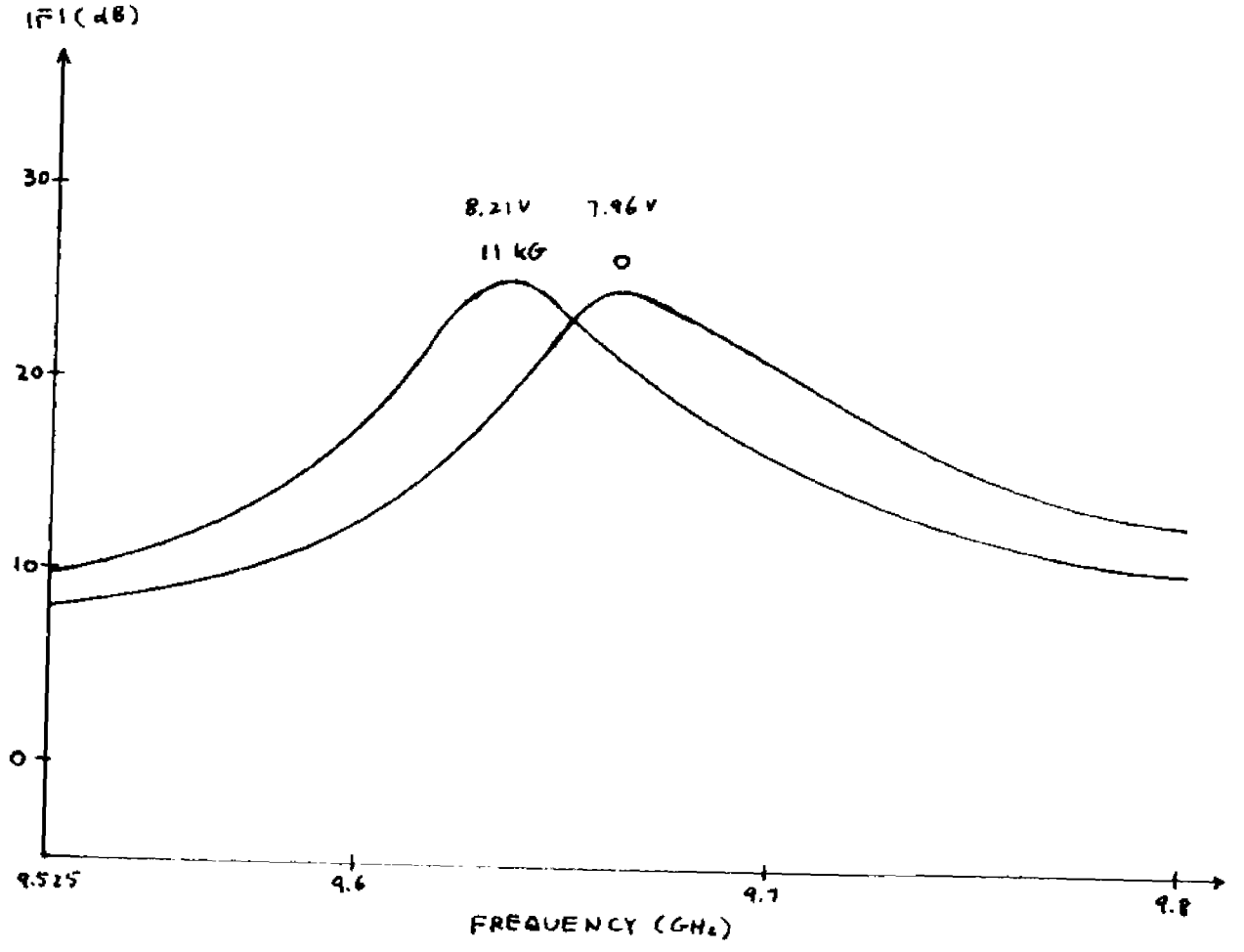

FIGURE 4.4.2 MEASURED $|\Gamma|$ VS. FREQUENCY FOR CONSTANT GAIN (DIODE #2)

of voltage increments is much less sensitive in this case. This lower sensitivity provides a more stable operation with the waveguide d-c block inserted in the circuit. This is necessary since the higher bias voltages may damage the network analyzer if d-c isolation is not provided. The effects of the magnetic field on device behavior is tested using the same procedure described in Sec. 4.2. Figure 4.4:2 shows that the frequency at which peak gain occurs is again lowered. This is expected from a reduction in drift velocity by the magnetic field; a result discussed in detail in Sec. 4.2. In view of the similarities between the results obtained here and that described in Sec. 4.2, correlation of the present measurements with theory will not be pursued.

4.4B Amplification Measurements with Heat Sink Inductance (L_S) Eliminated

As mentioned in Sec. 4.1, the heat sink inductance may be eliminated by causing a short circuit between the base of the diode just below the ceramic insulater and the aluminum substrate. Calculations revealed that gain is expected at a higher frequency, Fig. 4.4:3. Experimentally, gain is found to occur at $f \sim 12.2$ GHz, Fig. 4.4:4, agreeing with that calculated. The experimental results are displayed on a compressed Smith Chart which allows conversion of the compex reflection coefficent $\overline{\Gamma}$ into complex impedance or admittance. This is adventageous in

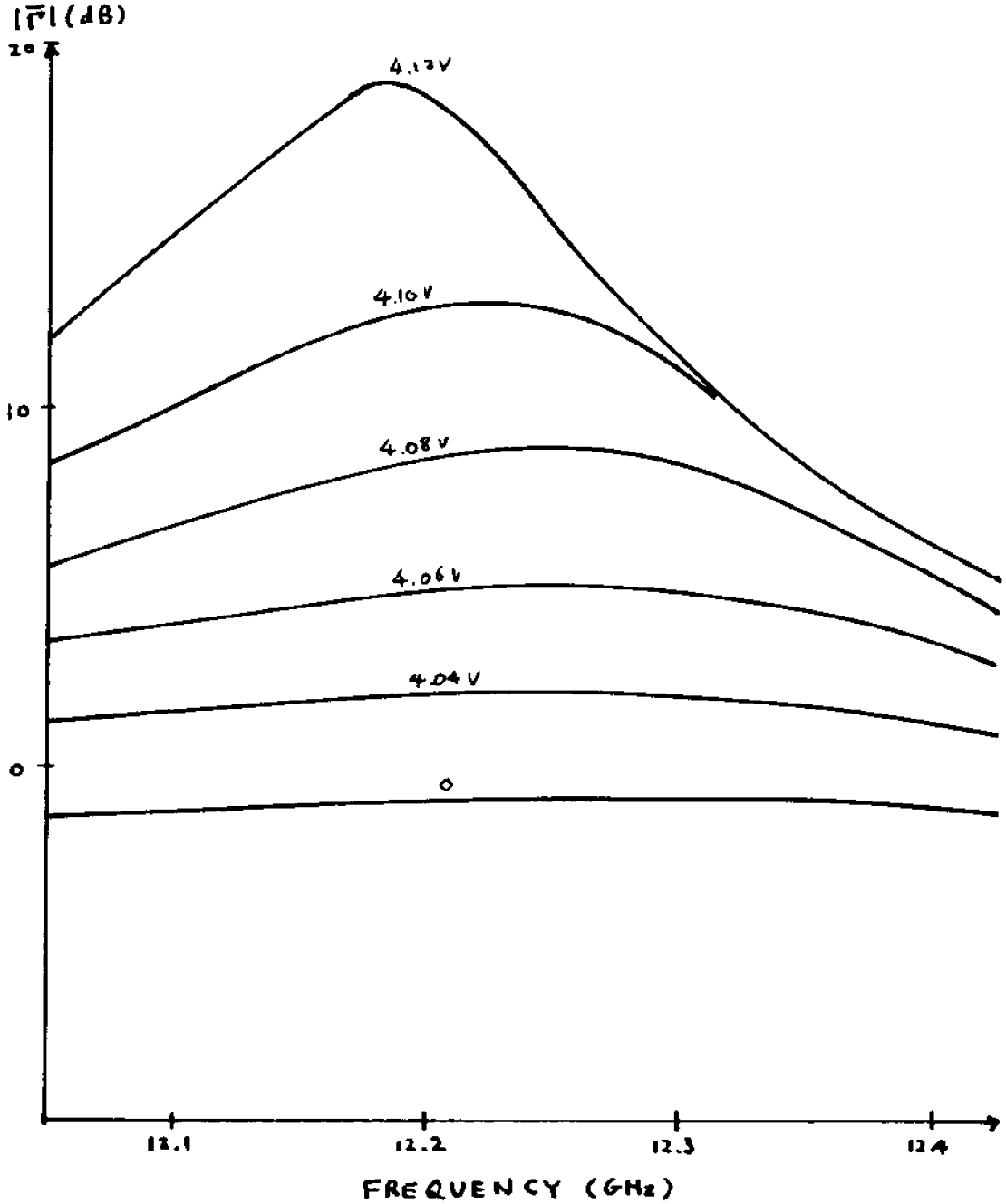

FIGURE 4.4:3 CALCULATED $|\Gamma|$ VS. FREQUENCY WITH REDUCED HEAT SINK INDUCTANCE

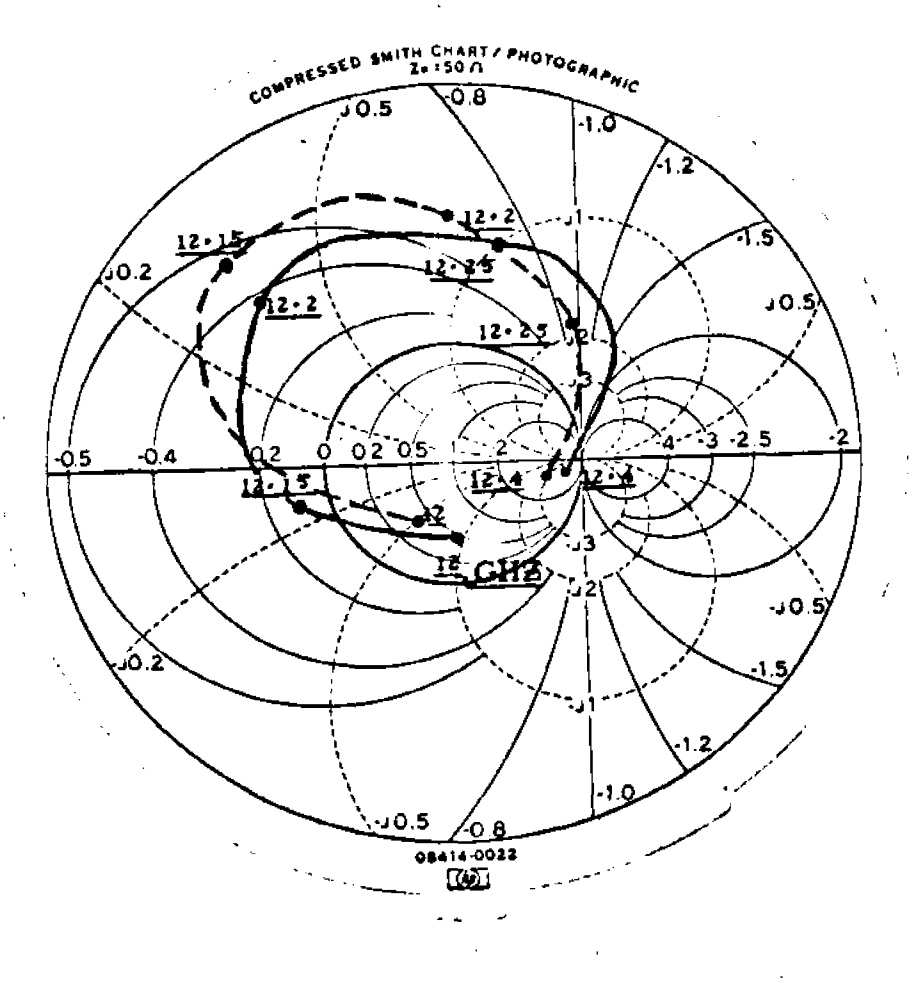

——— B = 0 V = 3.8 volts

- - - - B = 7.6 kG V = 3.986 volts

FIGURE 4.4.4 MEASURED Γ VS. FREQUENCY WITH REDUCED HEAT SINK INDUCTANCE

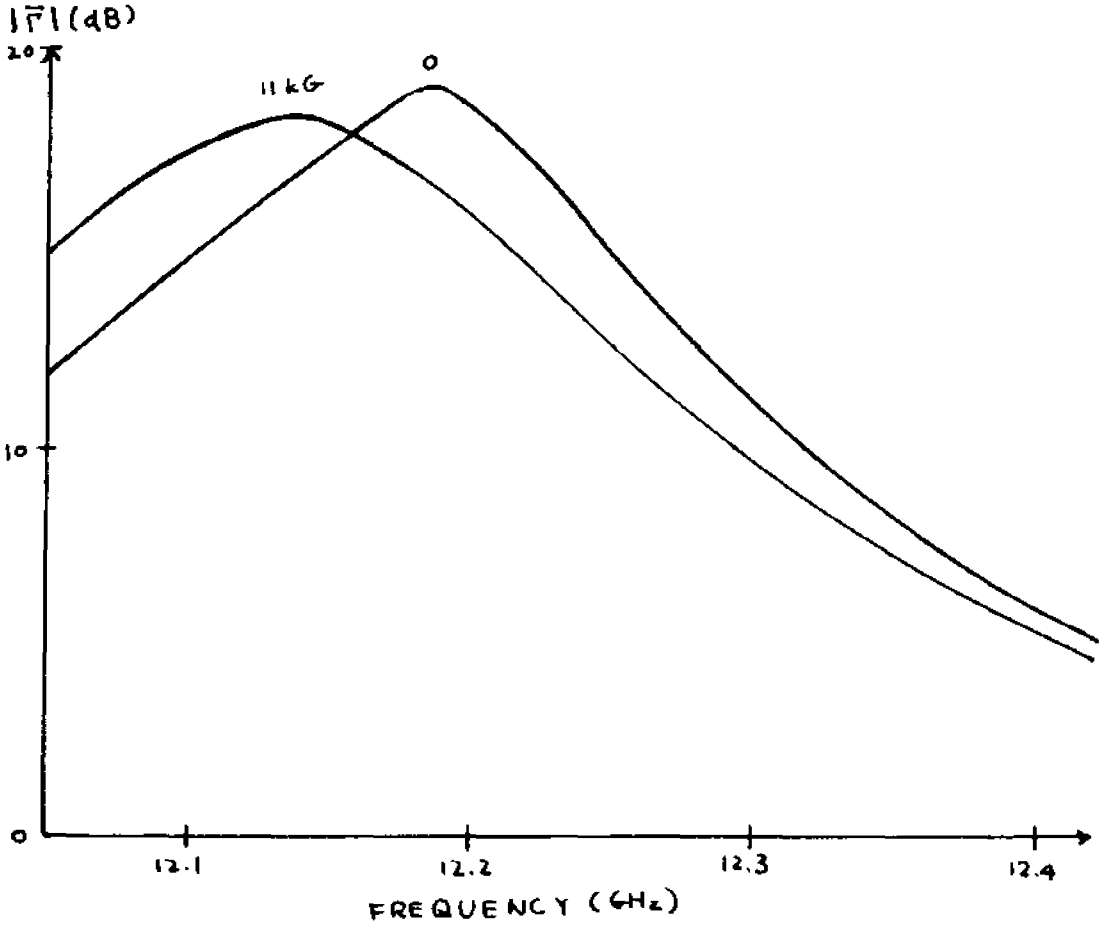

FIGURE 4.4.5 CALCULATED $|\Gamma|$ VS. FREQUENCY WITH REDUCED HEAT SINK INDUCTANCE (CONSTANT GAIN)

some situations. For example, in an attempt to provide matching for the device, it is necessary to work with the admittance function. For other purposes, for example, to estimate the 3-dB band width, the x-y display showing linear increments in frequency would be desirable.

The effect of the magnetic field in shifting the frequency at which peak gain occurs is found to be less than that described in Sec. 4.2. Figure 4.4:5 shows that a magnetic field of 11 kG shifts the peak gain by about 43 MHz. This is again verified experimentally as Table 4:1 shows.

Table 4:1 Dependence of Peak Gain Frequency on Magnetic Field

B(kG)	V_b(V)	Δf(MHz)	
0	3.8	--	f_o = 12.18 GHz
7.6	3.98	-26.5	
11.0	4.18	-46.5	

CHAPTER 5 SUMMARY, CONCLUSIONS AND SUGGESTIONS FOR FUTURE STUDIES

The purpose of this dissertation is to investigate the behavior of transferred electron devices in the presence of a transverse magnetic field. The results of the investigation establish the magnetic field as a diagnostic tool in evaluating the modeling and certain parameters for the device. Towards this end, magneto-resistance effects in GaAs were measured and calculated. In these measurements, it was found that the geometrical type of magnetoresistance dominated device behavior for the bias voltages of interest. To account for this effect, a simple analytical method based on a carrier temperature dependent mobility model was derived and used subsequently to predict the small signal properties at X-band. Using this method, good correlation between measured and calculated magnetoresistance effects were obtained. It was found that whereas the mobility is always a decreasing function of the bias voltage, the device only becomes unstable or amplifying when (dI/dV) becomes negative. Therefore, negative differential mobility is not the sole requirement for negative differential resistance. It was also found that with increasing magnetic field, the mobility becomes less sensitive to the bias voltage. Based on the carrier temperature model, this is an expected result since

increasing magnetic field reduces energy absorption by the carriers for a given voltage increment. On the other hand, when non-uniform electric fields across the sample are considered, this indicates that by increasing the magnetic field, a more uniform electric field distribution at a given bias voltage results. Since the non-uniform electric field model is not treated in this work, this is offered as a suggestion for future studies rather than a conclusion. Lastly, in connection with the static measurements, it was shown that for a device with large transverse dimensions compared to the length, the mobility may be calculated through measurements of current reduction by the magnetic field. The mobility thus obtained agreed with that calculated independently from the device resistance, doping concentration and geometries.

The modification of the static v_d-E characteristic by the magnetic field results in changes in the small signal behavior of the devices. In the constant bias voltage measurements, it was found that increasing magnetic field brings a device which is operating in the negative differential resistance region into the positive differential resistance region. This does not provide additional insight into what is already known from the static measurements. More interesting conclusions were drawn from constant small signal gain measurements with the magnetic field as a parameter. Theoretically, reduction in the drift velocity, v_d, at which small signal amplification

occurs gives rise to a reduction in the frequency at which the peak gain occurs. In the experiments v_d was varied by the magnetic field while constant small signal gain was maintained by adjusting the bias voltage. The frequency at which the peak gain occurs with the magnetic field as parameter was then recorded. In comparing the measured results to calculations, it was found that best correlations were obtained if microwave losses were accounted for by placing a 100-ohm resistance across the active device. Another model, which may have the same effect as the 100-ohm resistance, involves the introduction of a magnetic field dependent diffusion constant. However, in order to obtain this information, it is necessary to carry out statistical calculations of the carrier distribution function with the magnetic field as parameter. This is not attempted in this work and is suggested as a topic for future studies. In conclusion, this particular experimental procedure provides an independent means of evaluating the small signal admittance model. The correlation of theoretical and experimental results demonstrated in this work indicates that the small signal admittance has been properly modeled.

In the microwave calculations, the microstrip circuit was modeled by lumped circuit elements and appropriate sections of transmission lines. The values for these elements were obtained through direct measurements of the microstrip circuit using the network analyzer. The external circuit has an effect on the frequency charact-

eristics of the device. It was shown that a reduction in the heat sink inductance shifts the peak gain to a higher frequency. In addition, the external circuit was found to affect the stability of the amplifier; higher gain was made possible through the insertion of a 10-dB attenuator to the circuit. Therefore, the external circuit must be properly designed to obtain the most efficient amplifier operation.

In deriving the small signal admittance, the two carrier species model was used. The results were compared theoretically to that obtained through the average mobility model in the low frequency limit. It was found that the dispersion equation calculated through the two models are equivalent if the lower valley drift velocity, $v_{o\ell}$, in the two species model is interpreted as the average drift velocity, $\bar{v}$, in the average mobility model. To evaluate the two models individually, it is necessary to calculate $\bar{v}$ and $v_{o\ell}$ in terms of the measured d-c current. This is difficult since the d-c current does not provide information about the distribution of carriers among the two valleys. It is concluded that adequate correlations with theory were obtained if $v_{o\ell}$ is interpreted as $v_{o\ell} = (I/\rho_o A)$. The latter procedure lends support to the average mobility model. However, the average mobility model does not account for the intervalley relaxation time which is important in calculating the small signal admittance. This time constant, on the other hand, can

be explicitly introduced in the two valley model. The latter approach correctly predicts the increase in the effective dielectric constant. In conclusion, whereas the entire system of carriers is assumed to drift at an average velocity, the two species model is used to account for the capacitive effect due to intervalley transfer. Measurements of the frequency at which peak gain occurs with the magnetic field as a parameter supports this formulation.

The uniform static electric field approach was used throughout this work. The drift velocity of the carriers, calculated from the uniform electric field model, correctly predicts the frequency characteristics of the device. This would not be the case if considerable electric field distortions existed. It is concluded that the static electric field is approximately uniform across the entire sample. Direct measurements of the electric field distribution is difficult due to the small size of the sample. As a suggestion for future studies, this effect should be investigated more fully. In particular, magnetoresistance effects discussed earlier in this chapter suggest that in terms of the non-uniform field theory, increasing values of the magnetic field causes the distribution to be more uniform.

Since the magnetic field alters the small signal properties of transferred electron devices, it may be used as a tuning element. The frequency of the peak gain

was shifted by 600 MHz in the measurements with a magnetic field of approximately 16 kG. However, a more practical method which eliminates bulky equipment must be devised to produce the magnetic field. This may perhaps be achieved by introducing a current element adjacent to the transferred electron device.

Oscillator operation as well as noise properties of transferred electron devices under the influence of a magnetic field have not been treated in this work. These are suggested as other topics for future studies.

APPENDIX 1

Interpretation of the Experimentally Obtained Negative Differential Conductance (NDC)

In 1954, Shockley [45] showed that the static differential conductance for a two terminal sample with negative differential mobility is always positive provided that the cathode contact is well behaved. A well behaved cathode implies an ohmic contact with the cathode field maintained near zero. This result was generalized to arbitrary geometries and impurity distributions by Kroemer [63]. In the above proofs, diffusion effects were neglected.

The treatment which takes into consideration a possible electric field dependent diffusion constant was carried out by Hauge [62]. The numerical results showed that with $d\bar{D}/dE > 0$, stable solutions with NDC were obtained. However, no simple relationship exists for the NDC thus obtained and the negative slope in the v_d-E characteristic.

In the experimental results described in Chapter 4, in particular, in the effects of a transverse magnetic field on the small signal admittance, it was found that for $d\bar{D}/dE > 0$, agreement between theory and experiment is obtained. This supports the argument of the measured NDC in terms of an electric field dependent diffusion constant. However, there are other effects that must be considered as well. For example, since the static characteristic is measured with d-c biasing, the measured NDC may be due to

a temperature effect. In a recently publised paper on small signal admittance measurements [64], the use of a pulsed technique showed no evidence of NDC when a device exhibits small signal negative conductance.

In conclusion, the interpretation of the measured NDC in terms of a negative differential mobility can be done only on a phenomenological basis. However, in the present treatments, it is found to give adequate agreement between theory and experiments.

APPENDIX 2

Analytical Expressions for the Static v_d-E Characteristic of GaAs

To account for the measured static V-I characteristic of GaAs, an expression of the form

$$v(E) = \frac{\mu E + v_s (E/E_o)^4}{1 + (E/E_o)^4} \qquad (A2:1)$$

where μ = 8000 $cm^2/V\text{-sec}$, $v_s = 8 \times 10^6$ cm/sec and E_o = 4000 V/cm was used by Gunshor and Kak [65]. However, Monte Carlo calculations [41,53] indicate that the NDC region in the static v_d-E characteristic is a result not only of electron transfer to the upper valley, but also as a result of current saturation in the lower conduction valley. Therefore, in the present calculations, Eq. A2:1 is modified to the form

$$v(E) = \mu_\ell (n_\ell/n_o)E + \mu_u (n_u/n_o)E \qquad (A2:2)$$

$$\frac{n_\ell}{n_o} = \frac{1 + C_s (E/E_o)^n}{1 + (E/E_o)^n} \qquad (A2:3)$$

$$\mu_\ell = \begin{cases} 8000\ cm^2/V\text{-sec.} & E < E_s \\ 8000\ E_s/E & E > E_s \end{cases} \qquad (A2:4)$$

$$\mu_u = 120\ cm^2/V\text{-sec.} \qquad (A2:5)$$

$$(n_u/n_o) = 1-(n_\ell/n_o) \qquad (A2:6)$$

where E_s, C_s, E_o and n are constants. These constants are chosen such that the zero magnetic field v_d-E characteristic agrees with that obtained by Boardman et. al. [41]. Results by Boardman et. al. indicate that

the lower valley drift velocity saturates at $\sim 2.5 \times 10^7$ cm/sec. therefore

$$E_s \simeq 2.5 \times 10^7/8000$$
$$= 2.5/.8 \text{ kV/cm.}$$

For the remaining constants, C_s and E_o are chosen such that appropriate saturated drift velocity and NDC electric field values are obtained. The v_d-E characteristic is calculated from Eqs. A2:2-A2:6 and plotted on the same scale as that obtained by Boardman et. al.. The parameter n is varied until best graphical agreement is obtained. The final result, with C_s=.27, E_o=4.8 and n=3, is shown in Fig. 2.2:6.

APPENDIX 3

Comparison of the Two-Species Model and the Average Drift Velocity Model in GaAs

In the two-species model, each type of carrier is assumed to have a distinct mobility; the NDC is a result of the reduction in the high mobility carrier concentration as a result of intervalley transfer. On the other hand, the average drift mobility model assumes that the entire system of carriers is characterizable by the some average drift mobility; the NDC is described in terms of a reduction in the average drift mobility. The two descriptions give the same expression for current density under static situations. However, under small signal conditions, the two interpretations give different results. The essential feature in the comparison will not be lost while using the following simplifying assumption:

1. zero diffusion
2. the collision dominated model
3. for the two-species model, zero drift velocity in the upper valley, and
4. zero magnetic field

Using these assumptions, the equation Hakki [29] used for the two-species model may be written in the form

$$\epsilon SE_1 = \sum_{s=l,u} \rho_{1s}$$

$$= \rho_{ll} + \rho_{lu} \qquad (A3.1)$$

$$J_1 = \rho_{o\ell} v_{1\ell} + \rho_{1\ell} v_{o\ell} \qquad (A3:2)$$

$$v_{o\ell} = \mu_{o\ell} E_o \qquad (A3:3)$$

$$v_{1\ell} = \mu_{o\ell} E_1 \qquad (A3:4)$$

and $$SJ_1 + j\omega\rho_1 = j\omega \frac{\partial \rho_{o\ell}}{\partial E_o} E_1 \qquad (A3:5)$$

where all dependent variables are assumed to have the form

$$F = F_o + F_1 \exp(j\omega t + Sz) \qquad (A3:6)$$

The only solution to the dispersion equation is

$$S = -j \frac{\omega}{v_{o\ell}} - \frac{\rho_{o\ell}\mu_{o\ell}}{\epsilon v_{o\ell}} \left\{ 1 + \frac{E_o}{\rho_{o\ell}} \frac{\partial \rho_{o\ell}}{\partial E_o} \right\}$$

$$= -j \frac{\omega}{v_{o\ell}} - \frac{\rho_o}{\epsilon v_{o\ell}} \frac{\partial \bar{v}_o}{\partial E_o} \qquad (A3:7)$$

where the relationship

$$1 + \frac{E_o}{\rho_{o\ell}} \frac{\partial \rho_{o\ell}}{\partial E_o} = \frac{E_o}{\bar{v}_o} \frac{\partial \bar{v}_o}{\partial E_o} \qquad (A3:8)$$

has been used. Next, the average drift mobility approach employed by McCumber and Chynoweth [14], and similarly by Ohmi and Hasuo [33], is considered. The equations in this case are

$$\epsilon SE_1 = \rho_{1\ell} + \rho_{1u} \qquad (A3:9)$$

$$J_1 = \rho_o \bar{v}_1 + \rho_1 \bar{v}_o \qquad (A3:10)$$

$$SJ_1 + j\omega\rho_1 = 0 \qquad (A3:11)$$

and $$\bar{v}_1 = \frac{\partial \bar{v}_o}{\partial E_o} E_1 \qquad (A3:12)$$

The dispersion equation is solved to give

$$S = -j \frac{\omega}{\bar{v}_o} - \frac{\rho_o}{\epsilon \bar{v}_o} \frac{\partial \bar{v}_o}{\partial E_o} \qquad (A3:13)$$

Comparison of Eqs. A3:7 and A3:13 reveals that v_{ot} appears in the two-species model while $\bar{v}_o$ appears in the average drift mobility model. The physical origin of the discrepency is discussed in Sec. 3.2 in connection with the form of the dispersion equation (Eq. 3.2:24). Experimental evaluation of the two models is discussed in Secs. 4.2 and 4.3.

APPENDIX 4

Dependence of the Diffusion Constant on Electric Field with Drifted Maxwellian Distribution

For a system of carriers which obeys Einstein's relation

$$D = \frac{k_B T}{q} \mu \quad , \qquad (A4:1)$$

the relationship between the diffusion constant, D, and the electric field, E, is obtained through the steady state energy transport equation [48]

$$\frac{3}{2} \frac{k_B (T-T_o)}{\tau_e} = \frac{1}{2} \mu E^2 \quad . \qquad (A4:2)$$

For $T \gg T_o$, substitution of Eq. A4:1 into Eq. A4:2 results in

$$D = \frac{1}{3} \frac{\tau_e}{q} (\mu E)^2 \quad . \qquad (A4:3)$$

From Eq. A4:3

$$\frac{dD}{dE} = \frac{2}{3} \frac{\tau_e}{q} \mu^2 E \left(1 + \frac{E}{\mu} \frac{d\mu}{dE}\right)$$

$$= \frac{2}{3} \frac{\tau_e}{q} \mu^2 E \left(\frac{E}{\bar{v}} \frac{d\bar{v}}{dE}\right) \qquad (A4:4)$$

which indicates that (dD/dE) has the same sign as $(d\bar{v}/dE)$. In Secs. 4.2 and 4.3, the situation where (dD/dE) remains positive even when the device enters the NDC region is considered. This may be the case when the distribution function is non-Maxwellian [50,62].

APPENDIX 5

Computer Program

The following computer program calculates and plots values of SiL, Y_d, and I versus frequency. The parameters in the program represent typical values used in the actual calculations. The same plotting routine was used in generating v_d-E characteristics in Chp. 2.

```
1  REAL*4 L,N,MU,MU1
2  COMPLEX*8 S1,S2,Y1,R1,Z,ZZ,ZZ1,ZZ2,ZD
3  COMPLEX*8 YCP,ZLP,YCC,ZLC,ZLS,ZEQ,ZBL
4  DIMENSION A(61)
5  DATA DOT/'.'/,STAR/'*'/,BLANK/' '/,PLUS/'+'/
6  Q=1.6E-19
7  N=1.01E+15
8  L=1.0E-03
9  EPS=10.9*8.85E-14
10 D=200.
11 10 READ(5,*) E,YREMAX,YIMMAX
12 READ(5,*) B
13 WRITE(6,20)
14 20 FORMAT(10H       E    ,10H   YREMAX ,10H   YIMMAX )
15 WRITE(6,30) E,YREMAX,YIMMAX
16 30 FORMAT(F9.4,1X,2(F9.2,1X)//)
17 DO 40 J=1,61
18 40 A(J)=DOT
19 DO 50 J=1,7
20 JJ=J-1
21 JJJ=10*JJ+1
22 50 A(JJJ)=STAR
23 WRITE(6,60)(A(K),K=1,61)
24 60 FORMAT(7X,61A1)
25 E1=E
26 DO 70 II=1,20
27 I=II-1
28 E=E1
29 C1=-.088
30 C2=.7
31 MU=C1*E+C2
32 E2=E/SQRT(1.+MU*MU*B*B)
33 C11=-.088
34 C22=.7
35 MU1=C11*E2+C22
36 BMU1=MU1/(1.+MU1*MU1*B*B)
37 X1=C11*(1.-(MU*B*B*C1*E1)/(1.+MU*MU*B*B))/SQRT(1.+MU*MU*
   B*B)
38 DBMU1=X1*(1.-MU1*MU1*B*B)/(1.+MU1*MU1*B*B)**2.
39 Z1=1.+(E1/BMU1)*(DBMU1)
40 TN=4.5E-12
41 CC=MU1*((1.-MU1*MU1*B*B)/(1.+MU1*MU1*B*B)**2.)
42 EPSR=1.62E+12*MU1*TN*(-(4.E-13*CC)/TN-(E/BMU1)*DBMU1)
43 EPS1=EPS*(1.+EPSR)
44 BMU1=BMU1*1.0E+04
45 E1=E1*1.0E+03
46 UO=BMU1*E1
47 F=II*1.E+09
48 W=6.283*F
49 WD1=(Q*N*BMU1)/EPS1
50 WD=(UO*UO)/D
51 READ(5,*) AA
52 X=UO*(1.-AA)
```

```
53  BB=WD1*(-Z1)
54  DOL=D
55  WN=W
56  Z=CMPLX(-BB,WN)
57  S1=(-1./(2.*D))*(-X+CSQRT(X*X+4.*D*Z))
58  S2=(-1./(2.*D))*(-X-CSQRT(X*X+4.*D*Z))
59  ZZ=(1.-CEXP(S1*L))*(1.-(S1*L)/(S2*L))+S1*L
60  TA=2.95E-04
61  ZO=50.
62  C=EPS1*TA*(DOL/D)
63  F1=F/1.E+09
64  ZD=ZZ/(C*S1*Z)
65  XLP=W*.3E-09
66  ZLP=CMPLX(0.,XLP)
67  BCP=W*.27E-12
68  YCP=CMPLX(0.,BCP)
69  BCC=W*.5E-12
70  YCC=CMPLX(0.,BCC)
71  XLC=W*.12E-09
72  ZLC=CMPLX(0.,XLC)
73  XLS=W*.3E-09
74  ZLS=CMPLX(0.,XLS)
75  BL=W*.825E-10
76  XBL=100.*TAN(BL)
77  ZBL=CMPLX(0.,XBL)
78  ZEQ=ZBL+ZLC
79  ZEQ=1./(1./ZEQ+YCC)
80  ZEQ=1./(1./ZEQ+1./(ZLS+1./(YCP+1./(ZLP+ZD))))
81  ZEQ=ZEQ+ZLC
82  R1+(ZEQ-ZO)/(ZEQ+ZO)
83  Y1=1./R1
84  E1=E1/1.0E+03
85  DO 100 J=1,61
86  100 A(J)=BLANK
87  YRE=REAL(Y1)
88  YIM=AIMAG(Y1)
89  YIM=ATAN2(YIM,YRE)
90  YER=CABS(Y1)
91  YIM=YIM*(180./3.1416)
92  YRE=20.*ALOG10(YRE)
93  M=(YRE/YREMAX)*35+36
94  M=M-25
95  IF(M.GE.61) M=61
96  IF(M.LE.1) M=1
97  A(M)=PLUS
98  IF(YIM.GE.100.) GO TO 112
99  GO TO 113
100 112 J=(YIM/YIMMAX)*35+26
101 GO TO 114
102 113 J=(YIM/YIMMAX)*35+36
103 114 IF(J.GE.61) J=61
104 IF(J.LE.1) J=1
105 A(J)=STAR
```

```
106 IF(M.GT.J) GO TO 11
107 MM=J
108 GO TO 22
109 11 MM=M
110 22 IF(MM.LT.36) MM=36
111 A(36)=DOT
112 70 WRITE(6,110)(F1,(A(K),K=1,MM))
113 110 FORMAT(F7.3,61A1)
114 GO TO 10
115 END
```

REFERENCES

1. B. K. Ridley and T. B. Watkins, "The Possibility of Negative Resistance Effects in Semiconductors", Proc. Phys. Soc. (London), vol. 78, pp. 293-304; August 1961.

2. H. Ehrenreich, "Band Structure and Electron Transport in GaAs", Phys. Rev., vol 120, pp. 1951-1963; December 15, 1960.

3. J. B. Gunn, "Microwave Oscillations of Current in III-V Semiconductors", Solid State Comm., vol. 1, pp. 88-91; September 1963.

4. J. B. Gunn, "Instabilities of Current in III-V Semiconductors", IBM J. Res. Dev., vol. 8, pp. 141-159; April 1964.

5. J. B. Gunn, "Instabilities of Current and of Potential Distribution in GaAs and InP", Plasma Effects in Solids, Dunod, Paris, pp. 199-216; 1964.

6. C. Hilsum, "Transferred Electron Amplifiers and Oscillators", Proc. IRE, vol. 50, pp. 185-189, February 1962.

7. B. K. Ridley, "Specific Negative Resistance in Solids", Proc. Phys. Soc. (London), vol. 82, pp. 954-966, December 1963.

8. H. Kroemer, "Theory of the Gunn Effect", Proc. IEEE (corresp), vol. 52, p. 1736, December 1964.

9. A. R. Hutson et. al., "Mechanism of the Gunn Effect from a Pressure Experiment", Phys. Rev. Letters, vol. 14, pp. 639-641, April 19, 1965.

10. M. Shyam et. al., "Effects of Variation of Energy Minima Seperation in Gunn Oscillators", IEEE Trans. on Electron Devices, vol. ED-13, pp. 63-67, January 1966.

11. J. G. Ruch and G. S. Kino, "Measurement of the Velocity-Field Characteristic of Gallium Arsenide", Appl. Phys. Letters, vol. 10, pp. 40-42, January 15, 1967.

12. P. N. Butcher and W. Fawcett, "Calculation of the Velocity-Field Characteristic for GaAs", Phys. Letters, vol. 21, pp. 489-490, 1966.

13. P. N. Braslau and P.S. Hauge, "Microwave Measurements of the Velocity-Field Characteristic of GaAs", IEEE Trnas. on Electron Devices, vol. ED-17, pp. 616-622, August 1970.

14. D. E. McCumber and A. G. Chynoweth, "Theory of Negative Conductance Amplification and of Gunn Instabilities in 'Two-Valley' Semiconductors", IEEE Trans. on Electron Devices, vol. ED-13, pp. 4-21, January 1966.

15. H. Kroemer, "Nonlinear Space-Charge Domain Dynamics in a Semiconductor with Negative Differential Mobility", IEEE Trans. on Electron Devices. vol. ED-13, pp. 27-40, January 1966.

16. R. W. H. Engelmann and C. F. Quate, "Linear, or 'Small-Signal', Theory for the Gunn Effect", IEEE Trans. on Electron Devices, vol. ED-13, pp. 44-52, January 1966.

17. J. S. Heeks, "Some Properties of the Moving High-Field Domain in Gunn Effect Devices", vol. ED-13, pp. 68-78, January 1966.

18. B. W. Hakki and S. Knight, "Microwave Phenomena in Bulk GaAs", IEEE Trans. on Electron Devices, vol. ED-13, pp. 94-104, January 1966.

19. H. W. Thim and M. R. Barber, "Microwave Amplification in a GaAs Bulk Semiconductor", IEEE Trnas. on Electron Devices, vol. ED-13, pp. 110-113, January 1966.

20. J. A. Copeland, "Electrostatic Domains in Two-Valley Semiconductors", IEEE Trans. on Electron Devices (corresp.), vol. ED-13, pp. 180-191, January 1966.

21. J. A. Copeland, "Stable Space Charge Layers in Two-Valley Semiconductors", J. Appl. Phys., vol. 37 pp. 3602-3609, August 1966.

22. H. Kroemer, "Detailed Theory of the Negative Conductance of Bulk Negative Mobility Amplifiers, in the Limit of Zero Ion Density", IEEE Trans. on Electron Devices, vol. ED-14, pp. 476-492, September 1967.

23. H. W. Thim, "Computer Study of Bulk GaAs Devices with Random One-Dimensional Doping Fluctuations", J. Appl. Phys., vol. 39, pp. 3897-3904, July 1968.

24. H. W. Thim and M. R. Barber, "Observation of Multiple High-Field Domains in GaAs", Proc. IEEE (letters), vol. 56, pp. 110-111, January 1968.

25. M. R. Barber, "High-Power Quenched Gunn Oscillations", Proc. IEEE (Letters), vol. 56, pp. 752-753, April 1968.

26. J. A. Copeland, "Theorectical Study of a Gunn Diode in a Resonant Circuit", IEEE Trans. on Electron Devices, vol. ED-14, pp. 55-58, February 1967.

27. J. A. Copeland, "LSA Oscillator Diode Theory", J. Appl. Phys., vol. 38, pp. 3096-3101, July 1967.

28. W. C. Tsai and A. Rosenbaum, "Bias Circuit Oscillations in Gunn Diodes", IEEE Trans. on Electron Devices, vol. ED-16, pp. 196-208, February 1969.

29. B. W. Hakki, "Amplification in Two-Valley Semiconductors", J. appl. Phys., vol. 38, pp. 808-818, February 1967.

30. H. W. Thim, "Linear Microwave Amplification with Gunn Oscillators", IEEE Trans. on Electron Devices, vol. ED-14, pp. 517-522, September 1967.

31. J. A. Copeland, "Characterization of Bulk Negative Resistance Diode Behavior", IEEE Trans. on Electron Devices, vol. ED-14, pp. 461-463, September 1967.

32. H. W. Thim, M. R. Barber, B. W. Hakki, S. Knight and M. Uenohara, "Microwave Amplification in a dc-Biased Bulk Semiconductor", Appl. Phys. Letters, vol. 7, p. 167, September 1965.

33. T. Ohmi and S. Hasuo, "Unified Treatment of Small-Signal Space-Charge Dynamics in Bulk-Effect Devices", IEEE Trans. on Electron Devices, vol. ED-20, pp. 303-316, March 1973.

34. B. S. Perlman, "Microwave Amplification using Transferred Electron Devices in Prototype Filter Equalization Networks", RCA Rev., vol. 32, March 1971.

35. B. S. Perlman, L. C. Upadhyayyula, and R. E. Marx, "Wide-Band Reflection-Type Transferred Electron Amplifiers", IEEE Trans. Microwave Theory Tech., vol. MTT-18, pp. 911-921, November 1970.

36. S. Y. Narayan and F. Sterzer, "Stabilization of Transferred Electron Amplifier with Large N_0l Products", Electron. Letter, vol. 5, pp. 30-31, January 1969.

37. B. S. Perlman, C. L. Upadhyayula, and W. W. Siekanowitz, "Microwave Properties and Application of Negative Conductance Transferred Electron Devices". Proc. IEEE, vol. 59, pp. 1229-1237, August 1971.

38. H. Kroemer, "The Gunn Effect Under Imperfect Cathode Boundary Conditions", IEEE Trans. on Electron Devices, vol. ED-10, pp. 819-837, Nov. 1968.

39. H. L. Grubin, M. P. Shaw, and P. R. Solomon, "On the Form and Stability of Electric-Field Profiles Within a Negative Differential Mobility Semiconductor", IEEE Trans. on Electron Devices, vol. ED-20, pp. 63-78, January 1973.

40. P. R. Solomon, M. P. Shaw, H. L. Grubin and R. Kaul, "An Experimental Study of the Influence of Boundary Conditions on the Gunn Effect", IEEE Trans. on Electron Devices, vol. ED-22, pp. 127-139, March 1975.

41. A. D. Boardman, W. Fawcett and J. G. Ruch, "Monte Carlo Determination of Hot Electron Galvanomagnetic Effects in Gallium Arsenide", Phys. Stat. Sol. (a) vol. 4, pp. 133-141, 1971.

42. A. Sasaki and T. Tanaka, "Effects of Magnetic Field on Electron Transport Properties in Gallium Arsenide", Proc. on the 3rd Conf. on Solid State Devices, Tokyo, 1971. Supplement to Oyo Buturi, vol. 41, 1972.

43. W. Heinle, "Influence of Magnetic Field on the Gunn Effect Characteristic of GaAs", Phys. Stat. Sol. (a) vol. 2, pp. 115-121, 1971.

44. M. E. Levinshtein, T. V. Lvova, D. N. Nasledov and M. S. Shur, "Magnetic Field Influence on the Gunn Effect", Phys. Stat. Sol. (a) vol. 1, pp. 177-187, 1970.

45. W. Shockley, "Negative Resistance Arising From Transit Time in Semiconductor Diodes", Bell Sys. Tech. J., vol. 33, pp. 799-826, July 1954.

46. T. R. Jervis and E. F. Johnson, "Geometrical Magnetoresistance and Hall Mobility in Gunn Effect Devices", Solid-State Electronics, vol. 13, pp. 181-189, 1970.

47. H. J. Lippmann and F. Kuhrt, Z. Naturf. 13a, 474 (1958).

48. A. K. Jonscher, "Transport of Hot Injected Plasmas in Semiconductors", Proc. Phys. Soc., vol. 84, pp. 767-779, October 1964.

49. E. M. Conwell and M. O. Vassell, "High-Field Distribution Function in GaAs", IEEE Trans. on Electron Devices, vol. ED-13, pp. 22-27, Jan. 1966.

50. E. M. Conwell and M. O. Vassell, "High-Field Transport in n-Type GaAs", Phys. Review, vol. 166, February 15, 1968.

51. H. L. Grubin and R. Kaul, "The Influence of Boundary Conditions and the Bias on Amplification From Negative Differential Mobility Elements", IEEE Trans. on Electron Devices, vol. ED-22, pp. 240-247, May, 1775.

52. R. E. Collin, "Fundations for Microwave Engineering", Chp. 3, McGraw Hill, 1966.

53. H. D. Rees, "Time Response of the High-Field Electron Distribution Function in GaAs", IBM J. Res. Develop, pp. 537-542, September 1969.

54. F. Sterzer, "Transferred Electron (Gunn) Amplifiers and Oscillators for Microwave Applications", Proceedings of the IEEE, vol. 59, pp. 1155-1163, August 1971.

55. B. S. Perlman, C. L. Upadhyayula and W. W. Siekanowicz, "Microwave Properties and Applications of Negative Conductance Transferred Electron Devices", Proceedings of the IEEE, vol. 59, pp. 1229-1237, August 1971.

56. A. K. Talwar and W. R. Curtice, "An Experimental Study of Stabilized Transferred Electron Amplifiers", IEEE Trans on Microwave Theory and Tech., vol. MTT-21, pp. 477-481, July 1973.

57. J. G. Koning, R. E. Goldwasser, R. J. Hamilton, Jr., and F. E. Rosztocze, "Gunn-Effect Amplifiers for Microwave Communication Systems in X, Ku, and Ka Bands", IEEE Trans on Microwave Theory and Tech., vol. MTT-23, pp. 367-374, April 1975.

58. M. C. Steele and B. Vural, "Wave Interaction in Solid State Plasmas", McGraw Hill, 1969.

59. B. B. Robinson and B. Vural, "Double-Stream Interaction in a Thin Semiconductor Layer", RCA Review, vol. 29, pp. 270-280, June 1968.

60. I. W. Pence and P. J. K'ian, "Broad-Band Equivalent-Circuit Determination of Gunn Diodes", IEEE Trns. Microwave Theory Thech., vol. MTT-18, pp. 784-790, November 1970.

61. W. Hayt, Jr., "Engineering Electromagnetics", 2nd Edition, Chp. 9, McGraw Hill, 1967.

62. P. S. Hauge, "Static Negative Resistance in Gunn Effect Materials with Field-Dependent Carrier Diffusion", IEEE Trans. on Electron Devices (corresp.), vol. ED-18, pp. 390-391, June 1971.

63. H. Kroemer, "Generalized Proof of Shockley's Positive Conductance Theorem", Proc. IEEE (lett.), vol. 58, pp. 1844-1845, November 1970.

64. R. Spitalnik, M. P. Shaw, A. Rabier and J. Magarshack, "On the Mechanism for Microwave Amplification in 'Supercritically' Doped n-GaAs", Appl. Phys. Lett., vol. 22, 15 February 1973.

65. R. L. Gunshor and A. C. Kak, "Lumped-Circuit representation of Gunn Diodes in Domain Mode", IEEE Trans. on Electron Devices, vol. ED-19, pp. 765-770, June 1972.

AUTOBIOGRAPHICAL STATEMENT

Colmon Wood-Chuen Wong was borned in Kwong Tung, China, on May 27, 1947. Early in his childhood, he moved to Hong Kong where he lived until arriving at New York in 1964. Having finished the senior year at Seward Park High School in Manhattan, he attended The City College of New York where he received the B.E.E. and M.E.E. degrees in 1970 and 1971 respectively. He has since completed his doctoral work with the Electrical Engineering Department and expects to receive the Ph. D. degree in 1976.

From 1970 to 1975, Mr. Wong was employed by The City College of New York as a part time member of the instructional staff with the Electrical Engineering Department.

Mr. Wong was married in 1970 and now resides with his wife, Tammy, in Brooklyn, New York.